The Hong Kong Polytechnic University

Department of Mechanical Engineering

Phase-field Simulation of Void Evolution

Xiao Zhi-hua

A thesis submitted in partial fulfillment of the requirements for the degree of Doctor of Philosophy

April 2013

CERTIFICATE OF ORIGINALITY

I hereby declare that this confirmation report is my own work and that, to the best of my knowledge and belief, it reproduces no material previously published or written, nor material that has been accepted for the award of any other degree or diploma, except where due acknowledgement has been made in the text.

_____

Xiao Zhi-hua (name of student)

Dedicate to my parents

ABSTRACT

Void in metal is an empty space encased by a sharp metallic surface. The void formation and growth process in irradiated metal is a complicated process involving multiple spatial (from 10^{-1} to 10^{2} nanometers) and temporal (from nanoseconds to several days, months or even years) scales, as well as interactions with other types of defects, such as point defects (vacancies and self-interstitials), line defects (dislocations), plane defects (grain boundary) and volume defects (precipitates). Since metal with the supersaturated point defects is in a meta-stable state, local random fluctuations of vacancy concentration may result into the nucleation of void embryos. After the nucleation, the void embryo will grow or shrink depending on whether the net vacancies or interstitials flow in. Action of the void surface tension causes a vacancy emission from the void. Due to the dependence of the vacancy emission rate on the void surface curvature, void embryos with sizes larger than some critical one will continuously grow from the supersaturated solution of vacancies, while the smaller embryos will be re-dissolved.

Since it is difficult to simulate the complex sharp interface structure

using a numerical method for the cases of void ensemble, which involves a complex topological change of surface of multiple voids in a system, the phase-field method, using the concept of a diffuse interface, is a good alternative choice for the simulation of void evolution. The phase-field method is a powerful numerical simulation tool for studying microstructure evolution during phase transformation. In order to quantitatively simulate void evolution in metals using the phase-field method, the free energy functional of the system is first developed. In this functional the vacancy concentration is the only order parameter, which evolution is governed by the Cahn-Hilliard equation. The vacancy concentration is unity in the void, close to zero in the matrix, and between one and zero within the diffuse interface region. Thus, in the phase-field approach voids are treated as a kind of precipitates of vacancies. In this thesis, a single void dynamics after the nucleation, when only vacancies are present in the metal matrix, is quantitatively studied under various conditions by using a phase-field method. The results obtained with sharp boundary approach of void evolution of classical thermodynamics are used as the benchmark for the results obtained with the phase-field method.

Since the realistic void-metal interface is very sharp, in order to

effectively model the void evolution through using a diffuse interface to mimic the sharp interface, the phase-field model should be built properly with the physical mechanisms of void evolution maintained. In order to be consistent with the classical thermodynamics, the phase-field model should be able to reproduce the classical thermodynamics of void evolution in conditions under the sharp interface limit. The void-metal diffuse interface is customarily modeled by a Ginzburg-type gradient energy term with a coefficient which is parameterized from surface tension. The interfacial energy in the diffuse interface approach consists of two parts: the gradient energy due to the variation of vacancy concentration across the interface, and the local free energy due to the vacancies in non-equilibrium state within the diffuse interface. The competition between these two parts determines the thickness of the void-metal interface. The larger the local free energy due to the non-equilibrium vacancies, the narrower the interface will be; and the larger the gradient energy, the wider the interface will be. Within the interface region, the local free energy due to the non-equilibrium vacancies is equal to the gradient energy for flat interface case in equilibrium state because the chemical potential is constant zero across the interface in equilibrium state. For the curved interface case, the relationship between these two kinds of energy is more complicated because the chemical

potential is spatially non-zero constant across the interface in equilibrium state. The chemical potential in the curved interface case is inversely proportional to the void radius in equilibrium state.

In the present work, following the results obtained by A. A. Semenov and C. H. Woo, the gradient energy coefficient is treated as a constant independent of void size. Realistic concentrations of single vacancies, which correspond to the real experimental conditions, are used in the simulations. The real, rather than the reduced, time is used as well. This allows us to make a direct comparison between the results obtained by the phase-field model and those derived from the sharp boundary approach.

The simulations are performed by using the material parameters of molybdenum and copper in three-dimensional space. The vacancy concentration varies across many orders of magnitude across the interface region. In order to maintain the stability of numerical scheme, tiny time steps and spatial grid sizes are used. For the high supersaturation of vacancy concentration, the developed phase-field model reproduces very well the results of the sharp boundary approach on the behavior of single void evolution within the classical thermodynamics framework. Around the critical point for void evolution, due to the sensitivity of void growth

behavior to the parameters of system conditions, the results obtained with phase-field method deviate slightly from those obtained with sharp boundary approach. The ultrafine spatial scales of the void-metal diffuse interface and the fourth-order parabolic non-linear partial differential equation of the Cahn-Hilliard equation, both of which require using a very tiny time step and spatial grid size, present a challenge to numerically efficient modeling of the evolution of a void ensemble under irradiation conditions because this tiny time step and spatial grid size result in enormous calculations for numerical simulations in three-dimensional Cartesian coordinates of a system of large domain.

PUBLICATIONS

Journal Papers:

1. Z.H. Xiao, A.A. Semenov, C.H. Woo and S.Q. Shi, "*Single Void Dynamics in Phase Field Modeling*", Journal of Nuclear Materials, **439**, pp.25~32, 2013.

2. H.B. Huang, X.Q. Ma, Z.H. Liu, F.Y. Meng, Z.H. Xiao, P.P. Wu, S.Q. Shi and L.Q. Chen, "*Micromagnetic simulation of spin-transfer switching in a full-Heusler Co2FeAl0.5Si0.5 alloy spin-valve nanopillar*", Journal of Applied Physics, **110**, 033913, 2011.

3. Huang HouBing, Ma Xing-Qiao, Yue Tao, Xiao ZhiHua, Shi San-Qiang and Chen Long-Qing, "*Magnetization switching modes in nanopillar spin valve under the external field*", Science in China G: Physics, Mechanics and Astronomy, **54**, pages 1227-1234, 2011.

4. Z.H. Xiao, A.A. Semenov, C.H. Woo and S.Q. Shi, "*Phase field modeling of single void evolution in copper*", submitted to Modelling and Simulation in Materials Science and Engineering, 2013.

5. S. Q. Shi and Z.H. Xiao, "*Quantitative free energy functional for phase field modeling of binary alloys*", submitted to Chemical Physics Letters, 2013.

Conference Papers:

1. Z.H. Xiao, S.Q. Shi, C.H. Woo and A.A. Semenov, "*Phase Field Simulation of Void Growth in Metal*", at the 15th Annual Conference of HKSTAM, the 7th Jiangsu-Hong Kong Forum on Mechanics and It's Application, and the 2nd Symposium on the Development of Mechanics in Macau, March 11~12, 2011, Hong Kong & Macau, China.

2. S.Q. Shi, Z.H. Xiao, C.H. Woo and A.A. Semenov, "*Modeling of Void Formation in Irradiated Metals*", at the 17th International Conference on Ion Beam Modification of Materials (IBMM 2010), August 22-27, 2010, Montreal, Quebec, Canada.

ACKNOWLEDGMENTS

I would like to express my sincere gratitude to my chief supervisor, Prof. San-Qiang Shi, for his constant supports on me over these years. He spent considerable time on me and gave great tolerance to the mistakes I always made and my slow speed on the research. I am also grateful to my co-supervisor Prof. Chung-Ho Woo and Dr. Alexei A. Semenov. They spent a lot of time on my work and giving me guidance. Especially, Dr. Alexei Semenov discussed almost all the most important parts of this work with me. I learned a lot from him.

I also would like to thank Prof. Long-Qing Chen for his valuable advice on my research and Prof. Ken Elder for his help on the numerical methods. And many thanks to my dear friend, Dr. Wailun Chan, for teaching me some software tools, such as EndNote and CorelDRAW that were used to draw some cartoon pictures in this thesis.

TABLE OF CONTENTS

LIST OF TABLES

LIST OF FIGURES

Chapter 1: Introduction

1.1 Motivations

The first observation of irradiation-induced voids was carried out in stainless steel using neutron irradiation in 1967 by Cawthorne and Fulton [1]. Later voids were found in nickel by Norris in 1970 [2], using electron irradiation, and in other irradiated metals by Evans [3-5]. The presence of voids in materials will cause microstructural change of materials and influence the thermo-mechanical properties of materials, including changes such as those of thermal conductivity, ductility and creep properties, and even structural instabilities such as volumetric swelling and cracking, especially under long period irradiation conditions. Such irradiation-induced microstructural change is a very complex phenomenon that spans a wide range of length and time scales. The volumetric swelling of the material due to formation of voids leads to density decrease, which has a significant impact on the yielding behavior of structural materials. In order to design radiation-resistant materials for nuclear reactor components, researchers should understand the underlying physical mechanism of void formation and be able to predict the effect of irradiation conditions on morphological

evolution of voids and their subsequent impact on material properties. Thus, researchers pay a lot of attentions to this area and many experimental and theoretical works have been done since the first observation of void in irradiated metal. Many theoretical models and methodologies, such as classical nucleation theory and rate theory, are employed to study void evolution qualitatively and quantitatively.

However, these theories can only explain simple cases, or they are mean field theories that can only give spatial averages. It is desired to develop a predictive simulation tool based on fundamental thermodynamics for investigating the kinetics of void under irradiated conditions. To better understand the process of microstructural evolution, such a tool should be able to obtain spatial resolution of microstructural evolution in the irradiated materials. The rapidly changing landscape of computational materials science now shows great promise for theoretical predictions of microstructural evolution during materials processing, environmental attack and phase transformation. The phase-field method has become increasingly popular since early 1990, due to breakthroughs in its computational methodologies. It has been successfully applied to predict structural evolution on scales ranging all the way from nano-, micro- and meso-scale, to the macroscale. Thus the phase-field method is expected to be an

appropriate tool to give the spatial resolution of microstructure evolution of a system with void nucleation and growth.

A physical void in metal is an empty space encased by a sharp metallic surface. Within this space, there are no atoms, nor are there vacancies, which are present in the metallic matrix. These voids are formed through the classical nucleation and growth mechanism according to the classic nucleation theory. The void embryos are nucleated through stochastic fluctuations of vacancy concentration at discrete sites under the condition of supersaturated vacancy concentration. The vacancy concentration in the metallic matrix is very dilute, even under irradiation conditions with continuous production of vacancies. Due to the curvature of the void surface and the thermal fluctuation, the vacancies are continuously emitted from the void surfaces. Meanwhile, vacancies and self-interstitials flow into void. These processes result in the elimination or addition of atoms on the void surface. If the net amount of vacancies that jump into the void cannot balance those that jump out, the void will shrink, or even re-dissolve.

Since, in irradiated metal, vacancies and interstitials are created in equal numbers by the irradiation of energetic particles, such as electrons, neutrons or ions, there should be no net voids left, because the vacancies and

interstitials will be annihilated by recombination with each other when they meet. However, an asymmetry in the number of freely migrating vacancy defects over self-interstitials in the matrix of irradiated metal will result in void growth through certain bias mechanisms, which include dislocation bias [6] and production bias [7-9]. These mechanisms, which mainly originate from the behavioral difference between vacancies and self-interstitials, generally cause an asymmetry in the numbers of existing freely migrating defects. Because of the dislocation bias mechanism, more interstitials will diffuse into the sinks such as dislocation loops and network dislocations. And with the production bias mechanism, more self-interstitials will be produced in the form of interstitial clusters. These defect clusters are produced by the aggregation of point defects, or even directly produced in collision cascades generated by the irradiation of energetic particles, mainly heavy particles such as neutrons or ions.

The void nucleation and growth process is a phase transition process, which is determined by the laws of thermodynamics. There is a sharp interface between the void and matrix phase that plays a very important role in void nucleation and evolution due to the presence of surface tension. The void evolution process is also a kind of void surface moving process, which is a Stefan problem. Conventionally, solving this problem requires explicitly

tracking of the position of the moving surface and applying the boundary conditions to it. It is difficult to deal with, especially for the evolution of void ensembles.

Rather than the tricky explicit tracking of the position of void surface in the above sharp boundary approach (SBA), phase-field methodology offers us a more simple and convenient method to deal with it, via indirect tracking of the void surface, based on the concept of diffuse interface. In the phase-field model (PFM), the infinitely thin sharp surface is replaced by the diffuse interface with finite thickness. This description of void surface by diffuse interface results in a vacancy concentration field that is assumed to be continuously distributed everywhere in space, including voids, where the local concentration of single vacancies approaches unity. Based on this assumption and the conservation of vacancies, the void and the matrix are uniformly treated through the vacancy concentration as an order parameter governed by the Cahn-Hilliard equation [10]. The boundary conditions at the interface are implicitly incorporated into the model, which leads to the description of void evolution without tracking the interfacial positions. Thus, the interfacial boundary conditions are automatically satisfied around the interface. The mass conservation is also satisfied, as the vacancies flowing into the void correspond to the atoms flowing out from it.

A system involving the void growth and shrinkage with the motion of the void surface is a system in a non-equilibrium state. According to the principles of non-equilibrium thermodynamics, the driving force of system evolution is the difference in the chemical potentials of various parts of the system. The driving force (the gradient of chemical potential) determines the flux of point defects [11]. Since there are no point defects inside the void, the chemical potentials of point defects in the void are equal to zero, and the fluxes are determined by the corresponding values of chemical potentials in the metallic matrix.

From the foregoing, the principles of the non-equilibrium thermodynamics of void evolution should be correctly built in the phase-field framework with the underlying physical mechanism maintained, which can reflect the kinetic characteristic of the void growth or shrinkage. Since the vacancy concentration in the PFM becomes an order parameter which has physical meaning only within the matrix, the thermodynamic potential in the regions where the concentration cannot be treated as dilute should be interpolated by using phenomenological terms. Thus, construction of the Cahn-Hilliard-type thermodynamic potential [10, 12-14] is crucial for the correct development of a phase-field model. This potential conventionally consists of the two terms: the bulk free energy and the

Ginzburg-type gradient energy [12]. The bulk free energy should be a double well function whose two local minimum values correspond to matrix phase and void phase, respectively. The gradient energy term is a key ingredient in the PFM, as it ensures the thermodynamic equivalence of the physical and the emulated void.

The conventional method or theory mostly used to study void evolution and ordering in irradiated metal is rate theory [15, 16]. Due to the mean field character, rate theory has some limitations for the study of void nucleation and growth. Due to its strong ability to simulate microstructure evolution, several attempts have been made to use the phase-filed method for the study of the void evolution. The two-dimensional phase field method has been used to model void growth and void ordering in irradiated metals in recent years.

The first phase field simulation of void evolution in two dimensions in irradiated metal was done by Hui-Chia Yu and Wei Lu who proposed a phase-field model based only on the Cahn-Hilliard equation [17]. The void nucleation and growth process were treated as a phase separation process by spinodal decomposition. The elastic interaction was taken into account and was of the central importance for the void ordering in simulations of an

annealing process in the metals molybdenum and nickel, respectively. The elastic anisotropy and elastic interaction between void surface and vacancies result in anisotropic diffusion of vacancies, even if the diffusivity is isotropic, as the vacancies migrate faster along the elastically compliant directions, which further causes the void ordering. Very large unrealistic thermodynamic equilibrium vacancy concentration and initial vacancy concentration, which are 0.1 and 0.32 respectively, are used in the simulation.

The group of Srujan Rokkam, et al. proposed a phase-field model based on both the Cahn-Hilliard equation and the Allen-Cahn equation [18-20]. They studied the void nucleation and growth process behavior under the condition of supersaturated vacancy concentration in the matrix with stochastic vacancy generation rate by building a phase field model in two dimensions using the Cahn-Hilliard equation coupled with the Allen-Cahn equation [18]. The source fluctuations instead of thermal fluctuation of vacancies, which is the basis of the mechanism of classical nucleation models, were used as the initial driving force for the void nucleation. Landau-type free energy was used in the functional of the Allen-Cahn equation. In this model the elastic interaction was not taken into account. An order of 10^{-4} for thermodynamic equilibrium vacancy concentration at the melting point of copper (1276K) was used. The interaction between different

voids through the competition for vacancies was studied. The spinodal decomposition mechanism was used to realize the void nucleation process in Rokkam et al's simulations. Ostwald ripening and void nucleation and growth behavior were studied also, under different conditions, such as under the influence of grain boundary and self-interstitials. Based on the same model, they studied the influence of grain boundary on void nucleation behavior in irradiated polycrystalline metals [19]. Furthermore, they incorporated the self-interstitials into this model and the influence of self-interstitials on void nucleation and growth behavior were studied [20].

Shenyang Hu *et al*. built a phase-field model based only on the Cahn-Hilliard equation by incorporating the self-interstitial atoms, in order to study the evolution of a void ensemble in a metal with vacancy diffusion and 1-D migration of self-interstitials during irradiation [21]. The influence of diffusivity of self-interstitials on the formation of void lattice was studied. Large diffusivity of self-interstitials compared to the diffusivity of vacancies favored the void ordering, while increasing the generation rate of interstitials delayed the formation of the void lattice. In their paper [22] they built a phase-field model based on the Cahn-Hilliard equation without taking into account the self-interstitials, in order to study the void migration in a temperature gradient field. Furthermore, they extended their model to take

into account the generation and recombination of vacancies and self-interstitials, in order to study void migration and evolution [23].

However, as pointed out in Ref. [24] by A. A. Semenov and C. H. Woo, there are many problems or drawbacks on the research of void evolution using PFM in the above-mentioned published works [18-23].

First, these works of Hui-Chia Yu and Wei Lu, Srujan Rokkam et al, and Shenyang Hu et al assumed very high thermal equilibrium vacancy concentration (10^{-4} to 10^{-2} atomic fraction) in the matrix, which is far from the real physical value (about 3.3×10^{-11} for molybdenum at half melting temperature (1442K), and 3.17×10^{-10} for copper at half melting temperature (679K)).

Second, very high initial vacancy concentrations, ranging from 10^{-2} to 10^{-1} atomic fraction, were used in these simulations, at temperatures ranging from 500k to 1000k, and these concentrations are far from those of experimental reality (experimental observations of vacancy concentration for void formation are on the order of 10^{-10} and 10^{-8} for molybdenum and copper, respectively).

Finally, the void nucleation and growth process is not the same as the

phase separation process in a binary system through spinodal decomposition. However, these papers treat the void nucleation process as a spinodal decomposition process.

There usually are two types of phase separation mechanisms: nucleation and growth mechanism and spinodal decomposition mechanism. The mainly difference between them is that there is free energy barrier for the phase transition through the nucleation and growth, while there is not such energy barrier for spindoal decomposition. For a system at a temperature above a critical point, there is only one phase and the ratios between components can be arbitrary due to the domination of effect of entropy over enthalpy in the free energy at high temperature. Phase separation of a system is possible when temperature is below the critical point. If phase separation for a system start from an initial supersaturated meta-stable state, which is in an area termed binodal region in the phase diagram, there is an energy barrier for phase transition. The overcoming of this energy barrier via spontaneously stochastic thermal fluctuation can lead to the formation of new phase embryos abruptly and locally. The new phase embryos may grow or shrink away under certain conditions. This is the phase separation mechanism of nucleation and growth. Below the critical temperature, in addition to the binodal region, there is another region in the

phase diagram, called spinodal region in which system is in an unstable state. If phase separation for a system starts from this spinodal region, an infinitesimal fluctuation in concentration will result in continuous global phase separation, because there is no energy barrier. This is the phase separation mechanism of spinodal decomposition. The void embryos are nucleated abruptly and locally and the vacancy concentration in a small region should reach unity very quickly and uniformly. Therefore, considering the physical consistency, the spinodal decomposition mechanism cannot be used to mimic the void nucleation process. Due to the characteristics of PFM, it can only be used to model the void evolution process after the nucleation. The nucleation process should be treated in another way.

In addition to the above problems, there is another drawback to the phase-field model of studying void migration in a gradient temperature field under different conditions that was employed by Shenyang Hu's group [21], in which the Cahn-Hilliard equation based on the free energy functional they propose will not reproduce the diffusion equation or satisfy Fick's second law in the matrix.

The theoretical foundation of phase-field modeling for void evolution was built by A. A. Semenov and C. H. Woo [24, 25]. Through analyzing the

characteristics of void nucleation and growth in classical nucleation theory, they built a model by only using the Cahn-Hilliard equation to connect the void evolution of classical thermodynamics and that of the phase-field approach. In this model, in which the nucleation of a single void in an infinite domain was considered, the total free energy change due to the single void formation through stochastic fluctuation of vacancy concentration was assumed to be equal to the corresponding total free energy functional change used in the Cahn-Hilliard equation. Through this equivalence of the voids according to classical thermodynamics with sharp boundary and those in the phase-field model with a diffuse interface, the gradient energy coefficient for a flat interface, as well as for a curved interface, can be determined by reproducing the thermodynamic properties of the void in an equilibrium state in the classical nucleation model with the phase-field model. Semenov and Woo also analyzed the influence of void radius on the gradient energy coefficient, as well as the thickness of the void-matrix interface. Based on their work, the quantitative study of void evolution via the phase-field model can be realized.

1.2 Outline of content

The major goal of the present work is to make phase field simulations of a single void evolution in a three-dimensional domain after its nucleation mainly by following the framework proposed by A. A. Semenov and C. H. Woo [24, 25]. In order to realize this target, a Cahn-Hilliard type free energy functional is constructed properly by interpolating the free energy of a system with only void and vacancies present according to classical thermodynamics. The key point in constructing the free energy functional is to choose a proper gradient energy coefficient, which is derived by following the work of A. A. Semenov and C. H. Woo in ref. [24], and to construct a double well function of bulk free energy. The sharp boundary approach and the rate theory are used as benchmarks to study single void evolution in a spherical domain.

In Chapter 2, general introduction of background and concepts related to this work will be given. The two mechanisms of diffusion-controlled phase transition are introduced in section 2.1. Section 2.2 gives general introductions to the sharp boundary approach and to the rate theory. Section 2.3 gives general introductions to the phase-field method. In section 2.4, brief introductions of several major types of defects are given. Correspondingly different irradiation conditions are given in section 2.5. The bias mechanisms for net vacancies available for void formation are

introduced in section 2.6.

Chapter 3 gives a detailed theoretical description of the sharp boundary approach to void formation and growth, as well as a description of void evolution in rate theory. Chapter 4 describes the theory of phase-field modeling of void evolution in detail. Section 4.1 is a general introduction of the total free energy in the system. The total chemical potential is described in section 4.2. Section 4.3 presents information concerning the bulk free energy that was constructed. The chemical potential due to bulk free energy and uphill diffusion behavior are discussed in section 4.4. Section 4.5 is concerned with the interfacial energy, and the derivation processes of the gradient energy coefficient for a flat interface and a curved interface are presented. In section 4.6, the governing equation (Cahn-Hilliard equation) of vacancy diffusion is discussed.

Chapter 5 gives the numerical methods in detail to solve Cahn-Hilliard equation in spherical coordinates and Cartesian coordinates. Chapter 6 presents the results and discussions of single void evolution under different conditions by using PFM, SBA and RT. In section 6.1 and 6.2, a single void dynamics in the spherical coordinates are studied by using the material parameters of molybdenum and copper, respectively. Section 6.3 presents the

study of a single void dynamics in Cartesian coordinates by using PFM. In the final chapter, the conclusions of the simulation results are made and suggestions for further research are formulated.

Chapter 2: Literature review

Since it is related to the defects ranging from zero-dimensional point defects to two- or three- dimensional extended defects and their motions and interactions, void evolution covers the span from microscale to mesoscale spatially, and from picosecond to several days, months or even years temporally. Thus, it is a very complicated problem involving many concepts and mechanisms. In this chapter, the major concepts and mechanisms used in this work are presented.

2.1 Two mechanisms of diffusive phase transition

2.1.1 Nucleation and growth

There is always thermal fluctuation of solute particle concentration in a solution when the absolute temperature is above zero. The small new phase embryos will be nucleated at thermally fluctuating sites, the chance of occurrence of which increases with temperature. The new phase embryos may also be nucleated directly by input stochastic excitations from external

environment, such as the influence of stochastically energetic incident particles on void nucleation in radiated metal. A phase of supersaturated concentration of solute particles is in a meta-stable state which is a prerequisite condition for nucleation. However, the thermal fluctuation-induced nucleus results in the instability of the formerly meta-stable state of the parent phase of supersaturated concentration of solute particles, and the nucleus grows further to form a stable void (new phase) if its radius is larger than a critical radius (to be discussed in a later chapter); otherwise, it will disappear quickly. An interface is formed between the nucleus and the parent phase. The presence of this interface brings about, in the new phase, a surface tension which inclines to shrink the embryo by emitting the solute particles to the parent phase which surrounds it. This interface imposes an energy barrier to the nucleation. If the energy of the thermal fluctuation in the solution is smaller than this barrier, the embryo will be re-dissolved. If this barrier is overcome, the new thermally stable phase will be formed. The growth and shrinkage of the new phase is only through the motion of the interface as schematically shown in Fig. 2.1*a*.

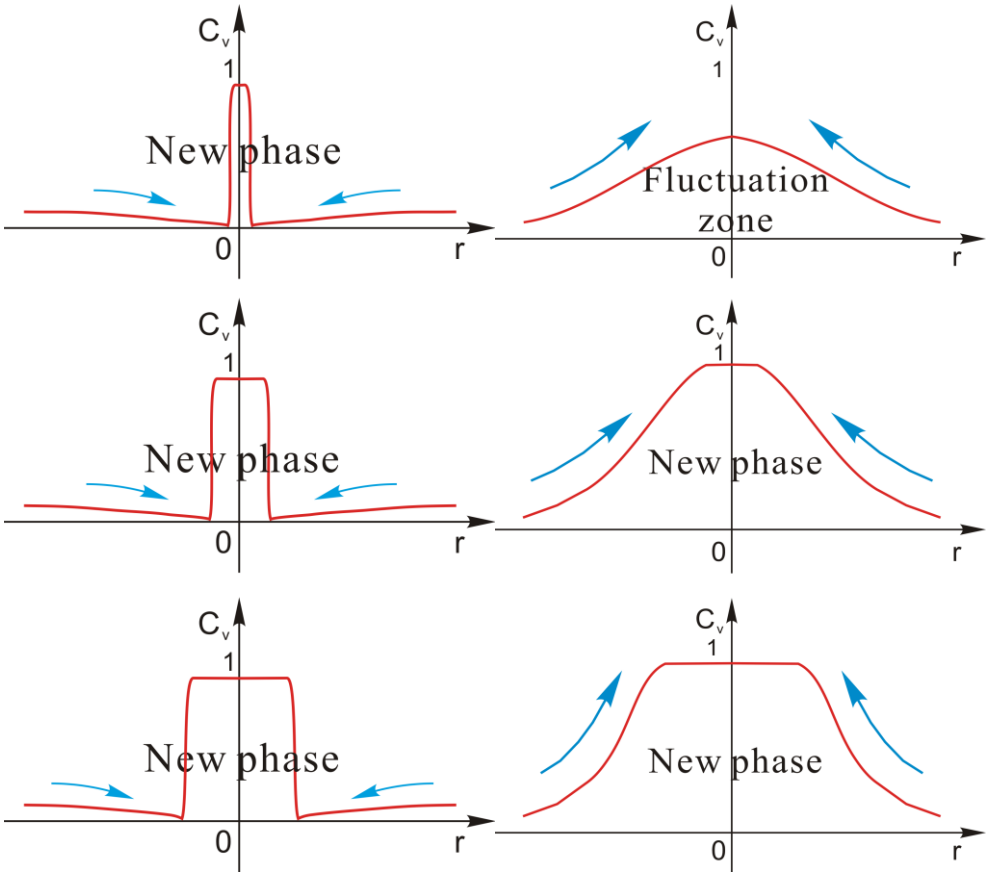

(*a*) (*b*)

Fig. 2.1. Schematic illustration of the mechanisms of spinodal decomposition and nucleation and growth, (*a*) nucleation and growth through normal diffusion, (*b*) spinodal decomposition through up-hill diffusion.

There are two types of mechanisms of nucleation: homogeneous nucleation and heterogeneous nucleation. Homogeneous nucleation is nucleation without preferential nucleation sites, and occurs spontaneously and randomly. Heterogeneous nucleation forms at preferential sites such as phase boundaries or impurities, which facilitate nucleation. It requires less

energy than homogeneous nucleation because the effective surface energy at preferential sites is lower - thus lowering the free energy barrier. The supersaturation needed for nucleation is reduced as well. Thus, heterogeneous nucleation occurs much more often than homogeneous nucleation.

2.1.2 Spinodal decomposition

Nucleation requires a large composition fluctuation, a result of thermal fluctuation or a result of directly stochastic irradiation by energetic particles in the case of void nucleation, as mentioned in the previous section. However, there is another type of phase formation mechanism, in which no nucleation stage is present. This is called spinodal decomposition. This mechanism differs from nucleation and growth mechanism not only because it occurs without a nucleation process but also because it occurs uniformly throughout the material (not just at discrete nucleation sites) as shown in Fig. 2.1*b*. Spinodal decomposition will make a solution of two or more components separate into distinct regions with distinctly different chemical compositions and physical properties through up-hill diffusion, which inclines to make each region rich in one component to form a new phase. Uphill diffusion

occurs when the second derivative of free energy with respect to composition becomes negative, which results in solute diffusion from a low concentration zone to a high concentration zone in the solution. It has a negative diffusion coefficient. The corresponding critical concentration (or minimum solute concentration) for uphill diffusion can be obtained by equating to zero the second derivative of free energy with respect to composition.

When the new phase is formed, there is an interface between the different phases and hence a rise in the system's free energy which is the same as in the nucleation and growth mechanism. If the free energy decrease due to the solute flowing from the low concentration zone (old phase) to the high concentration zone (new phase) is less than the free energy increase due to the formation of the interface, the new phase will shrink by outflow of solutes to the old phase. Conversely, the new phase will grow by inflow of solutes. The spinodal decomposition mechanism can be used to provide a means of producing a very finely dispersed microstructure that can significantly enhance the physical properties of the material, such as in the formation of precipitates in metal.

2.1.3 The difference between spinodal decomposition

mechanism and nucleation and growth mechanism

Spinodal decomposition mechanism is temperature dependent. There is no spinodal decomposition mechanism above the critical temperature at which the solvent and solute are miscible and the solutes can be dissolved in the solvent in any proportion as Fig.2.2 shown. Below that critical temperature, there are two regions: the meta-stable region, or nucleation and growth region, and unstable, or spinodal, region. Within the meta-stable region the system is stable in regard to small fluctuations but is unstable in regard to large fluctuations. In the spinodal region an arbitrarily small fluctuation in composition will make the homogeneous system unstable, which results in one part of the system getting more concentrated at the expense of another; hence the phase involves continuous separation. Thus, there is no thermodynamic barrier for this mechanism to form new phases inside the spinodal region and the decomposition is controlled solely by diffusion. It is in simple contrast to the nucleation and growth mechanism, and can be treated purely as a diffusion problem. Many of the characteristics of such decomposition can be described by an approximate analytical solution to the Cahn-Hilliard equation.

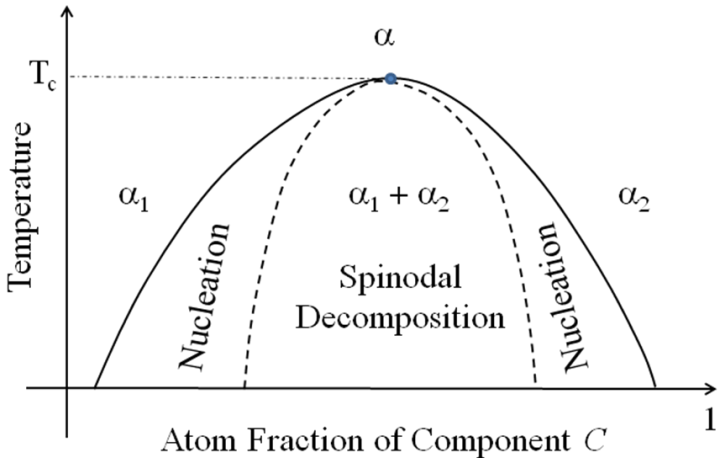

Fig. 2.2. The phase diagram of two diffusive phase transition mechanisms.

Usually, nucleation according to the nucleation and growth mechanism is large in degree and small in extent while spinodal decomposition is small or even infinitesimal in degree but large in extent, and composition fluctuation spreads throughout a large volume. Thus, interface thickness in the spinodal decomposition mechanism is large, while that in the nucleation and growth mechanism is small or even zero. In the spinodal decomposition case the interfacial energy consists of gradient energy and bulk free energy, due to the composition variation through the interface and finite width of the interface; while in the sharp interface case of nucleation and growth mechanism, the interfacial energy is determined by the surface tension and the corresponding surface area.

2.2 Sharp boundary approach and rate theory

2.2.1 Sharp interface

Interfaces play a vital role in the phase transition process. In conventional theoretical analysis and simulations of phase transition and micro-structural evolution, the interfaces between two phases are considered to be infinitely sharp, with zero thickness. The sharp interface model was originally proposed by Gibbs [26]. Some physical properties, such as composition, are assumed to vary discontinuously from one phase to another phase across the sharp interface, and the chemical potential of solute particles changes continuously across a flat sharp interface. For two phases separated by a curved sharp interface, the presence of surface tension results in a jump, not only in composition, but also in pressure or even in the chemical potential of solute particles [27] across the sharp interface. The physical characteristics of the sharp interface can be described as surface tension and interface curvature. The interfacial energy is proportional to the interfacial area, with the surface tension as the proportionality constant.

In modeling based on sharp interface, a set of differential equations are solved with flux and other mechanical conditions matched and mass conserved at the interface. Some variables are discontinuous across the

interface. The position of the moving interface should be explicitly tracked mathematically. Thus, such models are very difficult to simulate, especially for the complex phase morphologies. Sharp interface simulations are mostly restricted to one-dimensional systems or simplified phase morphologies - those, for example, that involve spherical grains.

2.2.2 Classical nucleation theory

Conventionally, in the classical nucleation theory the phase interface is treated as a sharp interface whose physical property is depicted by surface tension. The classical nucleation theory [28] is based on the changes in Gibbs free energy associated with the formation of a nucleus or embryo in a supersaturated solution. There is a free energy barrier, or nucleus formation energy, for new phase embryo formation, which is determined by the temperature, surface tension and solute particle concentration super-saturation ratio in the solution. The solute particle concentration super-saturation ratio should be greater than one. It is the ratio of solute particle concentration in the parent phase to the thermal equilibrium solute particle concentration (or saturated solute particle concentration). The nucleation rate is inversely proportional to the free energy barrier. Whether

the embryo will grow or not is determined by the derivative of free energy difference between those solute particles in the new phase and those in the parent phase with respect to the embryo radius; or by whether a solute particle jump from parent phase to new phase will result in a decrease of the system free energy or not. The free energy consists of two parts: the interfacial part and the volume part. Since the interfacial energy originates from surface tension and is proportional to the embryo surface area, it is the dominant part of the free energy if the embryo size is small because its curvature is very large. The volume part of free energy is dominant when the size of the embryo is large because it is proportional to the volume of embryo.

The interfacial energy will increase if the embryo absorbs a solute particle because the surface area is thereby increased. However, the volume part of free energy will drop if a solute particle jumps from parent phase into embryo because the chemical potentials of solute particles in the old (parent) phase and the new one are different. Therefore, the embryo will grow if absorbing a particle results in an increase of interfacial energy smaller than the decrease of the volume part of free energy. The embryo will shrink if the emission of a particle from it results in a decrease of interfacial energy greater than the increase of the volume part of free energy. In other words, if

the free energy released by forming the embryo's volume is enough to create its surface, the embryo will grow; otherwise, it will shrink. Regardless of whether the embryo grows or shrinks, the total free energy should not increase for a spontaneous evolution process. Thus, the driving force for phase transformation is the difference in Gibbs free energy between the final and initial states of the system.

The phase transition through the mechanism of nucleation and growth can generally be divided into two stages, namely, the nucleation stage and the growth stage. For the nucleation stage, the nucleation process is totally determined by the local discrete stochastic fluctuation of concentration of solute particles. The nucleation rate in classical nucleation theory is inversely proportional to the free energy barrier in an Arrhenius relationship, which describes how many embryos per units of time and volume exceed the critical size. Thus the classical nucleation theory is widely used to predict the rate of first-order phase transitions. For the growth stage, the diffusion of solute particles plays the dominant role once the embryo is nucleated. There may be an effect, called 'Ostwald ripening', after the nucleation, which is that the large embryo grows at the expense of the small one because, in order to be stable, the small embryo requires large solute concentration in the matrix due to its large curvature.

2.2.3 Rate theory

The rate theory [15, 16, 29-31] is the most used theory in studying void evolution. Many of the concepts and equations involved are borrowed from chemical kinetics. The theory proposes and builds on a concept called ‘loss media’ or ‘effective media’, which assumes that the discrete randomly distributed sinks can be approximated by a continuum distribution. It treats different extended defects as sinks, into or out of which the vacancies and interstitials will flow. The strengths of the various sinks are proportional to their density and size. The loss rate of vacancy and interstitial to the sinks is proportional to the sink strength. Vacancies and interstitials can also escape from the sinks due to thermal emission.

The sinks can be grouped into two types according to their capacity to absorb point defects: saturable sinks and unsaturable sinks. Coherent precipitates and impurity defects are saturable sinks; and dislocations, voids, grain boundary, gas bubbles and incoherent precipitates are unsaturable sinks. The sinks can also be divided into two types according to their preference for absorbing deferent types of defect: bias sinks and neutral sinks. Neutral sinks have no preference for interstitials or vacancies, but bias sinks do. Usually, a

dislocation is treated as a bias sink, which prefers to absorb more interstitials than vacancies; and other types of defects are treated as neutral sinks. Beside the major concepts of sinks and sink strength, there are other concepts, such as defect generation rate, thermal emission rate of defects from sinks, and recombination rate of vacancy and interstitial in the matrix. All of the values mentioned above are spatially homogenous. Thus, rate theory is a mean field theory [15].

In order to determine the strength of one type of sink and vacancy distribution and interstitials distribution, a sink with radius R is planted at the center of a spherical region that is free of other sinks. This spherical region is embedded in the effective medium [15]. Then the boundary value problem of the diffusion equation of vacancies and interstitials with other terms (generation rate, thermal emission rate and loss rate in sinks) can be solved, with spherical coordinates by assuming that the steady state is reached at each moment. This is a good approximation due to the short relaxation time of the diffusion field of vacancies and interstitials. The continuity of defect concentration at the sink free-effective medium interface should be satisfied in solving diffusion equations in the two regions. The other sink strengths can be determined in the same way. The flux of point defects into and out of these sinks will be almost equal to the flux at the actual sinks in the real body.

The reciprocal of the square root of the sink strength is the mean free path of point defects in the effective media. With the rate theory, several system model parameters (such as generation rate of defects and magnitude of dislocation bias) should be obtained by fitting them to the experimental data.

2.3 Phase-field Approach

2.3.1 Diffuse interface

In contrast to the zero width of interface in the sharp interface model, the interface width with the diffuse interface approach is finite. The diffuse interface concept arises from the specific expression of gradient energy in the heterogeneous system proposed by Cahn and Hilliard [12]. Thus, the diffuse interface plays the vital role in the phase field method, in which the interface is treated the same as the matrix and new phases, and in which the evolution of phase-field variables is governed by the same phase-field equations. Those variables representing the microstructure gradually and continuously vary across the interface.

The mass conservation and other interfacial boundary conditions are automatically satisfied around the interface. The interface width is

determined by the competition between the gradient energy and the bulk free energy. The thicker interface will decrease the gradient energy, but it will increase the bulk free energy by introducing more materials, which is in non-equilibrium state, into the interface [12]. The larger the gradient energy coefficient is, the wider the width of the interface will be. In the matrix, the profiles of field variables are almost the same as in the sharp-interface model. The position of the interfaces is implicitly given by the profiles of phase-field variables in the microstructural evolution process of the whole system, therefore avoiding the necessity of explicit tracking of the interface position. The uphill diffusion occurring within the interface is the means for the new phases to grow. The effect of interfacial curvature of the new phase is implicitly contained in the gradient of phase-field variables across the interface.

Although the specific expression of gradient energy is given by Cahn and Hilliard [12], the gradient energy coefficient is difficult to determine. There are two ways to do so. The first is to use a systematic asymptotic expansion of phase-field variables in both the interfacial region (inner expansion) and in the bulk (outer expansion), and matched them order by order [32, 33]. The results give partial differential equations and a series of boundary conditions at the interface, which should correspond to the sharp

interface model. The comparison between the partial differential equations and the corresponding equations in the sharp interface model provides the values of the gradient energy coefficient and other parameters used in the phase-field model. The second method is to make the free energy in the sharp interface model equal to that in the diffuse interface model [24, 25]. The phase-field model should recover the sharp interface model when the interface width goes to zero. The main drawback with this is that, to properly model relevant physical phenomena, the interface must be extremely thin, which results in a large gradient of phase-field variables within the interface region. This large gradient of variables across the interface poses certain difficulties in the phase field simulations, which require small grid size and time step size for a resolution high enough to capture the physics of the problems studied. In addition to the above large gradient of order parameters across the interface, the high-order (fourth-order) derivative of phase-field variables is present in the Cahn-Hilliard equation, which imposes a constraint on the time-step size as well.

2.3.2 Phase-field method

The phase-field method is a mathematical technique based on the diffuse

interface, thermodynamics and kinetic principles to model microstructure evolution. In order to approach the problem, the phase field method usually uses the Cahn-Hilliard equation [10] and the time-dependent Ginzburg-Landau equation (or Allen-Cahn equation) [34, 35] to depict the evolution of conserved variables and non-conserved order parameters that are smooth and continuous functions over space and time, respectively. Both are nonlinear partial differential equations, which are solved numerically. Conserved variables are usually used to represent the different local compositions. The non-conserved order parameters are usually used to represent structural heterogeneities which consist of spatially distributed phases of different crystal structures, such as grains of different orientations, domains of different structural variants and structural defects. The thermodynamic potential - the free energy in classical thermodynamics - is approached by the free energy functional in the phase-field method.

As mentioned in the previous section, the introduction of Ginzburg-Landau type gradient energy into the phase-field model leads to the concept of diffuse interface which makes the simulation process without need to explicitly track the position of the interface between different phases for solving a Stefan problem during the microstructural evolution of the system. Thus this approach avoids the difficult mathematical problem of

applying boundary conditions to the interface, the solution of which would otherwise be required for the compositions to match properly on both sides of the interface. With the phase-field method, boundary conditions at the interface are incorporated into the model implicitly and the location of the interface is obtained from the numerical solution of the phase-field order parameters.

Because of the above inherent properties, the phase-field method can easily treat topological changes, such as coalescence of two phases or break up of interface. Therefore, the evolution of complex phase morphologies can be predicted without making any *a priori* assumptions about the shape of the phases. Due to the characteristics mentioned above, such as the employing of the order parameter to represent different phases and the use of the free energy functional to approach the thermodynamic potential - the free energy of classical thermodynamics, the phase-field method is of phenomenological character. The phenomenological parameters used in the phase-field method are determined from experimental and theoretical information. It is a good tool for quantitative study and understanding of the irreversible thermodynamics of a non-equilibrium system and the kinetics of phase transformations. The simulation scale, grid size and time step size are strongly limited by the physical thickness of the interface.

In addition to the effect of surface tension mimicked by the combination effect of Ginzburg-Landau type gradient energy and bulk free energy which mainly consists of the enthalpy and the free energy due to entropy, the other physical effects and interactions, such as thermal equilibrium defects concentration, elastic interaction, electrostatic interaction and magnetic interaction can also be incorporated into the phase-field method through the configuration of the total free energy functional of the system. The thermal equilibrium single defects concentration is realized through the incorporation of formation enthalpy of single defects and the mixing entropy of single defects into the bulk free energy. Due to the above-mentioned characteristics, the phase-field method is very useful for the study of phase transition and microstructure evolution.

After the proposal of the Cahn-Hilliard type of free energy functional [12] and the Cahn-Hilliard equation[10], the phase-field method was introduced by Fix [36] and Langer [37], and this was followed by a lot of theory analysis work [32, 38-42]. The first realistic numerical simulations using the phase field method were in solidification dynamics [43-50]. It was then used in other areas of research and has become a powerful tool for simulating microstructural evolution in a wide variety of materials, such as those involving solid-state phase transformation [51-53], grain growth and

coarsening [54-58], crack propagation [59-62], ferroelectrics [63-66], ferromagnetics [67-70], dislocation [71-75], and precipitates [76-81].

2.4 Defects in the metal

In order to understand the formation mechanism of voids under irradiation conditions, we first need to know the major types of defects in the irradiated metal. Defects in the metal can be grouped into two types: point defects and extended defects. Extended defects can be grouped into line defects, planar defects and volume defects. Point defects are considered to be zero dimensional. Line defects, planar defects and volume defects are considered to be one, two and three dimensional defects, respectively. The following sections give a simple introduction to these four types of defects.

2.4.1 Point defects

1. Single vacancy defects

Point defects include vacancies, interstitials and substitutionals. A vacancy defect is formed when an atom is missing from a normal lattice site in a

crystalline material. The neighboring atoms around the vacancy will not collapse due to the stability of crystal structure and only a slight inward relaxation and tensile stress will be produced in the lattice around the vacancy. The formation energy of a single vacancy is the energy needed to remove an atom from its interior lattice site and place it on the crystal surface. For temperatures within the range of absolute zero to melting point in the crystal, there is an equilibrium vacancy concentration (or saturated vacancy concentration) which is due to the fact that the thermally fluctuating atom at the lattice site has the probability to overcome the formation energy barrier of vacancies and jump from the interior lattice site to the crystal surface, with a vacancy left behind. A certain number of vacancies can lower the Gibbs free energy of the crystal, while the creation of vacancies will increase it through incidentally energetic particles from outside. The formation energy of vacancy in many metals is about 1 ev.

The thermal equilibrium vacancy concentration in the metal is governed by the Arrhenius equation, and increases exponentially with temperature. Mono- and di-vacancies play a major role in the migration mechanism of atomic diffusion. Due to thermal fluctuation, an atom adjacent to a vacancy may have some chance to jump to the vacant site by overcoming an energy barrier between the saddle point and the equilibrium

position. The energy needed to overcome the energy barrier, or the energy needed by atoms to break bonds with neighbors, and to cause the lattice distortions during jump, is called migration energy or activation energy. The vacancy diffusion is isotropic in three dimensions, and the diffusion is described as a random walk process. There is no correlation effect between any two consecutive jumps of a vacancy. The diffusion constant is defined as a phenomenological coefficient which relates a net flux of vacancies per unit area to the vacancy concentration gradient whose direction is opposite to the flux direction. The direction of the flow of atom is opposite to that of the vacancies. The system with vacancy diffusion is in a non-equilibrium state. There are two main self-diffusion mechanisms for vacancies: the mono-vacancy mechanism and the di-vacancy mechanism. For most metals, the mono-vacancy mechanism dominates over a wide temperature range; the di-vacancy mechanism plays a role near the melting temperature [82].

2. Single interstitial defects

An interstitial is a kind of anti-defect of vacancy, in which an atom is squeezed into a non-lattice site or two or more atoms occupy one or more lattice sites and the number of atoms larger than the number of lattice sites. A strong compression stress or strain is produced in the lattice around the

inserted atom, even a small impurity atom (foreign atom), and this gives rise to a large elastic interaction between interstitials and other defects. A self-interstitial defect occurs when a non-foreign atom is squeezed into a non-lattice site. When a self-interstitial meets a vacancy, both of them will be annihilated. Self-interstitials are likely present in pure crystals, in the form of dumbbells and crowdions.

A dumbbell is similar to a di-vacancy, which is orientated along one of the principal lattice directions. However, a dumbbell consists of two atoms that share the same lattice site , while a di-vacancy consist of two vacancies occupying two consecutive lattice sites respectively. There are two types of dumbbells, <100> and <110> dumbbells. Usually a <100> dumbbell is a stable configuration in fcc crystals, and a <110> dumbbell is a stable configuration in bcc crystals [83, 84]. Dumbbell diffusion is isotropic in three dimensions, the same as vacancy diffusion.

A crowdion is an additional atom inserted into a string of atoms so that all of them have a small displacement from their corresponding lattice sites, which are oriented along the close-packed lattice direction, and it migrates along this direction also. Crowdions are only oriented along one close-packed <110> lattice direction in fcc crystals and along a <111> lattice

direction (explained below) in bcc crystals.

In nonmagnetic bcc metals the <111> crowdion configuration is the ground state and the <110> dumbbell configuration is the meta-stable state [85, 86]. The difference of formation energy between that for the <111> crowdion and that for the <110> dumbbell configuration is small. In fcc metals the <100> dumbbell configuration is the ground state and the <110> crowdion configuration is the meta-stable state. Under thermal fluctuation, these two configurations can mutually convert to each other.

The formation energy for a single self-interstitial is higher than that for a single vacancy while the migration energy of self-interstitials is far smaller than that of vacancies in the same metal. So, interstitials generally diffuse faster than vacancies, because the bonding of interstitials to the surrounding atoms is normally weaker and because there are many more interstitial sites than vacancy sites to jump to.

The crowdion migrates along one dimension (a close-packed lattice direction) before converting to the dumbbell, which migrates in three dimensions isotropically. The diffusion path of a crowdion along one dimension is segmented due to the thermal conversion to a dumbbell or to a change to another close-packed direction. Thus, the diffusion of

self-interstitials consists of three-dimensional isotropic diffusion of dumbbells and of one-dimensional anisotropic diffusion of crowdions along those crystalline close-packed directions in crystals. The increase of temperature leads to a decrease in the proportion of crowdion in self-interstitials and to an increase in the frequency of thermal reorientations of crowdions in other close-packed directions, which largely shortens the crowdion mean free path in a given close-packed direction.

3. Substitutional defects

A substitutional defect occurs when a host atom located at a lattice site in a crystal structure is replaced by a different type of atom, which is an impurity. If the substitutional atom is smaller than the original atom, then the lattice around the substitutional atom is in tension, otherwise the lattice is in compression. The diffusion of substitutional defects relies on the concentration of vacancies and the activation energy to allow the defects to exchange positions with adjacent vacancies [87]. The pre-exponential factors and activation energies for diffusion of substitutional atoms are smaller than for self-diffusion of host atoms.

There is a binding energy between substitutional atom and vacancy, which leads to many migration steps of the impurity atom and the vacancy

without dissociation [88]. After the first jump of a substitutional atom to an adjacent vacant lattice site, the substitutional atom tends to exchange sites with the vacancy again. Such successive exchanges of position do not lead to an effective migration, but have a correlated effect on the diffusion processes of the substitutional atom and the vacancy, respectively. The substitutional atom can form saturable defect traps (vacancy type trap and interstitial type trap), which are at the recombination centers of vacancies and self-interstitials. A vacancy trap will only have a certain probability of trapping a vacancy, through the binding energy between the vacancy and the substitutional atom. A self-interstitial may flow into the trap and recombine with the vacancy. An interstitial trap is the counterpart of the vacancy trap: it will only trap an interstitial, and the vacancy will then flows in to recombine with the trapped interstitial. The trapped vacancy or interstitial will be reemitted from the trap by overcoming the binding energy.

2.4.2 Extended defects (defect clusters)

The minimum defect clusters are di-vacancy and di-interstitial. Two or more adjacent vacancies may bond together to form a di- or a multi- vacancy through the binding energy among them. Two vacancies that form a

di-vacancy are located at each other's first- or second- nearest neighbor lattice sites. The resulting di-vacancy is oriented along the line connecting the two vacancies. The di-interstitial consists of two adjacent dumbbells bonded together by binding energy. In addition to the above-mentioned di-vacancy and di-interstitial, and to other multi-vacancies and multi-interstitials, there are many other types of defect clusters. Defect clusters are agglomerations of many single point defects arranged in certain ways. They can be grouped into three types: dislocations (line defects), planar defects and volume defects. Defect cluster may disassociate through the emission of point defects due to surface tension, or line tension, and thermal fluctuation.

2.4.2.1 Line defects (Dislocations)

Dislocations are line defects. They may move under applied stress, and this is a mechanism for the origin of plastic deformation of crystals. Dislocations can dissociate into two or more dislocations and combine with other dislocations. There are distortions in the lattice around the line of dislocation. The magnitude of distortion and direction of lattices caused by dislocation are described by the Burgers vector. The elastic strain energy associated with

the dislocation is proportional to the square of the Burgers vector. For metallic crystal, the Burgers vector for a dislocation will point in the direction of close-packed crystallography, whose magnitude equals that of the inter-atomic spacing. Two dislocations meeting from opposite directions will result in the annihilation of both. The slip of dislocation results in permanent (plastic) deformation of crystal material. If the dislocation is fixed by other defects, or if its motion is impeded, the crystal material will become hard and brittle. Entanglement among dislocations hinders the motion of dislocation. An increase of dislocation density increases the chance of overlap of dislocations through cold working or other methods which can produce new dislocations in the crystal.

There are two primary types of dislocation, edge dislocation and screw dislocation. An edge dislocation can be viewed when an extra portion of a plane of atoms in the close-packed crystallographic plane is inserted into a crystal with the edge of the plane in the crystal's interior. A screw dislocation can be formed by cutting halfway through a crystal and sliding the two parts in opposite directions along the cutting plane to form a fault that looks rather like a spiral staircase. For an edge dislocation, the Burgers vector and motion direction are perpendicular to the dislocation line; for a screw dislocation, the Burgers vector is parallel to the dislocation line and

perpendicular to the direction of motion. The edge dislocation moves on the slip planes of the dislocation line and Burgers vector. The screw dislocation moves on the plane on which its line lies.

Both types of dislocation are formed under applied shear stress whose direction is parallel to that of the Burgers vector. The stress produced by the edge dislocation is asymmetrical. The atoms experience a compression stress near the section of the extra plane of atoms inserted into the crystal, while the atoms near section of the missing plane experience tensile stress. The stress produced by the screw dislocation is symmetrical with respect to the dislocation line. The atoms near the screw dislocation line experience a shear stress. Other types of dislocation are hybrids of these two basic dislocations. They include mixed dislocation which is of both edge and screw character and whose Burgers vector is neither perpendicular nor parallel to the line direction.

There is also a mechanism of dislocation motion other than the slip of dislocations discussed above. It is known as dislocation climb, and is realized through addition of vacancies or self-interstitials to the termination of the extra portion of a plane of atoms of the dislocation. Dislocation climb allows an edge dislocation to move perpendicular to, and hence out of, its

slip plane. This type of dislocation can be regarded as a source, or as a sink, of point defects in the crystal. Dislocation climb is temperature dependent - the climb will occur much more rapidly at high temperatures than at low temperatures due to the increase in vacancy migration at high temperatures. The compressive stress perpendicular to the extra half-plane of atoms of an edge dislocation favors positive climb, in which atoms are removed from the half-plane edge; while tensile stress favors the negative climb, by which atoms are added to the half-plane edge.

As mentioned in the previous sections the presence of vacancies and self-interstitials will lead the entropy of crystal to increase and the free energy of crystal to decrease. In a thermodynamic equilibrium state, the free energy originating from the formation enthalpy of vacancies and self-interstitials is offset by the free energy originating from the entropy of the disordered state, which leads to a thermal equilibrium concentration of both types of point defects, vacancies and self-interstitials. The presence of dislocations will lead to an increase of entropy and a decrease of free energy in the crystal. However, the energy of dislocation formation is much higher than that of a point defect, and the entropy is never able to balance the enthalpy in the free energy, so that dislocations are never in thermodynamic equilibrium with their surroundings.

According to its mobility, dislocations can be divided into two types: sessile dislocations and glissile dislocations. A sessile dislocation is one that cannot glide, but has to be moved by some form of mass transport, such as climb; a glissile dislocation is one that can move by pure slip. Similarly to substitutional atoms, sessile dislocation can form saturable defect traps as well. A sessile dislocation will trap defects with a certain probability, and will also attract their corresponding opposite kind of defect to migrate to them and recombine, - i.e, vacancy sessile dislocations will attract interstitials and interstitial sessile dislocations will attract vacancies - thus they become recombination center of point defects. The point defects may be reemitted into the matrix from the sessile dislocation by overcoming the energy binding the sessile dislocation and the point defects.

A dislocation line must either end on the surface of a crystal or at another dislocation, or form a closed loop called a dislocation loop. Dislocation loops have been found frequently in crystals. If a dislocation loop and its Burgers vector lie in the same plane in which the dislocation loop slips, the loop can expand or shrink by gliding under the applied stress. When the Burgers vector is not in the plane of the loop, the slip surface defined by the dislocation line and its Burgers vector is a cylindrical surface. Such a dislocation is called a prismatic dislocation loop. It glides

conservatively along the cylindrical slip surface. There are two types of prismatic dislocation loop: the vacancy type dislocation loop and the interstitial type dislocation loop. The prismatic dislocation loop can expand or shrink through climb influenced by its stacking-fault and line-tension forces and the supersaturation ratio of point defects in the crystal.

Under excess vacancy concentration the vacancy-type loop will grow by absorbing vacancies, while the interstitial-type loop will shrink. Under excess self-interstitial concentration the interstitial-type loop will grow by absorbing self-interstitials, while the vacancy-type loop will shrink. Increasing temperature will result in the decrease of growth rate of both types of loop, or even their shrinkage, because higher temperature leads to higher thermal equilibrium point defect concentration and vacancies and self-interstitials will be emitted from vacancy- and interstitial- type loops, respectively. The interaction between a prismatic dislocation loop and an edge dislocation can lead to a dislocation loop moving close to the edge dislocation without shrinking or expanding [89].

Some crowdion clusters may form perfect glissile dislocation loops. Like single crowdions, the crowdion clusters can move one-dimensionally by thermal activation, with extremely small migration energies [90]. An edge

dislocation can be thought of as an ensemble of crowdions or clusters of interstitials [91]. Usually, the interstitial dislocation loop is more stable than the vacancy dislocation loop, so that interstitial dislocation loops tend to exist longer than vacancy dislocation loops. The reason for this is that the emission of interstitials from both the interstitial dislocation loop and vacancy dislocation loop is very difficult due to the larger formation energy for interstitials than for vacancies, while the emission of vacancies is easy for both the interstitial dislocation loops and vacancy dislocation loops. However, the emission of vacancy will lead interstitial dislocation loops to grow and vacancy dislocation loops to shrink. Thus, the counterpart effect of shrinking interstitial dislocation loops and growing vacancy dislocation loops through thermal emission of interstitials is inhibited due to the large formation energy required for interstitials.

2.4.2.2 Planar defects

A planar defect is a discontinuity of the perfect crystal structure across a plane. There are many types of planar defects, such as free surface, phase interface, grain boundaries, twin boundary and stacking fault. Free surface is external. Grain boundary and twin boundary and stacking fault are internal

but same phase. Phase interface occur between different phases. In the following I will only introduce grain boundary and phase interface which are very important for the void evolution.

1. Grain boundaries

Crystal material generally consists of a number of crystal grains that are separated by a grain boundary. The crystalline structure of each grain is identical but the orientations of the grains are not. The grain boundary is a narrow zone where the atoms are not properly spaced or perfectly arranged. The range of grain size is from nanometers to millimeters. Grain boundaries limit the lengths and motions of dislocations. Therefore, making grain size smaller can strengthen crystal material. The grain size can be controlled by the cooling rate when the material is cast or heat treated. Generally, rapid cooling produces smaller grains, whereas slow cooling results in larger grains. A grain boundary can be curved, but it tends to be planar when in thermal equilibrium, and this minimizes the boundary area and hence the boundary energy.

There are two types of grain boundary. One is a low-angle boundary, in which two adjacent grains are tilted towards each other at a small angle. The grain boundary is composed of isolated dislocations. The other is a

high-angle boundary, with the misorientation of the two grains being large and arbitrary. The migration speed of atoms in the grain boundary is very fast, even at low temperature. Such a boundary is also a location of the point defect sinks and sources.

2. Phase interface defects

An interface is a very narrow region of contact between two phases, in which the properties are not that of either phase. New phases can nucleate from old phases when some thermodynamic conditions are satisfied. The growth and shrinkage of new phases are realized by the movement of the interface, which is controlled by the flow of particles between phases, across the interface.

There are two main types of phase, precipitates and cavities, which can form defects in otherwise solid metallic material. The phase interfaces between precipitates or cavities and the parent metallic phase is a sharp interface whose width is very small. A misfit strain is produced in the phase interface between precipitates and the parent phase, and surface tension is present in the phase interface between cavities and the parent phase. The conservation law of mass (defects) should be satisfied when across the phase interface. The concentration of defects is not a continuous function of

position across the phase interface, such as in the case of evolution of precipitates, by absorbing or emitting substitutional impurity atoms or, in the case of evolution of voids, by absorbing or emitting vacancies and self-interstitials. However, the chemical potential should be a continuous function of position across the phase interface when the system is in an equilibrium state.

2.4.2.3 Volume defects

1. Precipitates

A precipitate is a region where a lot of impurity atoms aggregate to form a new phase. It can be formed through nucleation, spinodal decomposition, or eutectoid decomposition. The presence of the second, new phase precipitates often causes crystal lattice distortions when the precipitate particles differ in size and crystallographic structure from the host atoms. The presence of smaller solute particles which consist of precipitate in a host lattice leads to a tensile stress, whereas larger solute particles which consist of precipitate lead to a compressive stress. A misfit strain or eigen-strain will be present at the interface between the original phase matrix and the precipitate.

There are two types of precipitates: coherent and incoherent. A coherent precipitate is a precipitate that has continuous lattice structure with, or atomic arrangement with, the matrix from which the precipitate is formed. An incoherent precipitate is one that has no continuous lattice structure with the crystal structure of the surrounding matrix. The precipitates will grow when the impurity atoms flows in and will shrink when they flow out. When the precipitate nuclei are formed, the impurity atoms will diffuse from small to large precipitate particles under the surface tension. This is the Ostwald ripening effect. The evolution of precipitates is mainly determined by the temperature, concentration of impurity atoms and the elastic interaction between them and other precipitates and defects.

There are strong elastic interactions between precipitates and dislocations. The precipitate particles can act as obstacles to impede the movement of dislocations and thereby strengthen alloys. Such a process of formation of uniformly dispersed precipitate particles is known as precipitation hardening or age hardening. Some types of precipitate will favor crack generation and propagation in the material, such as hydrides. The growth of hydrides may eventually lead to irreversible metal plastic deformation through crack generation and propagation, depending on temperature and hydride expansion during precipitation. The surface of

coherent precipitates can either trap interstitials or vacancies through a finite binding energy, the same as the substitutional atoms and sessile dislocations do. The surface of a coherent precipitate will form a recombination center of interstitials and vacancies to influence the swelling rate of the metal further. The trap capacity of coherent precipitates for point defects is finite due to the fact that defects are only trapped at the surface of coherent precipitates. The incoherent precipitates have unsaturable capacity for point defects and hence play a role like that of voids.

2. Voids (Cavities)

A void is an empty space encased by a metallic surface; it also can be viewed as an agglomeration of vacancies or precipitates of vacancies. Unlike the usual precipitate formation process, by which precipitates can be formed through any of the three methods mentioned previously, the formation of a void can only occur through the nucleation and growth process, which is a phase transformation process. There is a sharp phase interface between void and parent phase, and hence a surface tension. The void embryos can be nucleated either through the thermal fluctuation of vacancies or through the aggregation of large vacancy clusters generated by a neutron or other energetic particle irradiation to overcome the formation energy barriers of

void nuclei. Adding a vacancy or emitting an interstitial will favor void growth, and adding an interstitial or emitting a vacancy will favor void shrinkage. Whether the void will grow or not is mainly determined by the net flux of vacancy flow in or out.

A supersaturated vacancy concentration is required for the void to be stable or to grow. The void is of unrestricted capacity for the in-migration of vacancies and self-interstitials. The surface of the void is the center of recombination of vacancy and self-interstitial. The void evolution behavior is influenced by many physical parameters of the metal, such as the formation energy of vacancies, formation energy of self-interstitials, migration energy of vacancies, migration energy of self-interstitials, surface tension of void surface and temperature. Thus it is affected by vacancy concentration, self-interstitial concentration, migration speed of vacancies, migration speed of self-interstitial in the metallic matrix and void size. The void is the net accumulation of vacancies. The volume swelling of irradiated metal is the result of void formation in them. The swelling rate is the fraction of vacancies to the void in the metal, and each single vacancy contributes an approximate atomic volume to the overall volume increase of the crystal. Other types of defect will not have any significant effects on the volume change of the metal. The void evolution process (growth or shrinkage) is a

free energy dissipative process due to the diffusion and/or recombination of vacancies and self-interstitials. A tensile stress is produced around the void in the matrix. The voids tend to attract each other through elastic interaction. Since the range of elastic strain of the void is extremely small, the elastic interaction between two voids becomes significant only when they are very close. The elastic interaction between the void and the point defects is very small comparing to the elastic interaction between dislocation and point defects [16].

2.5 Irradiation conditions

The types of defect produced in the metal will be different under different irradiation conditions. Thus different irradiation conditions will produce different defect structures in irradiated metal and further result in different microstructure of irradiated metal. There are two major types of irradiations conditions in terms of the energy that the incident particles carry – electron irradiation and neutron or heavy ion irradiation.

2.5.1 Electron irradiation

Due to the energy that the incident particles carry, the types of defect

produced by collision vary. Under electron irradiation, the majority of point defects in a metal are generated in the form of isolated Frenkel pairs, created when an atom is kicked out from the lattice site, by the momentum transferred from the incident electrons, and squeezes into a non-lattice site to form a self-interstitial, with a vacancy left behind. The energy of incident electrons used in irradiation typically varies from the keV to MeV and a displacement threshold energy of the order of 10 - 50 eV has to be transferred from an electron to an atom to form a Frenkel pair [92]. The Frenkel pairs are produced and distributed statistically. The vacancy and self-interstitial in a Frenkel pair are easily annihilated through recombination after their generation. If a vacancy and a self-interstitial lie close to each other, there is a significant overlap of their lattice distortions. Upon thermal activation and elastic interaction the self-interstitial may migrate to the vacancy and recombine. Avoiding the recombination of vacancy and interstitial to form a stable Frenkel pair depends on the separation between them - usually several atomic distances. There is some probability that the vacancy and interstitial in a stable Frenkel pair will diffuse to different sinks before their mutual annihilation through recombination. The concentration of vacancies and self-interstitials is supersaturated under continuous electron irradiation. The momentum transferred from an incident electron to an atom

is not large enough to form defect clusters (such as vacancy type dislocation loops and interstitial type dislocation loops) directly, but defect clusters can still be formed through nucleation and growth in electron irradiated metal [93].

Electron radiation induced diffusion of point defects is a mechanism by which the migration of atoms is induced by the direct or indirect collision of an incident electron with atoms. This mechanism leads to an effect similar to that of the migration of atoms by thermal activation. This mechanism explains the defect cluster formation in electron-irradiated metal at very low temperature, at which the thermal motion of defects cannot be expected, especially for vacancies. The operation of this mechanism is the reason that defects can still migrate together to form clusters at very low temperature. Thus the voids can be present in the electron-irradiated metal, even at relatively low temperature. The first observation of void formation in nickel by electron irradiation was carried out by Norris in 1970 [2]. An initial bombardment with argon ion particles before the electron irradiation is needed for void formation - without it the void will not be formed. The gas atoms produced by ion bombardment play a role in the void formation under electron irradiation.

2.5.2 Neutron or heavy ion irradiation

The kinetic energy transferred initially from the collision of energetic incident particles, such as neutrons or heavy ions, with primary knock-on atoms is far greater than the displacement threshold energy. A displacement cascade will occur as a sequence of atomic collisions of primary knock-on atoms. There will be no more damage produced when knock-on atom energy eventually goes below the threshold displacement energy for damage production, because each generation of recoil atoms has, on average, less energy than the previous generation.

A thermal spike or displacement spike occurs in the process of displacement cascade produced by the energetic neutrons or ion particles irradiation. This is characterized by the formation of a transient under-dense region in the center of the cascade and an over-dense region around it. The core region of the cascade is disordered, melts for an short initial period, and then solidifies, with the original crystallographic orientation maintained [92, 94]. The atoms are ejected from the core region of the cascade to the over-dense region, where a high concentration of self-interstitials will be formed. After the cascade, the core region cools down as a result of the

kinetic energy being transferred to the ambient through phonons and electrons The core region then becomes a under-dense region full of vacancies and without self-interstitials [95]. The removal of atoms from the core region of the cascade results in a vacancy-rich depleted zone after resolidification. The vacancy population in the depleted zones can agglomerate and collapse athermally into dislocation loops and stacking-fault tetrahedra in many metals.

Therefore, in the created defects in the displacement cascade process, there are not only point defects such as mono-vacancies, single self-interstitials and Frenkel pairs, but also defect clusters, such as dislocation loops and even void embryos. Both vacancies and interstitials and their clusters are produced in a highly localized and segregated pattern, with their distributions spatially separated from each other. These defect clusters may be either mobile or immobile. The first observation of irradiation-induced voids was carried out in stainless steel using neutron irradiation in 1967 by Cawthorn and Fulton [1], and this was the start of research in this area.

2.6 Bias mechanisms for net vacancies available for void formation and growth

2.6.1 Dislocation bias

There is a preferential absorption of self-interstitials over vacancies at dislocations through a mechanism called stress induced preferential absorption, which operates when the long-range elastic interaction between dislocations and self-interstitials is larger than that between dislocations and vacancies. Thus the dislocations will attract self-interstitials more strongly than vacancies, which results in a slightly higher rate of self-interstitial absorption to dislocations than that of vacancies through migration. Therefore, net vacancies will be left for void formation and swelling, because the numbers of vacancies and of self-interstitials created are equal in the irradiation process, in particular, under electron irradiation condition. This mechanism of void formation and swelling is known as dislocation bias [6]. Thus, there will be no volume swelling if there is no void nucleation and growth, because the vacancies and self-interstitials will be annihilated by recombination or absorption at sinks, such as dislocations or grain boundaries, without volume change. The mutual interaction, by using mobile defects as the media, between the climb and motion of edge dislocations and

the void nucleation and growth determines the evolution of the micro- and macro-structure of material.

2.6.2 Production bias

As mentioned previously, both vacancies and interstitials in cascade damage are generated not only in the form of Frenkel pairs but also in the form of clusters. The vacancy clusters, such as vacancy dislocation loops, are produced in the core region of the cascade; the ejected atoms from the core region form the interstitial dislocation loops in the matrix around the core region. At relatively high temperatures vacancy loops are thermally unstable due to line tension and shrink by emitting vacancies. Thus the immobilization of vacancies in vacancy loops is only temporary. Re-emitted vacancies will be available as freely migrating vacancies to various sinks, including voids. Due to the large binding energy of self-interstitials, which is close to their formation energy, self-interstitial clusters are thermally stable even at relatively high temperatures, until they are removed by growing loops or climbing dislocation segments, or are annihilated by the excess of vacancies. Thus self-interstitials are locked in interstitial loops from the moment they are created.

The lifetime of interstitial clusters is dominated by their destruction, when interstitial clusters are annihilated by the excess of vacancies or by growing loops or climbing dislocation segments, and is considerably longer than that of vacancy clusters, which is dominated by thermal annealing. Therefore, vacancies are emitted from vacancy clusters and are available for voids to grow, while fewer, or no, self-interstitials which would cause the void to shrink, are emitted from immobile interstitial clusters. Thus, there is also an asymmetry in the production of mobile point defects. This mechanism that results in net freely migrating vacancy defects in the matrix is called production bias [7-9].

The difference in the stability and lifetime between vacancy clusters and interstitial clusters generated during the cascade process gives rise to the biased production of available vacancies and self-interstitials. This production bias mechanism can only occur under neutron or heavy ion irradiation conditions and is absent in the case of Frenkel pair production under electron irradiation. The dislocation bias mechanism can operate under both electron irradiation and neutron or heavy ion irradiation, conditions. The number of self-interstitials tied up in the clusters represents approximately the number of vacancies available for void growth, and this number basically determines the strength of the production bias. Both the

production bias and the dislocation bias occur because the preferential trapping of interstitial atoms at dislocations provides the excess of vacancies required to sustain the void. The net result of the production bias is the same as that of the dislocation bias: the provision of an excess of vacancies. However, the physical processes involved in the two mechanisms are very different. In the case of the dislocation bias, the strain-field interaction drives the self-interstitial atoms to migrate to dislocations, where they are preferentially annihilated. In the case of production bias, the interstitial-interstitial interaction (and not the interstitial-dislocation elastic interaction) locks up the interstitials in dislocation loops.

Chapter 3: The sharp boundary approach of void evolution

The sharp boundary approach (SBA) or classical nucleation theory treats the void as a spherical vacuum space encased by a sharp metallic surface in which there are no atoms and vacancies [24, 96]. The void embryos are nucleated at discrete sites locally and occasionally by the large stochastic fluctuation of vacancies overcoming an energy barrier which is about one third of the surface energy of the corresponding void embryos. The vacancies diffuse from the high concentration zone to the low concentration zone in the matrix under the driving force produced by the gradient of chemical potential. As previously mentioned, the formation of vacancies need an external force or thermal fluctuation to act on atoms to break the bonds between them and kick them away from lattice sites, which will increase the enthalpy of the system. There is a minimum energy E_v^f needed to form a single vacancies. The formation energy of n vacancies is almost linearly proportional to the number of vacancies, which can be written as nE_v^f, because the vacancies in the metal are in a weak solution whose concentration is very dilute and the interaction among vacancies is very

small [97]. For simplicity, we assume that the volume of a single vacancies is equal to the atomic volume of the metal and that an atomic volume Ω is added to the volume of the void when a vacancy jumps into the void. Based on this assumption and the fact that the vacancy concentration is far smaller than unity in the irradiated metal, the vacancy concentration C_v is defined as $n/N=n\Omega \approx n/n_a$, where $N = n_a + n$ is the number of lattice sites per unit volume in the single crystal and equals to $1/\Omega$, n being the number of vacancies per unit volume and n_a the number of atoms per unit volume.

3.1 The Gibbs free energy of the system with the presence of vacancies

The isothermal and isobaric conditions are usually considered in experiments of void formation and evolution in metal under irradiation conditions because to fix the metal volume is more difficult than fixing the pressure. Therefore, the Gibbs free energy thermodynamic potential is chosen in studying void formation and evolution. The Gibbs free energy and the free energy density of metal with vacancies present can be written as follows:

$$F_{cl}\left(P,T,n_a,n\right)=\int_V\left[n_a\mu_0\left(P,T\right)+nE_v^f\left(P,T\right)-TS\left(n_a,n\right)\right]dV \qquad (3.1)$$

$$f_{cl}\left(P,T,n_a,n\right)=n_a\mu_0\left(P,T\right)+nE_v^f\left(P,T\right)-TS\left(n_a,n\right) \tag{3.2}$$

where $\mu_0(P,T)$ is the chemical potential of pure metal without vacancies, $E_v^f(P,T)$ the formation energy of a single vacancies, P the pressure, T the absolute temperature. $n_a\mu_0(P,T) + nE_v^f(P,T)$ is enthalpy, which is related to the chemical potential of every atom and the formation energy of vacancies. Thus the production of vacancies will increase the enthalpy of the system due to the energy required to break the bonds. The energy term, $-TS(n_a,n)$, in thermodynamic potential equation (3.2), is related to entropy originating from the thermal fluctuation. The competition between enthalpy due to the formation of vacancies and the energy due to entropy will minimize the local Gibbs free energy and dissipate the total Gibbs free energy of the system. The configurational, or mixing, entropy is rewritten as follows:

$$S=k_B\ln w \tag{3.3}$$

where k_B is the Boltzmann constant and w the number of microstates related to the vacancy distribution in the metal. The number of microstates is written as follows:

$$w=C_N^n=\frac{N!}{\left(N-n\right)!n!}=\frac{N!}{n_a!n!} \tag{3.4}$$

Thus

$$\begin{aligned} S &= k_B \ln w = k_B \ln \frac{(n_a + n)!}{n_a ! n!} \\ &\approx k_B \left[(n_a + n) \ln (n_a + n) - n_a \ln n_a - n \ln n \right] \end{aligned} \tag{3.5}$$

substituting equation (3.5) into equation (3.2), the Gibbs free energy density can be written as follows:

$$f_{cl}(P,T) = n_a \mu_0 (P,T) + n E_v^f (P,T) - k_B T \left[(n_a + n) \ln N - n_a \ln n_a - n \ln n \right] \tag{3.6}$$

The chemical potential of vacancies in a weak solution is

$$\begin{aligned} \mu_v (P,T) &= \frac{\partial f_{cl}(P,T)}{\partial n} \\ &= \frac{\partial \left\{ n_a \mu_0 (P,T) + n E_v^f (P,T) - k_B T \left[(n_a + n) \ln (n_a + n) - n_a \ln n_a - n \ln n \right] \right\}}{\partial n} \\ &= E_v^f (P,T) + k_B T \ln \frac{n}{n_a} \\ &= E_v^f (P,T) + k_B T \ln \frac{C_v}{1 - C_v} \\ &\approx E_v^f (P,T) + k_B T \ln C_v \end{aligned} \tag{3.7}$$

The approximation in above equation holds because the vacancy concentration is very dilute in metal.

We assume that the creation of vacancies and the addition of atoms to the system are independent of each other. The total number of lattice sites equals the sum of the number of atoms and the number of vacancies. Therefore, the expression of Gibbs free energy density can be written as follows:

$$\begin{aligned} f_{cl}(P,T) &= n_a\mu_0(P,T) + nE_v^f(P,T) \\ &\quad -k_BT\left[(n_a+n)\ln(n_a+n) - n\ln n - n_a\ln n_a\right] \end{aligned} \tag{3.8}$$

The chemical potential μ_a of atoms in the lattice with vacancies present can be obtained from following derivation:

$$\begin{aligned} \mu_a(P,T) &= \frac{\partial f_{cl}(P,T)}{\partial n_a} \\ &= \frac{\partial\left\{n_a\mu_0(P,T) + nE_v^f(P,T) - k_BT\left[(n_a+n)\ln(n_a+n) - n\ln n - n_a\ln n_a\right]\right\}}{\partial n_a} \\ &= \mu_0(P,T) - k_BT\ln\frac{n_a+n}{n_a} \\ &= \mu_0(P,T) - k_BT\ln\frac{N}{N-n} \\ &= \mu_0(P,T) + k_BT\ln(1-C_v) \\ &\approx \mu_0(P,T) - k_BTC_v \end{aligned} \tag{3.9}$$

Both the chemical potential of vacancies and that of atoms in the metal with vacancies present are functions of vacancy concentration. In fact, the Gibbs free energy density can be written as a function of vacancy concentration as well, which is useful because we can make an extrapolation from it to get the Gibbs free energy density that can be used in the phase-field method. Since we will mainly study the influence of vacancy behavior on void evolution, it will be convenient to focus only on the influence of vacancy concentration on the thermodynamic potentials, in this study. The configurational entropy and free energy density related to the vacancies can be written as follows:

$$\begin{aligned} S &= k_B \ln w = k_B \ln \frac{N!}{(N-n)!n!} \\ &= -Nk_B \left[C_v \ln C_v + (1-C_v) \ln (1-C_v) \right] \end{aligned} \tag{3.10}$$

$$\begin{aligned} \phi_{cl}(P,T,C_v) &= f_{cl}(P,T,n_a,n) - n_a \mu_0 (P,T) \\ &= nE_v^f (P,T) + Nk_B T \left[C_v \ln C_v + (1-C_v) \ln (1-C_v) \right] \\ &= N \left\{ C_v E_v^f (P,T) + k_B T \left[C_v \ln C_v + (1-C_v) \ln (1-C_v) \right] \right\} \\ &\approx \frac{1}{\Omega} C_v \left[E_v^f (P,T) + k_B T (\ln C_v - 1) \right] \end{aligned} \tag{3.11}$$

Since the vacancy concentration in metal is very dilute, the approximation in the last step of equation (3.11) is automatically satisfied. The construction of free energy density used in the phase-field method should base on expression (3.11). In other words, the free energy density used in the phase-field method should be able to reduce to expression (3.11) when the vacancy concentration is close to zero.

3.2 The void formation mechanism in the sharp boundary approach

According to classical nucleation theory, a super-saturated solution is in a meta-stable state, which is stable for the infinitesimal fluctuation due to the requirements for formation of a new phase surface and unstable for relatively large fluctuations which can overcome the energy barrier due to formation of

surface. A system evolves from a meta-stable state towards the stable equilibrium state through the nucleation and growth of new phases. The critical energy for the formation of a void is determined by competition between a volume free energy, which favors creation of the void, and a surface free energy, which favors its dissolution. The critical radius results from this competition. For a system involving only a flat external surface in the thermodynamic equilibrium state, the chemical potential $\mu_{ve}(P,T)$ of vacancies in the metal should be written as follows [26, 28, 98]:

$$\mu_{ve}\left(P,T\right)=E_v^f\left(P,T\right)+k_BT\ln C_{ve} \tag{3.12}$$

where C_{ve} is the saturated vacancy concentration, or thermal equilibrium vacancy concentration. We can choose this thermodynamic equilibrium state as a reference state by assuming that its chemical potential is equal to zero. Then the saturated vacancy concentration or thermal equilibrium vacancy concentration is given by:

$$C_{ve}=\exp\left[-E_v^f\left(P,T\right)/k_BT\right] \tag{3.13}$$

And the equation (3.7) can be rewritten as:

$$\mu_v\left(P,T\right)=k_BT\ln\left(SR\right) \tag{3.14}$$

where $SR = C_v/C_{ve}$ is the super-saturation ratio, which is supersaturated for

$C_v > C_{ve}$ and under-saturated for $C_v < C_{ve}$. The change in the Gibbs free energy thermodynamic potential due to the aggregation of m vacancies to form a void nucleus (formation energy of a void nucleus) is given by [26]:

$$\Delta\phi_{cl} = m\left[\mu_v'(P,T) - \mu_v(P,T)\right] + \gamma_s A \tag{3.15}$$

where $\mu_v'(P,T)$ is the chemical potential of vacancies in the reference state, which thus equals the saturated vacancy chemical potential $\mu_{ve}(P,T)$. It should be noted that $\mu_v'(P,T)$ is not the chemical potential of vacancies in the void, because there are no atoms in the void, and consequentially no vacancies. $\mu_v(P,T)$ is the chemical potential of supersaturated vacancy in the metal, γ_s the surface tension, and A the area of void surface. If the void is spherically symmetrical with a radius R, the void surface area $A = 4\pi R^2$ and $m = 4\pi R^3/(3\Omega)$.

The Gibbs free energy change consists of two parts. The first part, $m[\mu_v'(P,T) - \mu_v(P,T)]$, is the energy change due to the difference of m vacancies between the reference state and the supersaturated state in the metal, which is negative and decreases the system Gibbs free energy, and favors void formation and growth. The second part, $\gamma_s A$, is the energy needed to create the void surface, which is positive and increases the system Gibbs free energy, and suppresses void formation and growth. The equation (3.15)

can also be written as follows:

$$\Delta\phi_{cl} = -\frac{4\pi R^3}{3\Omega}\left[E_v^f\left(P,T\right) + k_B T \ln C_v\right] + 4\pi R^2 \gamma_s \tag{3.16}$$

According to the thermodynamics, the spontaneous process that the system inclines to is the process of reduction of system Gibbs free energy to reach a stable state, which requires that the differential of $\Delta\phi_{cl}$ with respect to void radius be negative in the process. Thus for void growth process $dR > 0$, it requires $d(\Delta\phi_{cl})/dR < 0$. For void shrinkage process $dR < 0$, it requires $d(\Delta\phi_{cl})/dR > 0$. The expression of the derivative of Gibbs free energy change $\Delta\phi_{cl}$ with respect to void radius R is written as follows:

$$\frac{d\Delta\phi_{cl}}{dR} = -\frac{4\pi k_B T}{\Omega} R^2 \ln\left(C_v / C_{ve}\right) + 8\pi R\gamma_s \tag{3.17}$$

If the jumping of vacancies into the void will result in the reduction of system Gibbs free energy, the void will grow; otherwise it will shrink. Thus there is a critical void radius for void evolution. If the void radius exceeds the critical value the jumping of vacancies into the void will result in the reduction of the system Gibbs free energy and the growth of the void; otherwise it will not. The critical void radius can be obtained by assuming that the derivative of Gibbs free energy change $\Delta\phi_{cl}$, with respect to void radius R, equals zero.

$$-\frac{4\pi k_B T}{\Omega} R^2 \ln\left(C_v / C_{ve}\right) + 8\pi R\gamma_s = 0 \tag{3.18}$$

From the above equation one can get the critical void radius for a system with vacancy concentration C_v in the matrix.

$$R_c = \frac{2\gamma_s \Omega}{k_B T \ln\left(C_v / C_{ve}\right)} \tag{3.19}$$

Fig. 3.1*a* and *b* show the critical void radius R_c as a function of vacancy concentration for molybdenum and copper, respectively. Fig. 3.1*c* and *d* show the critical void radius as a function of temperature for molybdenum and copper, respectively. The critical void radius decreases with the increase of vacancy concentration (see Fig. 3.1*a* and *b*) and increases with temperature when the vacancy concentration is fixed (see Fig. 3.1*c* and *d*). Each point in Fig. 3.1 represents a state of the system, and each state point on the curves in Fig. 3.1 represents an unstable equilibrium state, in which the void neither grows nor shrinks but will easily enter a non-equilibrium state (growth or shrinkage of void) under the influence of even a very small fluctuation of vacancy concentration. Thus, any deviation from this unstable equilibrium state induced by a small disturbance from the environment will result in the continuous growth (or shrinkage) of the void. For a void to be in an unstable equilibrium state, a small void requires high vacancy concentration in the

matrix, while, at higher temperatures, a larger radius is required for the void to be in an unstable equilibrium state.

Each curve in Fig. 3.1 separates the whole domain into two regions. Any state point in the top area on the right side of the curve in Fig. 3.1*a* and *b* corresponds to the growth of a void, or to thermally stable state, while the bottom area on the left side of the curve corresponds to the shrinkage of a void. Any point in the top area on the left side of the curve in Fig. 3.1*c* and *d* corresponds to the growth of a void, while any point in the bottom area on the right side of the curve corresponds to the shrinkage of the void.

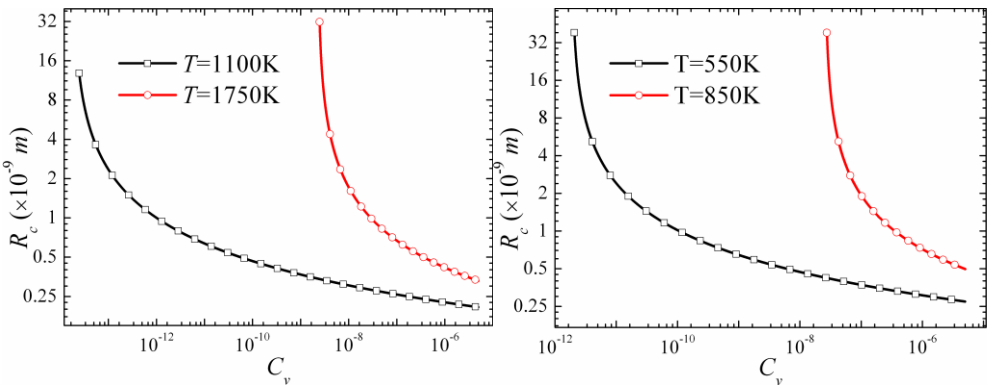

(*a*) (*b*)

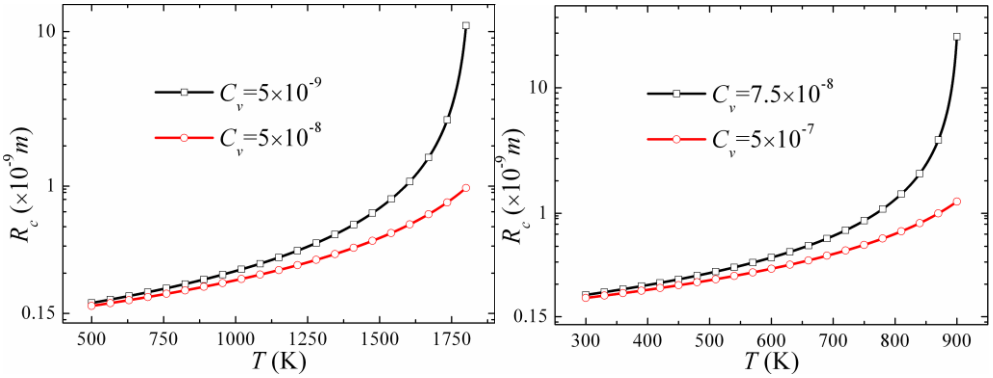

(*c*) (*d*)

Fig. 3.1. Critical void radius, R_c, as a function of vacancy concentration, C_v, in the matrix at two different temperatures (*a*) for molybdenum and (*b*) for copper, and as a function of temperature, *T*, for two different vacancy concentrations in the matrix (*c*) for Mo and (*d*) for Cu.

For a system with multiple voids, the voids with radius $R > R_c$ will grow and the voids with radius $R < R_c$ will shrink and dissolve. The vacancies emitted from the surface of shrinking voids into the matrix will favor the growth of larger voids. This phenomenon is known as Ostwald ripening. Corresponding to this critical void radius there is a critical vacancy concentration C_{veR} (or thermal emission vacancy concentration) required in the matrix for the system with a void with radius R to be in an equilibrium state.

$$C_{veR} = \exp\left[\left(2\gamma_s\Omega/R - E_v^f\right)/\left(k_BT\right)\right] \tag{3.20}$$

When the vacancy concentration in the matrix is bigger than C_{veR}, the void will grow and vise versa. A system with vacancy concentration in the matrix equaling to C_{veR} is very sensitive to vacancy concentration fluctuation because a small vacancy concentration increase or decrease will result in the continuous growth (or shrinkage) of the void.

The thermal equilibrium vacancy concentration, C_{ve}, is related to a flat surface; the thermal emission vacancy concentration, C_{veR}, is related to a curved surface. The ratio of C_{veR} to C_{ve} is the critical super-saturation ratio of vacancy concentration in the matrix for a void with a radius of R not to shrink.

$$SR_c = \frac{C_{veR}}{C_{ve}} = \exp\left[2\gamma_s\Omega/\left(Rk_BT\right)\right] \tag{3.21}$$

And the corresponding chemical potential is

$$\mu_{vR} = k_BT\ln\left(C_{veR}/C_{ve}\right) = \frac{2\gamma_s\Omega}{R} \tag{3.22}$$

The chemical potential in the matrix in an equilibrium state is inversely proportional to the void radius.

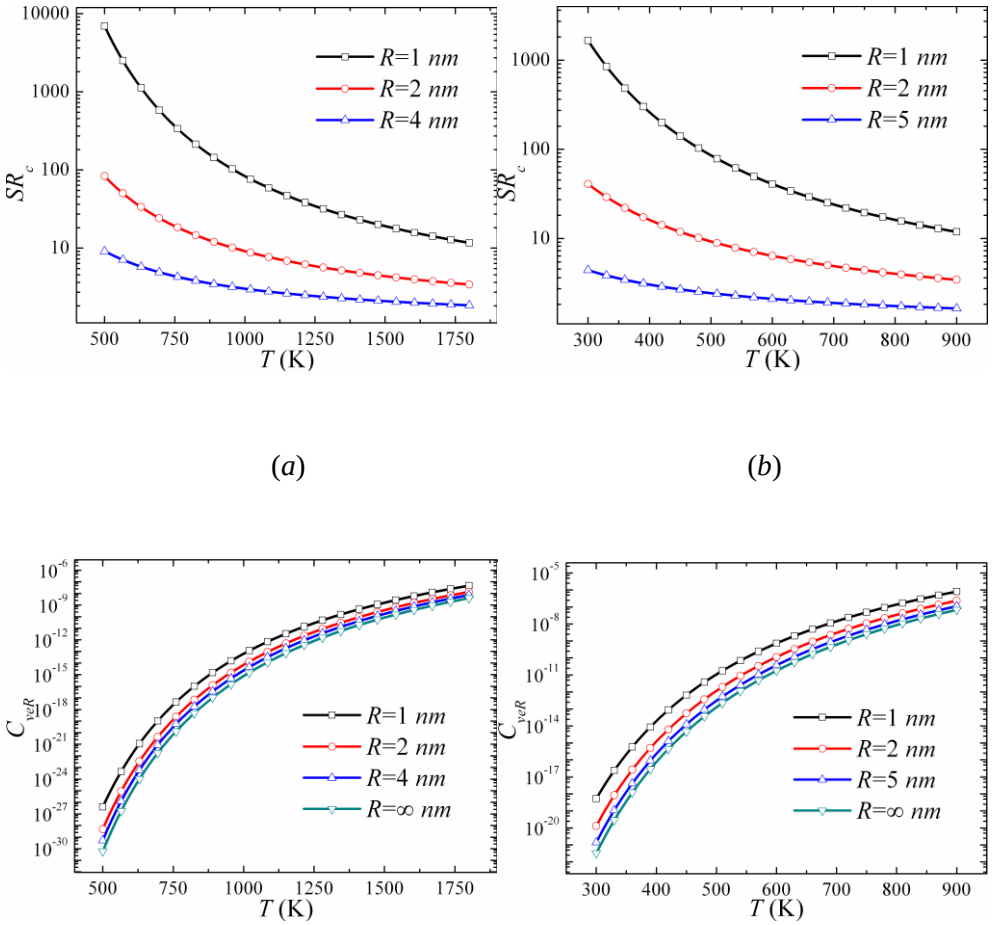

Fig. 3.2. Supersaturation ratios of vacancy concentration, SR_c, (*a*) for molybdenum and (*b*) for copper, and thermal emission vacancy concentration, C_{veR}, (*c*) for molybdenum and (*d*) for copper as functions of temperature, *T*, for voids of different radius, *R*.

The critical supersaturation ratio of vacancy concentration for a void in equilibrium with the system is determined by the absolute temperature and the radius of the void and is not related to the formation energy of the

vacancy. Fig. 3.2*a* and *b* show that SR_c decreases as temperature increases in molybdenum and copper, respectively, while the thermal emission vacancy concentration C_{veR} increases with temperature (Fig. 3.2*c* and *d*). The curves of C_{veR} are close to the curve of C_{ve} when the void radius approaches infinity (Fig. 3.2*c* and *d*). From the graphs in Fig. 3.2 we can see that the larger the void is, the smaller vacancy concentration or supersaturation ratio needed for a void to be in an unstable equilibrium state.

The equation (3.17) can be rewritten in terms of R_c as follows:

$$\frac{d\Delta\phi_{cl}}{dR} = -\frac{8\pi R^2\gamma_s}{R_c} + 8\pi R\gamma_s \tag{3.23}$$

In a meta-stable state, the vacancy concentration in the matrix is supersaturated ($C_v > C_{ve}$) or $\mu_v'(P,T) - \mu_v(P,T) < 0$. A thermal fluctuation in vacancy concentration may result in the nucleation of a void by the overcoming of a free energy barrier. This energy barrier, which is the maximum of formation energy [28] of the void, can be obtained by the integration of equation (3.23) with respect to void radius from 0 to R_c (or by directly substituting the critical void radius R_c into equation (3.16)). The formation energy is equal to one third of the surface energy.

$$\Delta\phi_{cl}\left(R_c\right) = \frac{4\pi R_c^2\gamma_s}{3} \tag{3.24}$$

It is indicated from equation (3.25) that the formation energy of void is totally determined by the surface energy of the void, and not related to the difference of chemical potential of vacancies in the reference state and in the supersaturated state in the matrix. The nucleation rate of voids mainly depends on the energy barrier [28]

$$\frac{dN_{void}}{dt} = N_{v0} \exp\left[-\frac{\Delta\phi_{cl}\left(R_c\right)}{k_B T} \right] \tag{3.25}$$

N_{v0} is the pre-exponential coefficient associated with the characteristic time scales of motion in the system (nucleation frequency). The nucleation rate of void is inversely proportional to the formation energy of void. The larger the void nucleus, the smaller the nucleation probability of it will be.

The above analysis is based on equilibrium thermodynamics, which can only be used to obtain some criterion to determine whether a void is stable or not under different conditions. In order to obtain the void growth rate or the microstructural evolution speed of system, the vacancy diffusion behavior in the metal should be studied.

3.3 Vacancy diffusion in the matrix

For any state deviating from thermodynamic equilibrium, there are thermodynamic driving forces to make the mass transport phenomenon occur. According to non-equilibrium thermodynamics, the local thermodynamic equilibrium can be assumed for a system close to equilibrium state. Thus the concepts of equilibrium thermodynamics can be extended to these non-equilibrium conditions, in which the flows are small and the driving forces gradually throughout in space. Based on these assumptions, we can obtain a linear relationship between the flows and the driving forces for the near-equilibrium system [99].

$$\mathbf{J}_i = \sum_j L_{ij}\mathbf{X}_j \tag{3.26}$$

where $\mathbf{J}_i$ is the flux of species i and $\boldsymbol{X}_j$ the driving force of species j. $\boldsymbol{X}_j$ is the gradient of chemical potential, which is related to concentration or density. L_{ij} are the kinetic coefficients which describe the cross-coupling effects of the different forces. They have the following relations:

$$L_{ij} = L_{ji} \tag{3.27}$$

Equation (3.27) is called the Onsager relations in irreversible thermodynamics. Equation (3.26) is an extension of Fick's first law. For a system containing the vacancies and self-interstitials, equation (3.26) can be

rewritten as follows:

$$\mathbf{J}_v = -\frac{M_{vv}}{\Omega}\nabla\mu_v(\mathbf{r},t) - \frac{M_{vi}}{\Omega}\nabla\mu_i(\mathbf{r},t) \tag{3.28}$$

$$\mathbf{J}_i = -\frac{M_{iv}}{\Omega}\nabla\mu_v(\mathbf{r},t) - \frac{M_{ii}}{\Omega}\nabla\mu_i(\mathbf{r},t) \tag{3.29}$$

where $\mathbf{J}_v$ is the flux of vacancies, $\mathbf{J}_i$ the flux of self-interstitials; ∇ the gradient operator; M_{vv} and M_{ii} the mobility of vacancies and self-interstitials, respectively; and $M_{vi} = M_{iv}$ is the mobility due to the mutual influence of diffusion of vacancies and self-interstitials. The gradient of chemical potential is the driving force for the diffusion of vacancies and self-interstitials. The other effects, such as the influence of the temperature gradient on the diffusion of point defects and the heat flow for a non-isothermal system, can be incorporated into the system in the same way. If M_{vi} is small, the diffusion of vacancies and self-interstitials are independent of each other.

In this work, the influence of vacancies on void evolution is the main concern. The effect of self-interstitials created by irradiation is ignored, which means that the concentration of vacancies calculated in this work is the net value after all possible annihilation mechanisms due to recombination and interaction of vacancies with other types of defects, such as

self-interstitials, dislocations, grain boundaries and so on. The elastic interaction between void and point defects will not be taken into account because its effect is relatively small [16]. The equation (3.28) is rewritten as follows:

$$\mathbf{J}_v = -\frac{M_v}{\Omega}\nabla\mu_v(\mathbf{r},t) \tag{3.30}$$

where M_v is given by

$$M_v = \frac{DC_v(\mathbf{r},t)}{k_B T} \tag{3.31}$$

where D is the diffusion coefficient. The diffusion coefficient is temperature dependent and a scalar for vacancies whose diffusion is isotropic.

$$D = D_0 \exp\left[-\frac{E_v^m}{k_B T}\right] \tag{3.32}$$

where D_0 is the pre-factor and E_v^m is the migration energy of vacancy. Substituting equations (3.7) and (3.31) into equation (3.30), one gets

$$\mathbf{J}_v = -\frac{D}{\Omega}\nabla C_v(\mathbf{r},t) \tag{3.33}$$

At positions where there are neither sources nor sinks, the conservation of mass should hold. The continuity equation and Fick's second law are written as follows:

$$\frac{\partial C_v(\mathbf{r},t)}{\partial t} = -\Omega \nabla \cdot \mathbf{J}_v \tag{3.34}$$

$$\begin{aligned} \frac{\partial C_v(\mathbf{r},t)}{\partial t} &= \Omega \nabla \cdot \left[\frac{M_v}{\Omega} \nabla \mu_v(\mathbf{r},t) \right] \\ &= \nabla \cdot \left[D \nabla C_v(\mathbf{r},t) \right] \end{aligned} \tag{3.35}$$

Through equation (3.35) the vacancy distribution in the matrix and the void growth rate can be obtained. In spherical coordinates, the diffusion equation (3.35) is rewritten as

$$\begin{aligned} \frac{\partial C_v(r,t)}{\partial t} &= \frac{1}{r^2}\frac{\partial}{\partial r}\left(Dr^2 \frac{\partial C_v(r,t)}{\partial r} \right) \\ &+ \frac{1}{r^2 \sin\theta}\frac{\partial}{\partial \theta}\left(D \sin\theta \frac{\partial C_v(r,t)}{\partial \theta} \right) + \frac{1}{r^2 \sin^2\theta}\frac{\partial}{\partial \varphi}\left(D \frac{\partial C_v(r,t)}{\partial \varphi} \right) \end{aligned} \tag{3.36}$$

For a system with spherical symmetry

$$\frac{\partial C_v(r,t)}{\partial t} = \frac{1}{r^2}\frac{\partial}{\partial r}\left(Dr^2 \frac{\partial C_v(r,t)}{\partial r} \right) \tag{3.37}$$

Based on the above analysis, the growth rate of a void (or the velocity of surface motion) is

$$\frac{dR}{dt} = -\Omega J_v\big|_{r=R} = D \left. \frac{\partial C_v(r,t)}{\partial r} \right|_{r=R} \tag{3.38}$$

For the derivation process of equation (3.38), see Appendix A. Equation (3.38) indicates that the void growth rate is proportional both to the diffusion constant of vacancies and the gradient of vacancy concentration at the void

surface or the gradient of chemical potential at the void surface. Thus the void growth rate is related to the migration energy of vacancies. However, the nucleation rate and the critical radius of voids are independent of the migration energy, while related to the formation energy of vacancies.

3.4 Rate theory of void evolution

The rate theory (RT) [15, 29-31] is based on chemical kinetics and is the most used theory for the study of void evolution. The vacancy concentration distribution in the matrix and the void growth rate in RT can be obtained by assuming that the steady-state of vacancy diffusion is reached at all times; therefore, the left hand side of equation (3.37) is equal to zero under certain boundary conditions. This is approximately true if the void evolution rate (dR/dt) is small. The time $\Delta\tau$ for the void surface to move the very tiny distance $\Delta R << R$ is about $\Delta R/(dR/dt) \cong R\Delta R/(DC)$. The corresponding relaxation time Δt of the vacancy diffusion field in front of the void surface is about $\Delta R^2/(2D)$. The vacancy concentration C in the solution is very dilute under experimental conditions and $\Delta R << R$, as a result, Δt is far smaller than $\Delta\tau$. Thus, it can be considered that the steady-state of the diffusion field in front of the void surface is reached, i.e., the time derivative in equation (3.37)

can be set approximately equal to zero. This is proved by our results in the next section, in which the void evolution curves obtained with SBA coincide with those obtained by this steady-state assumption, especially at high temperature.

Under the condition that the radius of the spherical region L is far greater than the void radius and in the absence of interstitials diffusion, the void growth rate can be written as: [100],

$$\frac{dR}{dt} = D(C_b - C_{veR})\frac{1}{R}, \quad \text{when} \quad L >> R \tag{3.39}$$

Otherwise,

$$\frac{dR}{dt} = -\Omega J\Big|_{r=R} = D(C_b - C_{veR})\frac{L}{R(L-R)} \tag{3.40}$$

The geometric structure of the above model is shown in Fig. 3.3. For the derivation of equations (3.39) and (3.40), see Appendix B. These equations are conventionally used in the rate theory treatment of void ensemble evolution under irradiation [15, 29, 30].

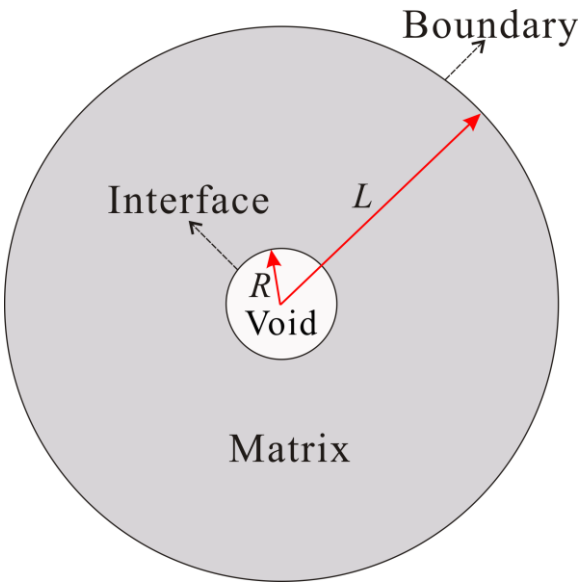

Fig. 3.3. Schematic illustration of a cross section of a spherical domain with a spherical void. R is the void radius, and L the radius of the system.

Whether the void will grow or shrink is determined by the difference between the vacancy concentrations at system boundary C_b and at void surface C_{veR}. The equilibrium state is reached when C_b equals C_{veR}, which means that the vacancies flowing in and out of the void balance each other; otherwise the system will be in a non-equilibrium state. The equation (3.39) is a good tool for us to understand the relationship between void growth rate and system parameters such as temperature, void radius and vacancy concentration at the boundary.

Chapter 4: Phase-field model of void evolution

In PFM for void evolution, the whole system is treated as a system composed of two phases: the phase of void and the phase of matrix. There is a diffuse interface between these two phases. The vacancy concentration is used as the order parameter, whose value is unity in the void and very small (within a range from 10^{-12} to 10^{-5}, according to the environment temperature) in the matrix but varies from almost zero (in the matrix) to unity (in the void) within the interface. Since the vacancy concentration in the void is far greater than in the matrix, in order to realize void growth the uphill diffusion within the interface zone is needed in the simulation. In addition, the vacancy concentration changes by many orders of magnitude within the narrow interface zone. This imposes a huge difficulty for the simulation of PFM of void evolution.

4.1 Total free energy functional

How to configure a free energy functional which can capture the physical character of void evolution under the vacancy diffusion in the matrix is of crucial importance. According to Cahn and Hilliard [12], the free energy of a non-uniform system can be rewritten as the sum of two contributions - the functions of the local composition and of its derivatives, respectively - based on the assumption that the local free energy of a non-uniform system depends both on its composition and on the composition of its near environment. For a system containing vacancies with cubic or isotopic symmetry, due to the invariant of local free energy to the symmetry operations of axis inversion and of rotation around a fourfold axis, without concerning the effect of external surface and neglecting terms in derivatives higher order than the second, the Taylor expansion of total free energy F can be written as follows:

$$F = \frac{1}{\Omega}\int_V f\left(C_v, \nabla C_v, \nabla^2 C_v, \cdots\right) d^3 r = \frac{1}{\Omega}\int_V \left[f_0\left(C_v\right) + \alpha\left(\nabla C_v\right)^2 \right] d^3 r \quad (4.1)$$

The integration is conducted over the total volume V, where $f(C_v, \nabla C_v, \nabla^2 C_v, \cdots)$ is the local free energy per lattice site of a system containing vacancies; $f_0(C_v)$ is the local free energy per lattice site of uniform vacancy concentration or local bulk free energy; $\alpha(\nabla C_v)^2$ is the free energy related to non-uniform vacancy concentration, or the Ginzburg-type gradient energy,

which describes some kinds of interactions between the vacancies locally; and α the gradient energy coefficient, which measure the strength or range of these interactions of non-uniform vacancy concentration. The total free energy functional F with the presence of vacancies in the matrix consists of bulk free energy F_b and gradient energy F_g.

$$F(C_v) = \frac{1}{\Omega}\int_V \left\{ f_0(C_v) + \alpha(\nabla C_v)^2 \right\} d^3r = F_b(C_v) + F_g(C_v) \qquad (4.2)$$

Higher-order gradient terms, such as $(\nabla^2 C_v)^2$, which can describe correlations on still smaller scales [33], can be included if necessary. It should be noted here that, although the free energy functional F is the interpolation of the true free energy (equation (3.2)) used in the thermodynamics, they are totally different [33]. The bulk free energy and gradient energy [12] are written as, respectively,

$$F_b(C_v) = \frac{1}{\Omega}\int_V f_0(C_v(\mathbf{r},t))\, d^3r = \frac{k_B T}{\Omega}\int_V \phi_b(C_v(\mathbf{r},t))\, d^3r \qquad (4.3)$$

$$F_g(C_v) = \frac{\alpha}{\Omega}\int_V [\nabla C_v(\mathbf{r},t)]^2 d^3r = \frac{k_B T \kappa^2}{\Omega}\int_V [\nabla C_v(\mathbf{r},t)]^2 d^3r \qquad (4.4)$$

where $\phi_b(C_v(\mathbf{r},t))$ is the free energy per lattice site, α relates to the surface tension, $\kappa^2 = \alpha/(k_B T)$ the reduced gradient energy coefficient, and κ is of a unit of length which characterizes an "interaction length" among vacancies.

In fact, the free energy functional expressed by equation (4.2) only takes into account the free energy originating from short range interaction. However, free energy accounts for long range interactions, such as the elastic interaction, electric dipole-dipole interactions and electrostatic interactions as well, and these can be introduced to the total free energy functional by adding following term [101]

$$F_l = \int_V \int_{V'} G(\mathbf{r} - \mathbf{r}') d^3 r d^3 r' \tag{4.5}$$

where $G(\mathbf{r} - \mathbf{r}')$ is a green function which describes long range interaction.

4.2 The chemical potential

The chemical potential of vacancies in the PFM is a variational derivative of the free energy functional with respect to vacancy concentration:

$$\mu(C_v) = \Omega \frac{\delta F(C_v)}{\delta C_v} = \frac{\partial f_0(C_v)}{\partial C_v} - 2\alpha \nabla^2 C_v \tag{4.6}$$

Equation (4.6) only holds for the condition that the vacancy concentration is fixed at the system boundary (Dirichlet boundary condition), or for the condition that the number of vacancies of the whole system is conserved (periodic boundary condition). For the derivation processes for equation

(4.6), see Appendix C. Any heterogeneity in chemical potential, which is the driving force $\nabla\mu(C_v)$, will produce a redistribution of chemical potential until it is constant throughout the whole system, and the system reaches an equilibrium state. In the SBA, the driving force $\nabla\mu(C_v)$ for vacancy diffusion can be reduced to ∇C_v, which means that any heterogeneity in vacancy concentration will produce a flow of vacancies until the vacancy concentration is homogeneous everywhere. Here in the PFM the driving force $\nabla\mu(C_v)$ can be reduced to ∇C_v only in the matrix. In the thermodynamic equilibrium state, the driving force $\nabla\mu(C_v)$ should be zero everywhere and the chemical potential should be spatially identical throughout the whole system. For a system containing a void with radius R in the thermodynamic equilibrium state in the PFM, the chemical potential at any position within the system should be equal to the chemical potential in the matrix obtained with SBA (see equation (3.22)). Thus, in a thermodynamic equilibrium state, by combining equation (4.6) and (3.22) we get

$$\mu_{vR} = \frac{\partial f_0(C_v)}{\partial C_v} - 2\alpha\nabla^2 C_v = \frac{2\gamma_s\Omega}{R} \tag{4.7}$$

The chemical potential in the system in the equilibrium state is inversely proportional to the void radius.

4.3 The bulk free energy

There are two requirements for the bulk free energy. First, in order to recover the SBA, the reduced bulk free energy per lattice site $\phi_b(C_v(\mathbf{r},t))$ must satisfy the corresponding limit [97], i.e., it should be consistent with the free energy density used in the SBA and RT (see equation (3.11)). Thus the reduced bulk free energy per lattice site should approach $k_BT(C_v\ln C_v/C_{ve} - C_v)$ for $C_v \to 0$. This can be written as follows:

$$\phi_b\left(C_v\right) = C_v \ln\left(C_v/C_{ve}\right) - C_v + \varphi\left(C_v\right) \tag{4.8}$$

Second, since the vacancy concentration is the order parameter, the reduced bulk free energy per lattice site, a phenomenological function with parameters fitted to experimental data, should be a double well function that has two global minima - for vacancy concentration at C_{ve} and at unity - which represent the matrix phase and void phase, respectively.

The following interpolation of equation (4.8) will be used in PFM:

$$\phi_b\left(C_v\right) = C_v \ln C_v + \left(1-C_v\right)\ln\left(1-C_v\right) + \frac{E_v^f}{k_BT} C_v\left(1-C_v\right) \tag{4.9}$$

This is a symmetrical double well function, symmetric around $C_v = 0.5$ with the two minima at $C \cong C_{e\infty}$ and $C \cong 1$. It is the extrapolation of the free

energy density in SBA (see expression (3.11)). From expression (4.9) one can find that, if C_v approaches zero, $k_BT\phi_b(C_v(\mathbf{r},t))/\Omega$ will be reduced to expression (3.11). Thus (4.9) satisfies the dilute solution limit.

Fig. 4.1 show the curves of ϕ_b for Mo and Cu at four different temperatures. The diagrams in the column to the right show the curves of ϕ_b around the point of saturated vacancy concentration, which is one of the minima of function ϕ_b.

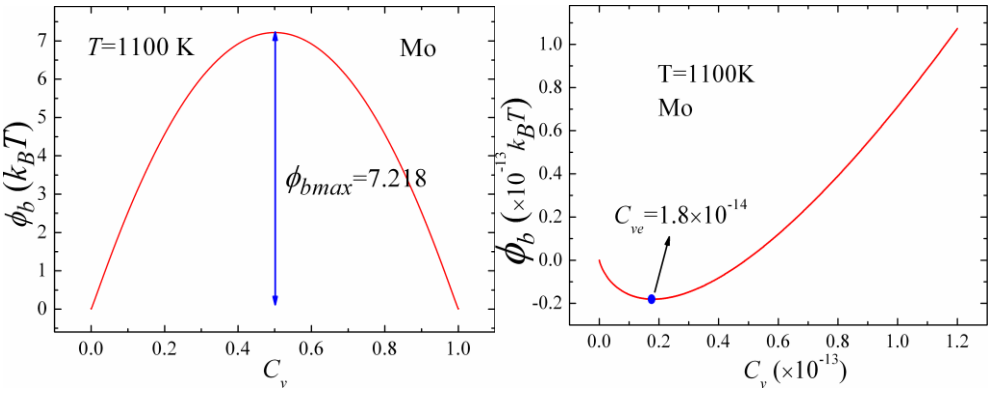

(*a*) (*b*)

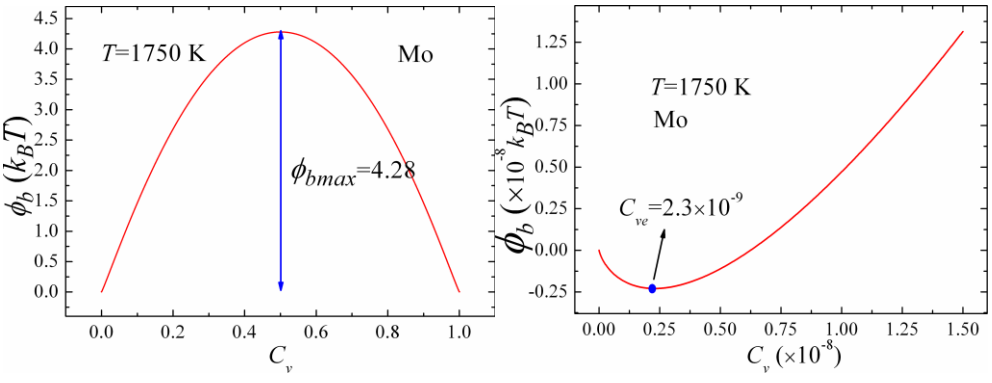

(*c*) (*d*)

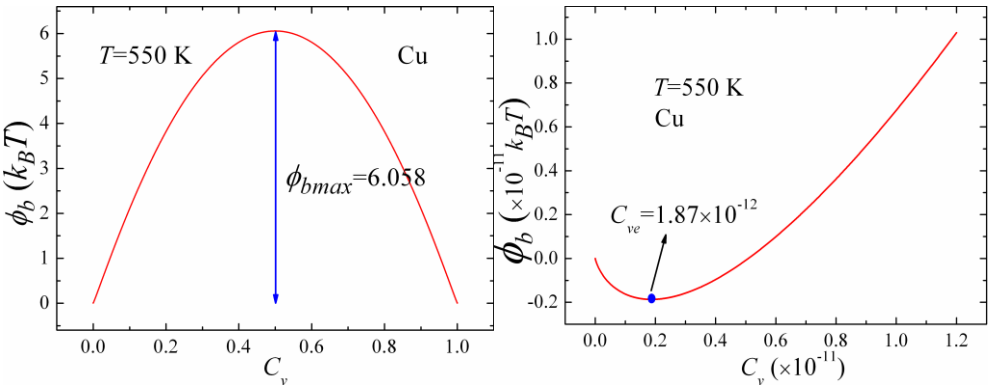

(*e*) (*f*)

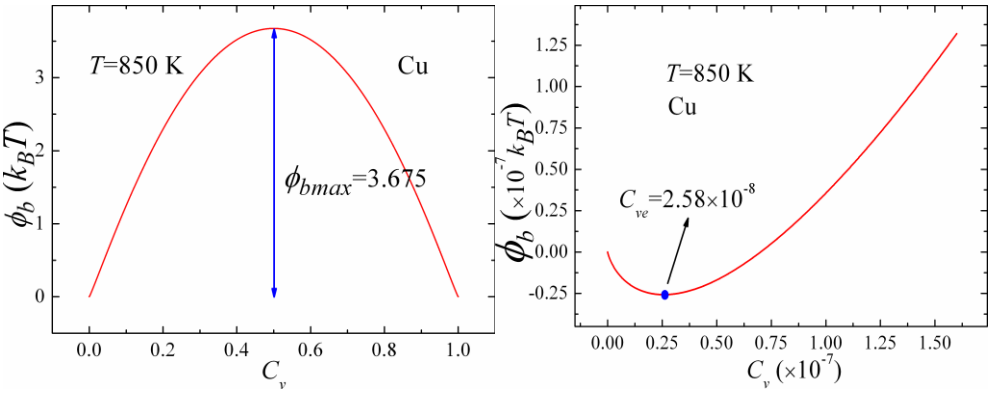

(*g*) (*h*)

Fig. 4.1. The curves of the bulk free energy, ϕ_b, for Mo at temperature 1100 K (*a*) (*b*) and 1750 K (*c*) (*d*), and for Cu at temperature 550K (*e*) (*f*) and 850K (*g*) (*h*). (*b*) (*d*) (*f*) (*h*), are the curves around the point of saturated vacancy concentration, C_{ve}, on the corresponding curves (*a*) (*c*) (*e*) (*g*), respectively. ϕ_{bmax} is the height of the energy barrier between two minima in the bulk free energy, ϕ_b.

The increase of temperature decreases the free energy barrier ϕ_{bmax} and

increases the saturated vacancy concentration. From Fig. 4.1, we can find that the maxima of bulk free energy for molybdenum are 7.2 k_BT and 4.3 k_BT at temperatures 1100 K and 1750 K, and for copper are 6.1 k_BT and 3.7 k_BT at temperatures 550 K and 850 K, respectively.

4.4 The bulk chemical potential and uphill diffusion

In order to be consistent with equation (3.30) used in the SBA, the flux per unit area in the PFM is rewritten as follows:

$$\begin{aligned}\mathbf{J}(\mathbf{r},t) &= -M\left(C_v\right)\nabla\frac{\delta F\left(C_v\right)}{\delta C_v}\\ &= -\frac{M\left(C_v\right)}{\Omega}\nabla\mu\left(C_v\right)\\ &= -\frac{M\left(C_v\right)}{\Omega}\nabla\left[\mu_b(C_v)-2\alpha\nabla^2C_v\right]\\ &= -D_e\left(C_v\right)\nabla C_v\end{aligned} \tag{4.10}$$

where

$$\mu_b\left(C_v\right)=\frac{\partial f_0\left(C_v\right)}{\partial C_v}=k_BT\frac{\partial\phi_b\left(C_v\right)}{\partial C_v}=k_BT\ln\left[\frac{C_v}{1-C_v}\right]+\left(1-2C_v\right)E_v^f \tag{4.11}$$

which is the bulk chemical potential and

$$D_e\left(C_v\right)=\frac{M\left(C_v\right)}{\Omega}\left\{\frac{\partial\mu_b\left(C_v\right)}{\partial C_v}-2\alpha\nabla^2\right\} \tag{4.12}$$

where the transport coefficient M is related to the diffusivity and is position dependent

$$M\left(C_v\right)=\frac{D}{k_BT}C_v(\mathbf{r},t)[1-C_v(\mathbf{r},t)] \tag{4.13}$$

which is the interpolation of formula (3.31). This type of formula of mobility combined with equation (4.10), can guarantee that the Cahn-Hilliard equation in the matrix is reduced to the diffusion equation (3.35) in the SBA. According to equation (4.10), the direction of vacancy flow is against the vacancy concentration gradient ∇C_v when $D_e(C_v)$ is smaller than zero. This phenomenon is called uphill diffusion. Assume that the vacancy concentration profile is of sinusoidal shape.

$$C_v=C_0+A(\mathbf{k},t)\cos(\mathbf{k}\cdot\mathbf{r}) \tag{4.14}$$

where **k** is wave vector, A(**k**,t) the amplitude, then

$$\begin{aligned}\mathbf{J}(\mathbf{r},t) &= -M\left(C_v\right)\nabla\left[\mu_b(C_v) - \frac{2\alpha}{\Omega}\nabla^2 C_v\right] \\ &= -\frac{M\left(C_v\right)}{\Omega}\nabla\left[k_B T\frac{\partial\phi_b\left(C_v\right)}{\partial C_v} - 2\alpha\nabla^2 C_v\right] \\ &= -\frac{k_B T M\left(C_v\right)}{\Omega}\left[\frac{\partial^2\phi_b\left(C_v\right)}{\partial C_v^2} - \frac{2\alpha}{k_B T}\nabla^2\right]\nabla C_v \\ &= -\frac{k_B T M\left(C_v\right)}{\Omega}\left[\frac{\partial^2\phi_b\left(C_v\right)}{\partial C_v^2} + \frac{2\alpha k^2}{k_B T}\right]\nabla C_v\end{aligned} \tag{4.15}$$

where, k^2 = **k** **k**. Since $M(C_v)$ is always positive, in order to make $D_e(C_v)$ smaller than zero, the following relation should be satisfied

$$\frac{\partial^2\phi_b\left(C_v\right)}{\partial C_v^2} + \frac{2\alpha k^2}{k_B T} < 0 \tag{4.16}$$

Since $0 < k < \infty$, the range of wave number k for the uphill diffusion should be determined. Substituting expression (4.11) into equation (4.16) gets

$$k^2 < -\frac{k_B T}{2\alpha}\frac{\partial^2\phi_b\left(C_v\right)}{\partial C_v^2} = -\frac{k_B T}{2\alpha}\left[\frac{1}{C_v\left(1-C_v\right)} - \frac{2E_v^f}{k_B T}\right] \le \frac{E_v^f - 2k_B T}{\alpha} \tag{4.17}$$

Thus, the range for the up-hill diffusion to occur is

$$0 < k < k_c \tag{4.18}$$

where

$$k_c = \sqrt{\frac{E_v^f - 2k_B T}{\alpha}} \tag{4.19}$$

This is the largest wave number for up-hill diffusion to occur, and the

corresponding wave length is

$$\lambda_c = \frac{2\pi}{k_c} = 2\pi\sqrt{\frac{\alpha}{E_v^f - 2k_BT}} \tag{4.20}$$

If the wave length of the sinusoidal of the vacancy concentration fluctuation is smaller than $2\pi\sqrt{\alpha/\left(E_v^f - 2k_BT\right)}$, no matter what its amplitude is, up-hill diffusion will not occur. For each basic wave whose wave number is smaller than k_c, there is a corresponding vacancy concentration $C_{vu}(k)$ for up-hill diffusion to occur.

$$C_{vu}\left(k\right) = \frac{1-\sqrt{1-\left[2k_BT/\left(E_v^f - \alpha k^2\right)\right]}}{2} \qquad \left(0 < k < k_c\right) \tag{4.21}$$

$C_{vu}(k)$ increases with the increase of both the temperature and wave number k. If k is close to zero, which corresponds to a long wave length, the vacancy concentration for uphill diffusion is

$$C_{vu} = \frac{1-\sqrt{1-\left(2k_BT/E_v^f\right)}}{2} \tag{4.22}$$

This means that the uphill diffusion will be more easily to occur for the vacancy concentration fluctuation in a larger area. A large fluctuation area of vacancy concentration with small amplitude can result in the decrease of the Gibbs free energy of the system and make the system unstable. In order to

realize the up-hill diffusion, the wave length should be infinite for the wave with infinitesimal amplitude. For molybdenum, $E_v^f/(k_BT)$ is about 31 at temperature 1100 K and 19.9 at temperature 1750K. κ is equal to 1nm at temperature 1100K and 0.63nm at temperature 1750K. The critical wave vector k_c is about 5.39×10^9 *rad*/*m* at temperature 1100K and 6.72×10^9 *rad*/*m* at temperature 1750 K, whose corresponding wave length λ_c is 1.166nm and 0.935 *nm*, respectively. Assuming that the vacancy concentration profile of a void is of a sinusoidal shape with $\lambda = 2R$, the value of κ^2k^2 is about 9.87 at temperature 1100 K and 3.92 at temperature 1750 K for a void with radius 1 *nm*. The corresponding critical vacancy concentration for uphill diffusion is 0.024 at temperature 1100 K and 0.032 at temperature 1750 K.

Any function of vacancy concentration profile can be expanded by using the sinusoidal basis (see equation (4.14)), which is a kind of Fourier transform.

$$C_v(\mathbf{r},t) = C_0 + \sqrt{\frac{2}{\pi}}\int_0^\infty A(\mathbf{k},t)\cos(\mathbf{k}\cdot\mathbf{r})d\mathbf{k} \tag{4.23}$$

The occurrence of up-hill diffusion does not require that the vacancy concentration profile is of a sinusoidal shape (or basic wave) whose wave

number $k < k_c$; it only requires that the Fourier expansion of vacancy concentration profile contains the basic wave with $k < k_c$. Thus, the critical vacancy concentration for spinodal decomposition to occur is equal to C_{vu} (see equation (4.22)), which can also be determined as follows

$$\frac{\partial^2 \phi_b\left(C_v\right)}{\partial C_v^2} < 0 \tag{4.24}$$

or

$$\frac{k_B T}{C_v\left(1-C_v\right)} - 2E_v^f < 0 \tag{4.25}$$

The critical value for uphill diffusion is determined by the bulk free energy. Fig. 4.2 show the curves of chemical potential and the critical vacancy concentration for uphill diffusion. The critical value for uphill diffusion for molybdenum is about 0.016 at temperature 1100 K and 0.026 at temperature 1750 K and for copper about 0.019 at temperature 550 K and 0.03 at temperature 850 K as shown in Fig. 4.2. These values are far greater than the vacancy concentration in the matrix, which guarantees that uphill diffusion will not occur in the matrix and only occur within the void-matrix interface. As such, the void formation and growth via spindoal decomposition of vacancy concentration (or uphill diffusion globally) can be avoided, to

ensure the vacancy diffusion in the matrix is the same as that obtained with SBA. The chemical potentials at critical vacancy concentration are 26.51 k_BT (1100 K) and 15.23 k_BT (1750 K) for molybdenum and 22.03 k_BT (550 K) and 12.95 k_BT (850 K) for copper.

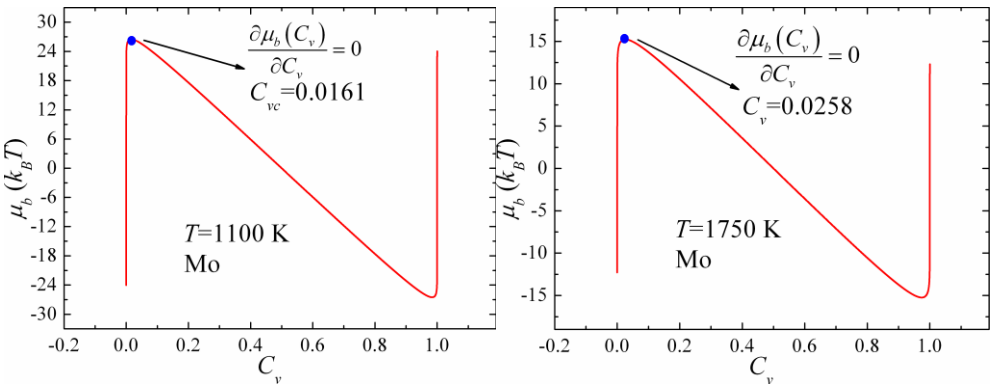

(*a*)

(*b*)

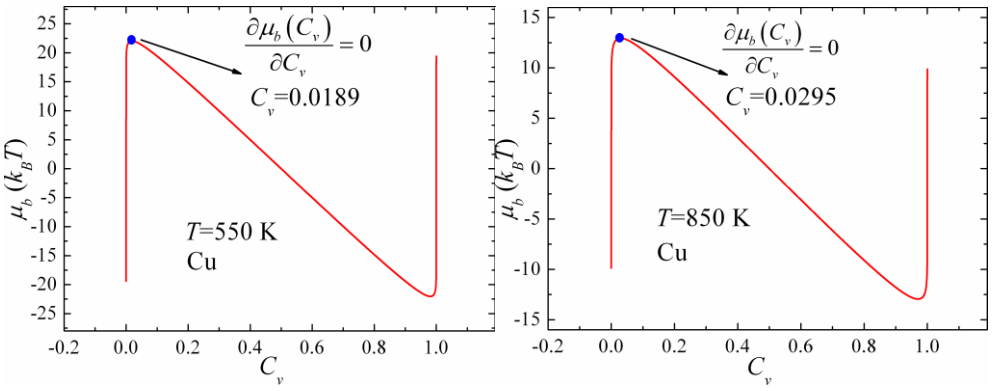

(*c*)

(*d*)

Fig. 4.2. Profile of chemical potential of molybdenum at temperatures 1100 K (*a*) and 1750 K (*b*) and of copper at temperatures 550 K (*c*) and 850 K (*d*). The blue

point on each curve corresponds to the critical point for uphill diffusion, and corresponding vacancy concentration, C_v, beside the blue point is the critical vacancy concentration for uphill diffusion.

4.5 The interfacial energy and gradient energy coefficient

In the phase field model the width of interface is finite. This finite interface thickness and the interfacial energy originate from finite correlation lengths on a microscopic scale. This interfacial energy is characterized by the surface tension in the case of the SBA. In order for the phase-field model to reproduce the void evolution in the SBA, the relation between the interfacial energy used in the PFM and the surface tension should be built. One can expect that the interface thickness and interfacial energy are proportional to surface tension. In this section, the interfacial energy and gradient energy coefficient will be studied.

The interfacial energy consists of two types of free energy within the interface: the bulk free energy and the gradient energy. The interface width is dictated by the competition between the chemical potential due to the gradient energy and that due to the bulk free energy which produce opposite

effects in determining the width. The bigger gradient energy coefficient will make the interface width larger. The wider, or the more diffuse, of the interfacial region, the smaller the contribution of the gradient energy will be. However, for wider interfaces, there are more materials, within which the phase-field variables are of non-equilibrium values, are introduced into the interfacial regions. These materials in non-equilibrium states will make the contribution of bulk free energy to the interfacial energy larger. Thus, larger values of the gradient energy coefficient result in more diffuse interfaces, whereas the larger bulk free energy (or height of barrier between the two wells in the bulk free energy function) result in sharper interfaces [12].

The interfacial energy in the PFM is written as follows:

$$\begin{aligned}\Delta F &= F\left(C_v\right) - F\left(C_{veR}\right) \\ &= \frac{1}{\Omega}\int_V \left\{ f_0\left(C_v\right) - f_0\left(C_{veR}\right) + \alpha\left(\nabla C_v\right)^2 \right\} d^3r \\ &= \frac{k_B T}{\Omega}\int_V \left\{ \phi_b\left(C_v\right) - \phi_b\left(C_{veR}\right) + \kappa^2\left(\nabla C_v\right)^2 \right\} d^3r\end{aligned} \tag{4.26}$$

The chemical potential formula (4.6) can be rewritten as follows:

$$\begin{aligned}\frac{\mu(\mathbf{r},t)}{k_BT} &= \frac{\Omega}{k_BT}\frac{\delta F(C_v)}{\delta C_v} \\ &= \frac{1}{k_BT}\left[\frac{\partial f_0(C_v)}{\partial C_v} - 2\alpha\nabla^2 C_v\right] \\ &= \frac{\partial \phi(C_v)}{\partial C_v} - 2\kappa^2\nabla^2 C_v \\ &= \ln\frac{C_v}{1-C_v} + \frac{E^f}{k_BT}(1-2C_v) - 2\kappa^2\nabla^2 C_v\end{aligned} \tag{4.27}$$

where $\alpha = \kappa^2 k_B T$, and κ-coefficient is of a unit length which characterizes an "interaction length" of vacancies. At equilibrium state, the chemical potential should be constant throughout the system.

$$\frac{\mu(C_v)}{k_BT} = \frac{\partial \phi(C_v)}{\partial C_v} - 2\kappa^2\nabla^2 C_v = const \tag{4.28}$$

This can also be derived as in Appendix D. According to the boundary conditions, $C_v = C_b = C_{veR}$ at $r \to \infty$. The chemical potential in the PFM is equal to that in the SBA. i.e., $\mu(C_v)/k_BT = \ln(C_{veR}/C_{ve})$. Therefore, in the equilibrium state, we have

$$\frac{\partial \phi_b(C_v)}{\partial C_v} - 2\kappa^2\nabla^2 C_v = \ln(C_{veR}/C_{ve}) \tag{4.29}$$

The gradient energy coefficient is the key point for the gradient energy. It will be derived and discussed in the following sections for the flat surface case and the curved surface case. The derivation of κ-coefficient follows the work by A. A. Semenov and C. H. Woo [24], under the assumptions that the

width of interface is small, κ is size independent, and the system is in the equilibrium state.

4.5.1 Flat interface

For a flat interface between the void and matrix, $C_{veR} = C_{ve}$ in equilibrium state. Equation (4.28) becomes one dimensional and

$$\frac{\partial \phi_b(C_v)}{\partial C_v} - 2\kappa^2 \frac{\partial^2 C_v}{\partial x^2} = 0 \tag{4.30}$$

Multiplying both side of equation (4.30) by dC_v/dx and integrating it with respect to x which is the spatial coordinates, then produces

$$\phi_b(C_v) - \kappa^2 \left(\frac{\partial C_v}{\partial x}\right)^2 = const \tag{4.31}$$

At a position far from the flat interface $x \to \infty$, dC_v/dx equals zero and $\phi_b(C_{ve})$ $\approx -C_{ve}$. Thus the constant is equal to $-C_{ve}$. The above equation becomes

$$\phi_b(C_v) + C_{ve} = \kappa^2 \left(\frac{\partial C_v}{\partial x}\right)^2 \tag{4.32}$$

Equation (3.30) indicates that, for a flat interface case, the chemical potential due to bulk free energy is offset it due to gradient energy in the equilibrium

state. From equation (4.32) we can find that the bulk free energy is equal to the gradient energy. Both of the bulk free energy and the gradient energy are half of the interfacial energy. Substituting equation (4.32) into equation (4.26) gets us

$$\begin{aligned}\Delta F &= F\left(C_v\right) - F\left(C_{ve}\right) \\ &= 2\frac{Sk_BT}{\Omega}\int_{-\infty}^{+\infty}\left[\phi_b\left(C_v\right) + C_{ve}\right]dx\end{aligned} \tag{4.33}$$

Where S is the interface area, $\Delta F/S = \gamma_s$. Combing equations (4.32) and (4.33), we have

$$\gamma_s = 2\frac{k_BT}{\Omega}\int_{C_{ve}}^{1}\left\{\kappa\left[\phi_b\left(C_v\right) + C_{ve}\right]\right\}^{\frac{1}{2}}dC_v \tag{4.34}$$

Assuming κ is independent of the vacancy concentration, one can get the expression of κ from equation (4.34).

$$\kappa = \frac{\gamma_s\Omega}{2k_BT}I_s \tag{4.35}$$

where $I_s = 1/I_1$ and

$$I_1 \approx \int_{C_{ve}}^{1-C_{ve}}\left[\phi_b(C_v) + C_{ve}\right]^{\frac{1}{2}}dC_v \tag{4.36}$$

Considering the specific expression of ϕ_b (see equation (4.9)), κ decreases with increasing of temperature.

At equilibrium state the interface width is given by

$$\Delta l \approx \int_{C_{ve}}^{1-C_{ve}} \frac{\kappa}{\left[\phi_b(C_v) + C_{ve}\right]^{\frac{1}{2}}} dC_v \tag{4.37}$$

which is derived from equation (4.32). From the above, one can see that a larger κ makes the interface wider and a higher bulk free energy across the interface makes the interface narrower. Equation (4.37) is approximately related to the maximum of reduced bulk free energy per lattice site $\phi_{b\max}$,

$$\Delta l \approx \kappa \left(\phi_{b\max}\right)^{-\frac{1}{2}} \tag{4.38}$$

(See Appendix E for the proof). The larger the maximum of bulk free energy is, the better the approximation of equation (4.38) will be. Due to the formula used in this thesis, it can be further expressed as follows:

$$\Delta l \approx \kappa \left(\phi_{b\max}\right)^{-\frac{1}{2}} = \kappa \left(\frac{E^f}{4k_B T} - \ln 2 \right)^{-\frac{1}{2}} \tag{4.39}$$

Since $\phi_{b\max}$ decreases with temperature increase, Δl increases with temperature increase. Based on equation (4.39), the width of interface is about 3.1Å at 1100K and 3.7Å at 1750K. Thus the grid size should be smaller than this width which imposes a strong constraint on the simulation size of system and on the time step size as well.

4.5.2 Curved interface

For simplicity, assume that the void is of spherical symmetry. The schematic geometric illustration model is shown in Fig. 3.3. In spherical coordinates, equation (4.29) is rewritten as follows:

$$\frac{\partial \phi_b(C_v)}{\partial C_v} - 2\kappa^2 \frac{1}{r^2}\frac{d}{dr}\left(r^2 \frac{dC_v}{dr}\right) = \ln\left(C_{veR}/C_{ve}\right) \tag{4.40}$$

Multiplying both side of equation (4.40) by dC_v/dr and integrating it with respect to r in spherical coordinates produces

$$\kappa^2\left(\frac{dC_v}{dr}\right)^2 - \phi(C_v) + C_v \ln\left(C_{veR}/C_{ve}\right) = -\int \frac{4\kappa^2}{r}\left(\frac{dC_v}{dr}\right)^2 dr \tag{4.41}$$

This can also be written as follows:

$$\frac{d}{dr}\left[\phi(C_v) - C_v \ln\left(C_{veR}/C_{ve}\right) - \kappa^2\left(\frac{dC_v}{dr}\right)^2\right] = \frac{4\kappa^2}{r}\left(\frac{dC_v}{dr}\right)^2 \tag{4.42}$$

For boundary conditions $C_v(r = 0) = 1$ and $C_v(r\to\infty) = C_{veR}$, then

$$\begin{aligned}\int_0^\infty \frac{4\kappa^2}{r}\left(\frac{dC_v}{dr}\right)^2 dr &= \phi(C_{veR}) + C_{veR}\ln\left(C_{veR}/C_{ve}\right) - \phi(1-C_{ve}) + \ln\left(C_{veR}/C_{ve}\right) \\ &= \ln\left(C_{veR}/C_{ve}\right)\end{aligned} \tag{4.43}$$

According to the SBA, the formation energy of a void with critical radius R_c is

$$\begin{aligned}\Delta F &= m\left[\mu_v'\left(P,T\right)-\mu_v\left(P,T\right)\right]+\gamma_s A \\ &= -\frac{4\pi R_c^3 k_B T}{3\Omega}\ln\frac{C_{veR}}{C_{ve}}+\gamma_s 4\pi R_c^2 \\ &= \gamma_s\frac{4\pi R_c^2}{3}\end{aligned} \tag{4.44}$$

The free energy change due to the formation of a void with critical radius, R_c, is

$$\Delta F = \frac{k_B T}{\Omega}\int_V\left[\phi\left(C_v\right)-\phi\left(C_{veR}\right)+\kappa^2\left(\nabla C_v\right)^2\right]dV \tag{4.45}$$

In order to obtain the gradient energy coefficient, κ, assume there is a perturbation of vacancy concentration

$$\delta C_v(\mathbf{r}) = C_v(\mathbf{r}) - C_v^0 \tag{4.46}$$

which is small $\left(\left|\delta C_v(\mathbf{r})\right| << C_v^0\right)$ everywhere, except in a small but finite volume $\delta V << V$, and satisfies the conservation condition, i.e.,

$$\int_V \delta C_v(\mathbf{r})dV = \int_{V-\delta V}\delta C_v(\mathbf{r})dV + \int_{\delta V}\delta C_v(\mathbf{r})dV = 0 \tag{4.47}$$

And assume

$$\delta V = \frac{4\pi R_c^3}{3} = \int_0^{R_{ph}} C_v(r)4\pi r^2 dr \tag{4.48}$$

and

$$V = \frac{4\pi R_{sd}^3}{3} \rightarrow R_{sd} = \left(\frac{3V}{4\pi}\right)^{\frac{1}{3}} \tag{4.49}$$

R_c is the radius of the void in the SBA model, R_{ph} the radius of the void defined in the phase-field method and R_{sd} the radius of the domain of the system. The relation between these radii is $R_c < R_{ph} << R_{sd} < \infty$.

The formation energy of a void with critical radius in the PFM can be rewritten as follows:

$$\begin{aligned}
\Delta F &= \frac{k_B T}{\Omega}\int_V \left\{\left[\phi(C_v) - C_v \ln\left(C_{veR}/C_{ve}\right) + \kappa^2(\nabla C_v)^2\right] + \left[C_v \ln\left(C_{veR}/C_{ve}\right) - \phi(C_{veR})\right]\right\} dV \\
&= \frac{k_B T}{\Omega}\int_V \left\{\left[\phi(C_v) - C_v \ln\left(C_{veR}/C_{ve}\right) + \kappa^2(\nabla C_v)^2\right] + \left[\delta C_v \ln\left(C_{veR}/C_{ve}\right) + C_{veR}\right]\right\} dV \\
&= \frac{k_B T}{\Omega}\int_V \left[\phi(C_v) - C_v \ln\left(C_{veR}/C_{ve}\right) + \kappa^2(\nabla C_v)^2 + C_{veR}\right] dV \\
&= \frac{k_B T}{\Omega}\int_0^{R_{sd}} \left[\phi\left(C_v\right) - C_v \ln\left(C_{veR}/C_{ve}\right) + \kappa^2\left(\frac{dC_v}{dr}\right)^2 + C_{veR}\right] 4\pi r^2 dr
\end{aligned} \tag{4.50}$$

Multiplying both sides of equation (4.42) by $4\pi r^3/3$ and integrating it with respect to r gets us

$$\frac{4\pi}{3}\int_0^{R_{sd}} r^3 d\left[\phi\left(C_v\right) - C_v \ln\left(C_{veR}/C_{ve}\right) - \kappa^2\left(\frac{dC_v}{dr}\right)^2\right] = \frac{16\pi\kappa^2}{3}\int_0^{R_{sd}} \left(\frac{dC_v}{dr}\right)^2 r^2 dr$$

$\rightarrow$

$$\frac{4\pi}{3}\left\{r^3\left[\phi(C_v)-C_v\ln(C_{veR}/C_{ve})-\kappa^2\left(\frac{dC_v}{dr}\right)^2\right]\right\}_0^{R_{sd}}$$
$$=4\pi\int_0^{R_{sd}}\left[\phi(C_v)-C_v\ln(C_{veR}/C_{ve})+\frac{\kappa^2}{3}\left(\frac{dC_v}{dr}\right)^2\right]r^2dr$$

$\rightarrow$

$$\frac{4\pi}{3}\left\{r^3\left[\phi(C_v)-C_v\ln(C_{veR}/C_{ve})-\kappa^2\left(\frac{dC_v}{dr}\right)^2\right]\right\}_0^{R_{sd}}+4\pi\int_0^{R_{sd}}\frac{2\kappa^2}{3}\left(\frac{dC_v}{dr}\right)^2r^2dr$$
$$=4\pi\int_0^{R_{sd}}\left[\phi(C_v)-C_v\ln(C_{veR}/C_{ve})+\kappa^2\left(\frac{dC_v}{dr}\right)^2\right]r^2dr$$

$\rightarrow$

$$\int_0^{R_{sd}}\left[\phi(C_v)-C_v\ln(C_{veR}/C_{ve})+\kappa^2\left(\frac{dC_v}{dr}\right)^2+C_{veR}\right]4\pi r^2dr=\int_0^{R_{sd}}\frac{2\kappa^2}{3}\left(\frac{dC_v}{dr}\right)^2 4\pi r^2dr \quad (4.51)$$

Combining equation (4.50) and (4.51) produces

$$\Delta F=\frac{k_BT}{\Omega}\int_0^{R_{sd}}\frac{2\kappa^2}{3}\left(\frac{dC_v}{dr}\right)^2 4\pi r^2dr \quad (4.52)$$

Expression (4.52) indicates that the gradient energy is 1.5 times of the formation energy of void. In fact, we also can derive an expression for ΔF without the need to use the gradient energy term by employing the same derivation process as above.

$$\Delta F = 2\frac{k_B T}{\Omega}\int_0^{R_{sd}} \left[C_v \ln\left(C_{veR}/C_{ve}\right) - \phi\left(C_v\right) - C_{veR}\right] 4\pi r^2 dr \qquad (4.53)$$

Equating ΔF in equations (4.44) and (4.52), one can get

$$\gamma_s \frac{4\pi R_c^2}{3} = \frac{k_B T}{\Omega}\int_0^{R_{sd}} \frac{2\kappa^2}{3}\left(\frac{dC_v}{dr}\right)^2 4\pi r^2 dr \qquad (4.54)$$

Obtaining the gradient energy coefficient results in

$$\kappa^2 = \frac{\gamma_s \Omega}{2k_B T}\frac{4\pi R_c^2}{\int_0^{R_{sd}} \left(dC_v/dr\right)^2 4\pi r^2 dr} \qquad (4.55)$$

Equating ΔF in equations (4.44) and (4.53), one can get the value of the integral in equation (4.53):

$$\int_0^{R_{sd}} \left[C_v \ln\left(C_{veR}/C_{ve}\right) - \phi\left(C_v\right) - C_{veR}\right] 4\pi r^2 dr = \frac{\gamma_s \Omega}{2k_B T}\frac{4\pi R_c^2}{3} \qquad (4.56)$$

The value of the integral on the left hand side of equation (4.56) should be positive and increase with R_c^2, not R_c^3. From equation (4.56) and (3.24), one can find that, in the equilibrium state, the right hand side of equation (4.56) is half of the formation energy of a void in the case of the SBA. Since in the equilibrium state, the chemical potential in the void is the same as it in the matrix, the left hand side of equation (4.56) is the bulk free energy due to the introduction of non-equilibrium material (vacancies) into the interfacial

region. Thus the bulk free energy due to the introduction of non-equilibrium material (vacancies) into the interfacial region is half of the formation energy of the void. This is total different from the case of flat surface, in which the gradient energy is equal to the bulk free energy of the non-equilibrium vacancies within the interface region and both of them are half of the interfacial energy. The reason of this phenomenon is following: In the flat surface case, the chemical potential in the matrix is zero, while in the curved surface case, the chemical potential in the matrix is not equal to zero, which is inversely proportional to the void radius, because of the curved surface present. Thus the differences between the chemical potential of vacancies in the interfacial region and that in the matrix region are different for the flat surface case and the curved surface case.

Since the vacancy concentration variation is mainly within the interface, equation (4.55) can be simplified to the following equation by assuming $r = R_c$.

$$\kappa^2 \approx \frac{\gamma_s \Omega}{2k_B T} \frac{1}{\int_0^{R_{sd}} \left(dC_v / dr \right)^2 dr} \tag{4.57}$$

In fact, one also can obtain the above expression through equation (4.43) by assuming $r = R_c$. Equation (4.43) can be simplified as follows:

$$\int_0^{R_{sd}} \frac{4\kappa^2}{r}\left(\frac{dC_v}{dr}\right)^2 dr \approx \frac{4\kappa^2}{R_c}\int_0^{R_{sd}}\left(\frac{dC_v}{dr}\right)^2 dr = \ln\left(C_{veR}/C_{ve}\right) = \frac{2\gamma_s\Omega}{k_B T R_c} \quad (4.58)$$

This indicates that the above derivation process of the gradient energy coefficient is correct. Equation (4.54) can reproduce the expression of the gradient energy coefficient for a flat surface (formula (4.35)) by using equation (4.57) as follows:

$$\begin{aligned}\kappa &= \frac{\gamma_s\Omega}{2k_B T}\frac{1}{\kappa\int_0^{R_{sd}}\left(\frac{dC_v}{dr}\right)^2 dr} = \frac{\gamma_s\Omega}{2k_B T}\frac{1}{\kappa\int_{C_{ve}}^{1}\left(\frac{dC_v}{dr}\right)dC_v} \\ &= \frac{\gamma_s\Omega}{2k_B T}\frac{1}{\int_{C_{ve}}^{1}\left[\phi_b\left(C_v\right)+C_{ve}\right]^{\frac{1}{2}}dC_v}\end{aligned} \quad (4.59)$$

In the case of flat surface in equilibrium state, in terms of the specific expression of bulk free energy used, for $\nabla^2 C_v = 0$ the equation (4.28) becomes

$$\frac{\partial\phi_b\left(C_v\right)}{\partial C_v} = \frac{\mu_b}{k_B T} = \ln\frac{C_v}{1-C_v} + \left(1-2C_v\right)\frac{E_v^f}{k_B T} = 0 \quad (4.60)$$

The solutions for equation (4.60) are $C_v = C_{ve}$, 0.5 and $1 - C_{ve}$, as shown in Fig. 4.3. $C_v = C_{ve}$ and $1 - C_{ve}$ are in the matrix and void, respectively; only when $C_v = 0.5$ is it within the interface.

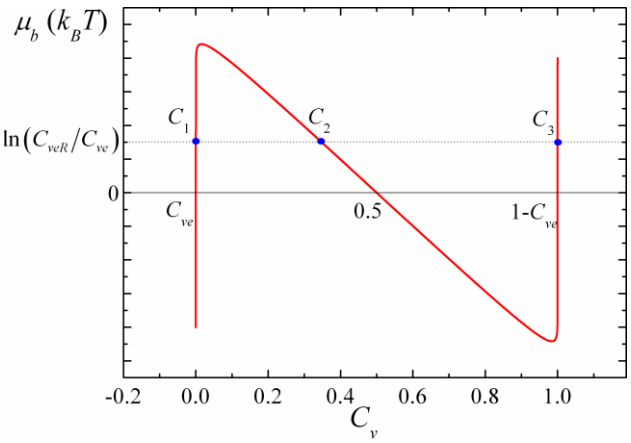

Fig. 4.3. The vacancy concentration for the position at which $\nabla^2 C_v=0$ in equilibrium state. μ_b is the chemical potential of vacancies due to bulk free energy. $\ln(C_{veR}/C_{ve})$ is the chemical potential of vacancies in a system with a void with radius R in equilibrium state. C_1, C_2 and C_3 are three equilibrium vacancy concentrations, and their positions are within the matrix, interface region and void, respectively.

For a spherical void case, the corresponding three equilibrium vacancy concentrations: C_{ve}, 0.5 and $1 - C_{ve}$ are no longer valid. The corresponding three equilibrium vacancy concentrations for a spherical void in equilibrium with the system will be discussed below. From equation (4.29) one can get

$$\frac{\partial \phi_b(C_v)}{\partial C_v} = \frac{\mu_b}{k_B T} = \ln\frac{C_v}{1-C_v} + (1-2C_v)\frac{E_v^f}{k_B T} = \ln(C_{veR}/C_{ve}) \qquad (4.61)$$

The corresponding three solutions for equation (4.61) are C_1, C_2 and C_3 (see Fig. 4.3). It is obvious that $C_1 = C_{veR}$ and $C_3 = 1 - C_{veR}$. The slope of the chemical potential curve in Fig. 4.3 is

$$\frac{1}{k_B T}\frac{\partial \mu_b}{\partial C_v} = \frac{1}{C_v\left(1-C_v\right)} - 2\frac{E_v^f}{k_B T} \tag{4.62}$$

Since the term $1/[C_v(1–C_v)]$ around C_v = 0.5 is far smaller than the term E_v^f/k_BT, whose value is about 62 at temperature 1100 K, the slope around C_v = 0.5 within a big range is almost constant, as shown in Fig. 4.3.

$$\left.\frac{1}{k_B T}\frac{\partial \mu_b}{\partial C_v}\right|_{C_v=0.5} = 4 - 2\frac{E_v^f}{k_B T} \tag{4.63}$$

And

$$\left.\frac{1}{k_B T}\frac{\partial \mu_b}{\partial C_v}\right|_{C_v=0.5} \approx \frac{0-\ln\left(C_{veR}/C_{ve}\right)}{0.5-C_2} \tag{4.64}$$

Combining equations (4.63) and (4.64), one gets

$$C_2 \approx 0.5 - \frac{\gamma_s \Omega / k_B T}{R_c\left(E_v^f / k_B T - 2\right)} \tag{4.65}$$

From the above equation it is obvious that the value of C_2 increases with the void radius and decreases with the increase of temperature. But the effect of temperature on C_2 is not as significant as that of the void radius. When the critical void radius approaches infinity, C_2 is close to 0.5, which reproduces the results of the flat surface case. For any void with finite radius, C_2 should be smaller than 0.5. At temperature 1100 K, the term $\gamma_s\Omega/k_BT$ is about 1 *nm*

and the term E_v^f/k_BT is about 31. For a void with a critical radius R_c=1 *nm*, C_2 is about 0.466. For a void with a critical radius R_c = 0.3 *nm* which only contains several vacancies, C_2 is about 0.385. Thus, the deviation of C_2 from 0.5 is very small for those voids which are not very tiny.

At the point C_v = 0.5, according to equation (4.40), one can get following relations:

$$\nabla^2 C_v\Big|_{C_v=0.5} = \frac{1}{r^2}\frac{d}{dr}\left(r^2\frac{dC_v}{dr}\right)\Bigg|_{C_v=0.5} = -\frac{\ln\left(C_{veR}/C_{ve}\right)}{2\kappa^2} \tag{4.66}$$

since $\ln(C_{veR}/C_{ve})$ is always bigger than zero

$$\nabla^2 C_v\Big|_{C_v=C_2} = \frac{1}{r^2}\frac{d}{dr}\left(r^2\frac{dC_v}{dr}\right)\Bigg|_{C_v=C_2} = 0 \tag{4.67}$$

Thus, within the interface, $\nabla^2 C_v < 0$ wherever $C_v > C_2$, and $\nabla^2 C_v > 0$ wherever $C_v < C_2$. This means that the vacancy concentration profile within the interface is convex wherever $C_v > C_2$ and is concave wherever $C_v < C_2$. Therefore, the place where $C_v = C_2$ is the inflection point, as shown in Fig. 4.4. The vacancy concentration at the inflection point decreases with a decrease in the critical radius of the void.

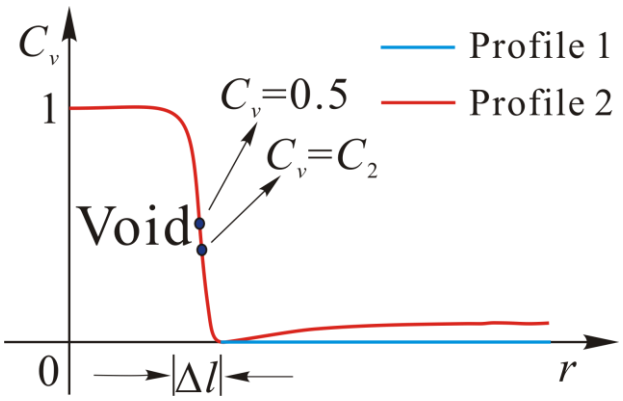

Fig. 4.4. a schematic illustration of vacancy concentration profile in spherical coordinates. Δl is the width of the interface, and C_2 is the vacancy concentration whose position is at R_2 which is an inflection point. Profile 1 corresponds to an equilibrium state, and profile 2 corresponds to a growth state.

Profile 1 in Fig. 4.4 corresponds to a void in equilibrium state; profile 2 corresponds to a void in growth state. The above analysis is useful for the following derivation for the gradient energy coefficient. Expanding $C_v(r)$ in the Taylor series around the point C_v = 0.5 on the vacancy concentration profile, we can get

$$C_v(r) = C_v(R_m) + (r - R_m)\left.\frac{dC_v}{dr}\right|_{r=R_m} + (r - R_m)^2 \left.\frac{d^2C_v}{dr^2}\right|_{r=R_m} \tag{4.68}$$

where R_m is the position of the point C_v = 0.5. Thus, the vacancy concentration at the point $C_v = C_2$ is

$$C_2 = C_v\left(R_2\right) = C_v\left(R_m\right) + \left(R_2 - R_m\right)\left.\frac{dC_v}{dr}\right|_{r=R_m} + \left(R_2 - R_m\right)^2 \left.\frac{d^2C_v}{dr^2}\right|_{r=R_m} \quad (4.69)$$

where R_2 is the position of the point C_v = C_2. Equation (4.66) can be rewritten as follows

$$\left.\frac{1}{r^2}\frac{d}{dr}\left(r^2\frac{dC_v}{dr}\right)\right|_{C_v=0.5} = \left.\frac{2}{R_m}\frac{dC_v}{dr}\right|_{r=R_m} + \left.\frac{d^2C_v}{dr^2}\right|_{r=R_m} = -\frac{\gamma_s\Omega}{\kappa^2 R_c k_B T} \quad (4.70)$$

Assuming $R_m \approx R_c$ is appropriate because R_m is almost at the middle of the interface. Combing equations (4.65), (4.69) and (4.70), we can get

$$\left.\frac{dC_v}{dr}\right|_{r=R_m} = -\frac{\gamma_s\Omega}{k_B T}\frac{\frac{1}{E_v^f/k_BT-2} - \frac{\Delta R^2}{2\kappa^2}}{\Delta R\left(R_c - \Delta R\right)} \quad (4.71)$$

$$\left.\frac{d^2C_v}{dr^2}\right|_{r=R_m} = -\frac{\gamma_s\Omega}{\kappa^2 R_c k_B T} + \frac{2\gamma_s\Omega}{k_B T R_c}\frac{\frac{1}{E_v^f/k_BT-2} - \frac{\Delta R^2}{2\kappa^2}}{\Delta R\left(R_c - \Delta R\right)} \quad (4.72)$$

where $\Delta R = R_2 - R_m$. From equation (4.65) we also can get the gradient of vacancy concentration at the point C_v = 0.5, which is written as follows:

$$\left.\frac{dC_v}{dr}\right|_{r=R_m} \approx \frac{C_2 - 0.5}{\Delta R} = \frac{-\gamma_s\Omega/k_BT}{R_c\left(E_v^f/k_BT - 2\right)\Delta R} \quad (4.73)$$

Since the terms $\gamma_s\Omega/k_BT$, ΔR and $E_v^f/k_BT - 2$ are positive, the slope dC_v/dr at the point $r = R_m$ where C_v = 0.5 is negative. In fact, the vacancy concentration gradient is always negative within the interface because the spherical coordinates are used and the vacancy concentrations in the void are

bigger than those in the matrix.

Equating equations (4.71) and (4.73) gets us

$$\kappa^2 = \frac{1}{2}\Delta R R_c \left(E_v^f / k_B T - 2 \right) \tag{4.74}$$

And substituting equation (4.74) into (4.72) gets us

$$\left. \frac{d^2 C_v}{dr^2} \right|_{r=R_m} = 0 \tag{4.75}$$

In fact, this result is also simply implied by equation (4.70). The first term on the left hand side and the term on the right hand side of equation (4.70) are inversely proportional to R_c, which means the value of the second term on the left hand side is far smaller than for the other two terms. Therefore, the second term is negligible and approach to zero. From above results we can find that κ^2 is proportional to ΔR which is the distance between two points at which both $(1/r^2)\mathrm{d}(r^2 dC_v/dr)/dr$ and d^2C_v/dr^2 are zero.

Assuming that the width of interface is Δl and the vacancy concentration gradient within the interface is a constant which is equal to the slope at the point $C_v = 0.5$ as Fig 4.5 shown, the slope at R_m can be expressed in terms of Δl, as follows:

$$\left.\frac{dC_v}{dr}\right|_{C_v=0.5} \approx \frac{C_{veR}-1}{\Delta l} \approx \frac{-1}{\Delta l} \tag{4.76}$$

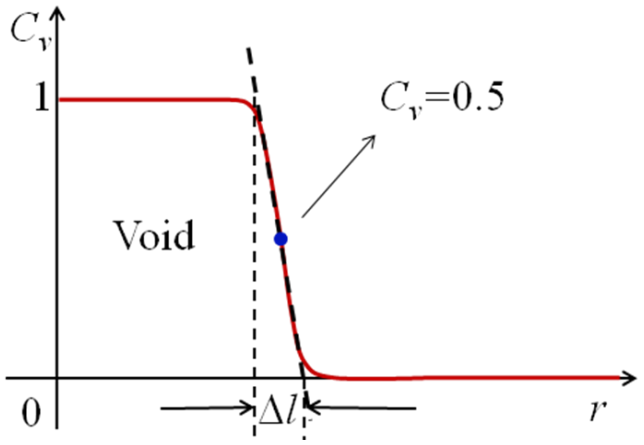

Fig. 4.5. the approximation of slope of vacancy concentration profile in the interfacial region by the value of the slope at the point where vacancy concentration is equal to 0.5. Δl is the width of the interface.

Equating equations (4.73) and (4.76) produces the value of ΔR.

$$\Delta R = \frac{\Delta l \gamma_s \Omega / k_B T}{R_c \left(E_v^f / k_B T - 2 \right)} \tag{4.77}$$

ΔR is inversely proportional to the critical void radius and increases with temperature. At temperature 1100 K, $\gamma_s\Omega/k_BT$ is about 2 *nm*, and E_v^f/k_BT is 31. For a void with a critical radius 2 *nm* and an interface width assumed to be 0.4 *nm*, ΔR is about 0.014 *nm*, which indicates that the distance between the

two points at C_v = 0.5 and C_v = C_2 on the vacancy concentration profile is very tiny.

Under the conditions used in the derivation of equation (4.76) and according to equation (4.55), κ^2 can also be expressed as follows:

$$\kappa^2 \approx \frac{\gamma_s \Omega}{2k_B T} \frac{4\pi R_c^2}{\left(dC_v/dr\right)^2 4\pi R^2 \Delta l} = \frac{\gamma_s \Omega}{2k_B T} \Delta l \tag{4.78}$$

It also can be directly attained by substituting equation (4.77) into (4.74). Equation (4.78) indicates the relation between the κ-coefficient and the interface thickness. In order to determine the value of the gradient energy coefficient, the interface width should be known. The exact determination of interface width Δl is very difficult; here we will use the interface width obtained in the flat surface case to approximate it, which is hold for large void. Substituting expression (4.37) into equation (4.78), one gets

$$\kappa = \frac{\gamma_s \Omega}{2k_B T} I_2 \tag{4.79}$$

where

$$I_2 = \int_{C_{veR}}^{1-C_{veR}} \frac{1}{\left[\phi_b(C_v) + C_{ve}\right]^{\frac{1}{2}}} dC_v \tag{4.80}$$

It should be noted that I_2 is different from I_s in the equation (3.34). κ is

approximately inversely proportional to *T*.

4.6 The Cahn-Hilliard equation

According to the conservation law of mass and the equation (4.10), the Cahn-Hilliard equation is usually written as follows [10]:

$$\frac{\partial C_v}{\partial t} = \Omega\nabla\cdot\mathbf{J}_v = \Omega\nabla\cdot\left[M\nabla\frac{\delta F\left(C_v\right)}{\delta C_v}\right] \tag{4.81}$$

Considering the free energy functional we construct, equation (4.81) can be further rewritten as follows:

$$\begin{aligned}\frac{\partial C_v(\mathbf{r},t)}{\partial t} &= \nabla\cdot\left\{M(\mathbf{r},t)\nabla\left[\mu_b(\mathbf{r},t)-2\kappa^2 k_B T\nabla^2 C_v(\mathbf{r},t)\right]\right\}\\ &= \nabla\cdot\left\{DC_v(\mathbf{r},t)\left[1-C_v(\mathbf{r},t)\right]\nabla\left[\frac{\partial\phi(C_v)}{\partial C_v}-2\kappa^2\nabla^2 C_v(\mathbf{r},t)\right]\right\}\\ &= \nabla\cdot\left\{DC_v(\mathbf{r},t)\left[1-C_v(\mathbf{r},t)\right]\nabla\left[\ln\frac{C_v(\mathbf{r},t)}{1-C_v(\mathbf{r},t)}+\frac{E^f}{k_B T}\left[1-2C_v(\mathbf{r},t)\right]-2\kappa^2\nabla^2 C_v(\mathbf{r},t)\right]\right\}\end{aligned} \tag{4.82}$$

This equation can be easily modified to include a noise term and terms related to vacancy-interstitial recombination. The spontaneous process governed by the Cahn-Hilliard equation (4.82) is a free energy dissipation process (see Appendix G). Equation (4.82) can be further simplified to

$$\frac{\partial C_v(\mathbf{r},t)}{\partial t} = D\nabla\cdot\left\{\left[1-2C_v(\mathbf{r},t)\left(1-C_v(\mathbf{r},t)\right)\left(\frac{E_v^f}{k_B T}+\kappa^2\nabla^2\right)\right]\nabla C_v(\mathbf{r},t)\right\} \equiv -\nabla\cdot\mathbf{J}_v(\mathbf{r},t) \tag{4.83}$$

which is a nonlinear equation and contains a fourth order gradient term. From equation (4.83) one can easily find that the Cahn-Hilliard equation (4.82) is reduced to diffusion equation (3.35) when the vacancy concentration approaches zero. In order to benchmark the model, the evolution of a single void planted in a spherical region in the spherical coordinates will be studied by using the PFM, SBA and RT, respectively. Then, the evolution of a single void with three-dimensional Cartesian coordinates will be studied. Due to the non-linearity and variable mobility, equation (4.82) is very difficult to solve. Numerical methods are needed to solve it.

Chapter 5: The numerical method of solving phase-field equations

In numerical calculation, using reduced time step size, grid size and parameters will be convenient. τ is the normalization factor of time, l the normalization factor of length, Δt the time step size, Δr the grid size, $\Delta t'$ the reduced time step size, and $\Delta r'$ the reduced grid size. $t'=t/\tau$, $r'=r/l$, $\Delta t'=\Delta t/\tau$, $\Delta r'=\Delta r/l$, $\kappa'=\kappa/l$, $D'=D\tau/l^2$, $M'=D'k_BTC_v(1-C_v)$. In the simulations, Δt is equal to τ and Δr is equal to l.

5.1 Spherical coordinates

In spherical coordinates, equation (4.82) is written as

$$\frac{\partial C_v(r,t)}{\partial t}=\frac{\partial}{r^2\partial r}\left\{r^2M(r,t)\frac{\partial}{\partial r}\left[\mu_b(r,t)-\frac{2\kappa^2k_BT}{r^2}\frac{\partial}{\partial r}\left(r^2\frac{\partial C_v(r,t)}{\partial r}\right)\right]\right\} \quad (5.1)$$

For reduced units, the equation is

$$\frac{\partial C_v(r',t')}{\partial t'}=\frac{\partial}{r'^2\partial r'}\left\{r'^2M'(r',t')\frac{\partial}{\partial r'}\left[\mu_b(r',t')-\frac{2\kappa'^2k_BT}{r'^2}\frac{\partial}{\partial r'}\left(r'^2\frac{\partial C_v(r',t')}{\partial r'}\right)\right]\right\} \quad (5.2)$$

A second-order 2-step explicit BDF/AB finite difference numerical scheme is used to solve this equation [102, 103]. It is a second order 2-step backward differentiation formulas method (BDF2) for the time derivative of vacancy concentration on the left hand side of equation (5.2) and a second-order 2-step Adams-Bashforth method (AB2) for the treatment of the right hand side terms of equation (5.2). A three-point central difference approximation for the treatment of the Laplace operator in space is used. This second-order scheme provides the best accuracy/cost ratio and is sufficiently accurate. The second-order 2-step BDF/AB finite difference numerical scheme for equation (5.2) is written as follows:

$$C_{vi}^{n+1} = \frac{1}{3}\left[4C_{vi}^{n} - C_{vi}^{n-1} + 2\Delta t'\left(2f_{vi}^{n} - f_{vi}^{n-1}\right)\right] \tag{5.3}$$

where

$$f_{vi}^{n} = \frac{1}{i^2\Delta r'}\left[\frac{(i+0.5)^2}{2}\left(M_{i+1}'^{n} + M_{i}'^{n}\right)\frac{\left(\mu_{i+1}^{n} - \mu_{i}^{n}\right)}{\Delta r'} - \frac{(i-0.5)^2}{2}\left(M_{i}'^{n} + M_{i-1}'^{n}\right)\frac{\left(\mu_{i}^{n} - \mu_{i-1}^{n}\right)}{\Delta r'}\right] \tag{5.4}$$

where $\mu_i^n = \mu_{bi}^{\ n} - 2k_BT\kappa'^2\nabla_r'^2 C_{vi}^{\ n}$ and $M_i'^n = D'C_{vi}^{\ n}\left(1-C_{vi}^{\ n}\right)/k_BT$. $\nabla_r'^2$ is the reduced Laplace operator in spherical coordinates. A three-point approximation for $\nabla_r'^2$ at a given time step *n* is

$$\nabla_r'^2 C_{vi}^{\ n} = \frac{1}{i^2\Delta r'}\left[(i+0.5)^2\frac{C_{vi+1}^{\ n} - C_{vi}^{\ n}}{\Delta r'} - (i-0.5)^2\frac{C_{vi}^{\ n} - C_{vi-1}^{\ n}}{\Delta r'}\right] \tag{5.5}$$

Since it is a second order finite difference method scheme in time, the value of vacancy concentration at the first time step is unknown. Here, the vacancy concentration at the first time step is obtained by the first order forward Euler method, which is written as

$$C_{vi}^{1} = C_{vi}^{0} + \Delta t' f_{vi}^{0} \tag{5.6}$$

where C_{vi}^{0} and f_{vi}^{0} are the initial values of C_{vi} and f_{vi}, respectively. In the numerical simulations, for convenience, both $\Delta t'$ and $\Delta r'$ are set equal to unity.

5.2 Cartesian coordinates

Equation (4.82) in three-dimensional Cartesian coordinates in reduced units is written as

$$\frac{\partial C_v(\mathbf{r}',t')}{\partial t'} = \nabla' \cdot \left\{ M(\mathbf{r}',t') \nabla' \left[\mu_b'(\mathbf{r}',t') - 2\kappa'^2 k_B T \nabla'^2 C_v(\mathbf{r}',t') \right] \right\} \tag{5.7}$$

Here, for solving the above equation, the second-order 2-step explicit BDF/AB finite difference numerical scheme is used as well. However, in space, due to the very small vacancy concentration in the matrix and the variation of many orders of magnitude of the vacancy concentration across

the interface, the conventional seven-point central difference approximation for the Laplace operator in three dimensions is not accurate enough. A 27-point stencil for discrete Laplacian approximations is used [104]. Other than the central point, the other 26 points are 6 points on the 6 faces, 12 points on the 12 edges and 8 points at the 8 corners. In three-dimensional Cartesian coordinates, the equation (5.3) is rewritten as follows:

$$C_{v(i,j,k)}^{n+1} = \frac{1}{3}\left[4C_{v(i,j,k)}^{n} - C_{v(i,j,k)}^{n-1} + 2\Delta t'\left(2f_{v(i,j,k)}^{n} - f_{v(i,j,k)}^{n-1}\right)\right] \tag{5.8}$$

where

$$f_{v(i,j,k)}^{n} = \frac{3}{13}\left[f_{vf(i,j,k)}^{n} + f_{ve(i,j,k)}^{n} + f_{vc(i,j,k)}^{n}\right] \tag{5.9}$$

$$\begin{aligned} f_{vf(i,j,k)}^{n} = {} & \frac{1}{\Delta x'}\left[M'^{n}_{(0.5,0,0)}D^{+}_{(1,0,0)} - M'^{n}_{(-0.5,0,0)}D^{-}_{(-1,0,0)}\right]\mu^{n} \\ & + \frac{1}{\Delta y'}\left[M'^{n}_{(0,0.5,0)}D^{+}_{(0,1,0)} - M'^{n}_{(0,-0.5,0)}D^{-}_{(0,-1,0)}\right]\mu^{n} \\ & + \frac{1}{\Delta z'}\left[M'^{n}_{(0,0,0.5)}D^{+}_{(0,0,1)} - M'^{n}_{(0,0,-0.5)}D^{-}_{(0,0,-1)}\right]\mu^{n} \end{aligned} \tag{5.10}$$

$$\begin{aligned} f_{ve(i,j,k)}^{n} = {} & \frac{1}{\sqrt{\Delta y'^2 + \Delta z'^2}}\left[M'^{n}_{(0,0.5,0.5)}D^{+}_{(0,1,1)} - M'^{n}_{(0,-0.5,-0.5)}D^{-}_{(0,-1,-1)} + M'^{n}_{(0,-0.5,0.5)}D^{+}_{(0,-1,1)} - M'^{n}_{(0,0.5,-0.5)}D^{-}_{(0,1,-1)}\right]\mu^{n} \\ & + \frac{1}{\sqrt{\Delta x'^2 + \Delta z'^2}}\left[M'^{n}_{(-0.5,0,0.5)}D^{+}_{(-1,0,1)} - M'^{n}_{(0.5,0,-0.5)}D^{-}_{(1,0,-1)} + M'^{n}_{(0.5,0,0.5)}D^{+}_{(1,0,1)} - M'^{n}_{(-0.5,0,-0.5)}D^{-}_{(-1,0,-1)}\right]\mu^{n} \\ & + \frac{1}{\sqrt{\Delta x'^2 + \Delta y'^2}}\left[M'^{n}_{(0.5,0.5,0)}D^{+}_{(1,1,0)} - M'^{n}_{(-0.5,-0.5,0)}D^{-}_{(-1,-1,0)} + M'^{n}_{(-0.5,0.5,0)}D^{+}_{(-1,1,0)} - M'^{n}_{(0.5,-0.5,0)}D^{-}_{(1,-1,0)}\right]\mu^{n} \end{aligned} \tag{5.11}$$

$$\begin{aligned} f_{vc(i,j,k)}^{n} = {} & \frac{1}{\sqrt{\Delta x'^2 + \Delta y'^2 + \Delta z'^2}}\{M'^{n}_{(0.5,0.5,0.5)}D^{+}_{(1,1,1)} - M'^{n}_{(-0.5,-0.5,-0.5)}D^{-}_{(-1,-1,-1)} \\ & + M'^{n}_{(-0.5,0.5,0.5)}D^{+}_{(-1,1,1)} - M'^{n}_{(0.5,-0.5,-0.5)}D^{-}_{(1,-1,-1)} + M'^{n}_{(-0.5,-0.5,0.5)}D^{+}_{(-1,-1,1)} \\ & - M'^{n}_{(0.5,0.5,-0.5)}D^{-}_{(1,1,-1)} + M'^{n}_{(0.5,-0.5,0.5)}D^{+}_{(1,-1,1)} - M'^{n}_{(-0.5,0.5,-0.5)}D^{-}_{(-1,1,-1)}\}\mu^{n} \end{aligned} \tag{5.12}$$

The forward difference and backward difference of chemical potential on the face points along x direction are written as follows:

$$D^{+}_{(1,0,0)}\mu^{n} = \frac{\mu^{n}_{(i+1,j,k)} - \mu^{n}_{(i,j,k)}}{\Delta x'}, \quad D^{-}_{(-1,0,0)}\mu^{n} = \frac{\mu^{n}_{(i,j,k)} - \mu^{n}_{(i-1,j,k)}}{\Delta x'} \tag{5.13}$$

The forward difference and backward difference of chemical potential along the y and z directions can be written in a similar format, following the same principle.

The forward difference and backward difference of chemical potential on the edge points along the (y,z) direction are written as follows:

$$D^{+}_{(0,1,1)}\mu^{n} = \frac{\mu^{n}_{(i,j+1,k+1)} - \mu^{n}_{(i,j,k)}}{\sqrt{\Delta y'^{2} + \Delta z'^{2}}}, \quad D^{-}_{(0,-1,-1)}\mu^{n} = \frac{\mu^{n}_{(i,j-1,k-1)} - \mu^{n}_{(i,j,k)}}{\sqrt{\Delta y'^{2} + \Delta z'^{2}}} \tag{5.14}$$

The forward difference and backward difference of chemical potential along (–y,z), (x,z), (–x,z), (x,y) and (–x,y) directions can be written in a similar format. Along the (x,y,z) direction, they can be written as follows:

$$D^{+}_{(1,1,1)}\mu^{n} = \frac{\mu^{n}_{(i+1,j+1,k+1)} - \mu^{n}_{(i,j,k)}}{\sqrt{\Delta x'^{2} + \Delta y'^{2} + \Delta z'^{2}}}, \quad D^{-}_{(-1,-1,-1)}\mu^{n} = \frac{\mu^{n}_{(i-1,j-1,k-1)} - \mu^{n}_{(i,j,k)}}{\sqrt{\Delta x'^{2} + \Delta y'^{2} + \Delta z'^{2}}} \tag{5.15}$$

In equations (5.9), (5.10), (5.11), and (5.12), the corresponding mobility coefficients before these forward difference terms and backward difference terms of chemical potential are

$$M'^{n}_{(0.5,0,0)}=\frac{M'^{n}_{(i+1,j,k)}+M'^{n}_{(i,j,k)}}{2},\quad M'^{n}_{(-0.5,0,0)}=\frac{M'^{n}_{(i,j,k)}+M'^{n}_{(i-1,j,k)}}{2} \tag{5.16}$$

$$M'^{n}_{(0,0.5,0.5)}=\frac{M'^{n}_{(i,j+1,k+1)}+M'^{n}_{(i,j,k)}}{2},\quad M'^{n}_{(0,-0.5,-0.5)}=\frac{M'^{n}_{(i,j-1,k-1)}+M'^{n}_{(i,j,k)}}{2} \tag{5.17}$$

$$M'^{n}_{(0.5,0.5,0.5)}=\frac{M'^{n}_{(i+1,j+1,k+1)}+M'^{n}_{(i,j,k)}}{2},\quad M'^{n}_{(-0.5,-0.5,-0.5)}=\frac{M'^{n}_{(i-1,j-1,k-1)}+M'^{n}_{(i,j,k)}}{2} \tag{5.18}$$

The mobility coefficients for the other directions are not listed here because they can be written by following the same principle. The chemical potential and reduced mobility at time step *n* in the above equations are written as follows, respectively:

$$\mu^{n}_{(i,j,k)}=\mu^{n}_{b(i,j,k)}-2k_BT\kappa'^{2}\nabla'^{2}C^{n}_{v(i,j,k)} \tag{5.19}$$

$$M'^{n}_{(i,j,k)}=D'C^{n}_{v(i,j,k)}\left(1-C^{n}_{v(i,j,k)}\right)\Big/k_BT \tag{5.20}$$

The 27-point stencil approximation for the Laplace operator in three-dimensional Cartesian coordinates is written as follows:

$$\nabla'^{2}C^{n}_{v(i,j,k)}=\frac{3}{13}\left[\nabla'^{2}_{f}C^{n}_{v(i,j,k)}+\nabla'^{2}_{e}C^{n}_{v(i,j,k)}+\nabla'^{2}_{c}C^{n}_{v(i,j,k)}\right] \tag{5.21}$$

where the finite difference of the Laplace operator on the face points is

$$\begin{aligned}\nabla_f'^2 C^{\,n}_{v(i,j,k)} = &\left[C^{\,n}_{v(i+1,j,k)} + C^{\,n}_{v(i-1,j,k)} - 2C^{\,n}_{v(i,j,k)} \right] \Big/ \Delta x'^2 \\ &+ \left[C^{\,n}_{v(i,j+1,k)} + C^{\,n}_{v(i,j-1,k)} - 2C^{\,n}_{v(i,j,k)} \right] \Big/ \Delta y'^2 \\ &+ \left[C^{\,n}_{v(i,j,k+1)} + C^{\,n}_{v(i,j,k-1)} - 2C^{\,n}_{v(i,j,k)} \right] \Big/ \Delta z'^2\end{aligned} \tag{5.22}$$

On the edge points it is

$$\begin{aligned}\nabla_e'^2 C^{\,n}_{v(i,j,k)} = &\left[C^{\,n}_{v(i,j+1,k+1)} + C^{\,n}_{v(i,j-1,k-1)} + C^{\,n}_{v(i,j+1,k-1)} + C^{\,n}_{v(i,j-1,k+1)} - 4C^{\,n}_{v(i,j,k)} \right] \Big/ \left(\Delta y'^2 + \Delta z'^2 \right) \\ &+ \left[C^{\,n}_{v(i+1,j,k+1)} + C^{\,n}_{v(i-1,j,k-1)} + C^{\,n}_{v(i+1,j,k-1)} + C^{\,n}_{v(i-1,j,k+1)} - 4C^{\,n}_{v(i,j,k)} \right] \Big/ \left(\Delta x'^2 + \Delta z'^2 \right) \\ &+ \left[C^{\,n}_{v(i+1,j+1,k)} + C^{\,n}_{v(i-1,j-1,k)} + C^{\,n}_{v(i+1,j-1,k)} + C^{\,n}_{v(i-1,j+1,k)} - 4C^{\,n}_{v(i,j,k)} \right] \Big/ \left(\Delta x'^2 + \Delta y'^2 \right)\end{aligned} \tag{5.23}$$

and on the corner points it is

$$\begin{aligned}\nabla_c'^2 C^{\,n}_{v(i,j,k)} = &\left[C^{\,n}_{v(i+1,j+1,k+1)} + C^{\,n}_{v(i-1,j-1,k-1)} + C^{\,n}_{v(i+1,j+1,k-1)} \right. \\ &+ C^{\,n}_{v(i-1,j-1,k+1)} + C^{\,n}_{v(i+1,j-1,k+1)} + C^{\,n}_{v(i-1,j+1,k-1)} \\ &\left. + C^{\,n}_{v(i+1,j-1,k-1)} + C^{\,n}_{v(i-1,j+1,k+1)} - 8C^{\,n}_{v(i,j,k)} \right] \Big/ \left(\Delta x'^2 + \Delta y'^2 + \Delta z'^2 \right)\end{aligned} \tag{5.24}$$

In the simulation, for the sake of convenience, $\Delta x'$, $\Delta y'$ and $\Delta z'$ are set equal to 1.

Chapter 6: Results and discussion

According to the study in paper [24, 25] at a given temperature the gradient energy coefficient can be treated as a constant without void-size dependence, not only for large voids, but also for voids with sizes comparable with those of a lattice constant. In the following, for the sake of convenience, the dynamics of a single void in the molybdenum and copper in the phase-field framework based on the work of A. A. Semenov and C. H. Woo [24, 25] will be studied, with the assumption that the gradient energy coefficient is constant for a fixed temperature. The concentration of single vacancies, C_v, which is a conserved variable, represents the only order parameter governed by the Cahn-Hilliard equation. And the real, rather than reduced, time is used in the simulations. A direct quantitative comparison between the results obtained with the PFM and those derived from the SBA can be also made.

6.1 Single void dynamics in spherical coordinates in material molybdenum

6.1.1 Boundary conditions and initial conditions

The following equation (4.82) is numerically solved for the case of a single spherical void, i.e., when a void of some initial radius is put in the center of a spherical volume with the radius, L, as shown in Fig. 3.3. Equation (4.82) is the fourth order in the spatial coordinates, and so requires four boundary conditions. They are taken as follows:

$$\nabla C_v(r,t)\big|_{r=0} = 0, C_v(r,t)\big|_{r=L} = C_b, \nabla^2 C_v\big|_{r=L} = 0, \nabla(\nabla^2 C_v)\big|_{r=L} = 0 \quad (6.1)$$

Here C_b is the vacancy concentration at the volume boundary. It is assumed to be fixed. The first condition in (6.1) results from the requirement for C_v to be differentiable. It can be easily seen from equations (4.81), (4.82) and (4.83) that the last two mean that far away from the void, both the chemical potential, μ, of vacancies and their flux, **J**, are independent of the void-metal interface characteristics, and are entirely determined by the vacancy concentration and its gradient, as the chemical potential of vacancies, μ, and their flux, **J**, are entirely determined by the vacancy concentration and its gradient in the sharp boundary case. The initial condition is

$$C_v(t=0)\big|_{r\le R_{ini}} \cong 1, C_v(t=0)\big|_{R_{ini}<r<L} = C_b \quad (6.2)$$

Due to a diffuse character of the interface, the void radius, R, cannot be

defined uniquely within the phase-field framework. Here, similar to [25], the value of R is defined as

$$R(t) = \left\{ 3 \int_{0}^{r_{\min}} r^2 C(r,t) dr \right\}^{1/3} \tag{6.3}$$

In equation (6.3), r_{min} is the spatial position, where vacancy concentration reaches the local minimum. Since, outside the void, vacancy concentration is very low and the diffuse interface is very sharp [25], possible alternative definitions of the void radius will result in minor differences in the value of R , but there are no significant differences.

In SBA, the boundary and initial conditions are

$$C_v(r,t)\big|_{r=R} = C_{veR}, C_v(r,t)\big|_{r=L} = C_b, C_v(t=0)\big|_{R_{ini}<r<L} = C_b \tag{6.4}$$

For C_{veR}, which depends on void radius and temperature, see equation (3.20). The equations (3.37) and (3.38) will be solved by using a numerical tool called PDECHB software package [105, 106]. Since this is a moving boundary problem (R changes with time), in order to sovle the above two equations by PDECHB, one needs to transform equations (3.37) and (3.38) to a fixed boundary problem. They become the following:

$$\frac{\partial C_v(x,t)}{\partial t} - \frac{1-x}{L-R}\frac{dR}{dt}\frac{\partial C_v(x,t)}{\partial x} = \frac{1}{\left[R+(L-R)x\right]^2}\frac{1}{L-R}\frac{\partial}{\partial x}\left\{D\left[R+(L-R)x\right]^2\frac{1}{L-R}\frac{\partial C_v(x,t)}{\partial x}\right\} \tag{6.5}$$

$$\frac{dR}{dt} = D\frac{1}{L-R}\frac{\partial C_v(x,t)}{\partial x}\bigg|_{x=0} \tag{6.6}$$

where, $x = (r - R)/(L - R)$, $r = R + (L - R)x$, L the radius of the spherical region, and r the length of the matrix in the spherical region. The value of x is in the interval [0,1]. For the derivation process of equations (6.5) and (6.6) see Appendix F. The boundary conditions and initial conditions become

$$C_v(x,t)\big|_{x=0} = C_{veR},\ C_v(x,t)\big|_{x=1} = C_b,\ C_v(x,t=0) = C_b \tag{6.7}$$

6.1.2 Model parameters and material parameters

In PFM, a spherical domain with the radius L = 11.8 *nm* is discretized along the radial direction into a uniform grid with the grid size l = 0.147 *nm*. The value of l is chosen as less than the characteristic width of the interface, which is determined by the gradient energy coefficient, κ. It is found in [25] that the value of κ may be treated as relatively constant, almost independent of the void size. Depending on temperature, it is maintained at about one or two lattice constants a_0 [24, 25]. In the phase-field approach the gradient

energy coefficient is usually considered as an adjustable parameter and the value of I_2, depending on temperature, is about 0.75. In the following numerical calculations, for simplicity, the integral I_2 is assumed to be equal to unity. From equation (4.79), this assumption means that the effective value of the surface tension is actually equal to γ_s/I_2. For the numerical scheme to be stable the time step, τ, is taken to be $\tau = 10^{-15}$ *s*.

Material parameters used in the calculations correspond to the case of molybdenum. They are listed in Table 6.1. Temperatures in the calculations are chosen so that the void evolution may be both significantly affected and practically unaffected by the vacancy emission from the void.

Table 6.1

Material parameters for molybdenum.

Parameter	Value
Vacancy formation energy, E_v^f [a]	3.0 eV
Vacancy migration energy, E_v^m [a]	1.62 eV
Vacancy diffusivity pre-exponential, D_0 [a]	1.3×10^{-5} m^2/s
Surface tension, γ_s [b]	2.05 J/m^2
Lattice constant, a_0 [a]	3.1 A
Atomic volume, Ω	$a_0^3/2$

[a] Reference [107].

[b] Reference [108].

To mimic the real experimental conditions all numerical calculations are performed for the very low values of vacancy concentration C_b (~ 10^{-9} – 10^{-7}).

6.1.3 Vacancy concentration profile and chemical potential profile

It follows from equation (3.39) that the void growth rate does not depend explicitly on time. Taking into account the smallness of the time step, τ, this property makes much easier the comparison between the void dynamics following from the PFM and the SBA. Indeed, instead of considering the void evolution over long time periods during which significant changes in the void radius can be realized, we may just compare the void growth rates at different values of the initial void radius, R_{ini}. The equivalence in the growth rates would obviously mean the equivalence in the void evolution during the corresponding period of time. The characteristic time required for the vacancy diffusion field to approach its steady-state spatial distribution is of

the order of $t_R = R_{ini}^2/(2D)$. Thus, for the purpose of the present study, it is sufficient to consider the void evolution during the time intervals $t >> t_R$.

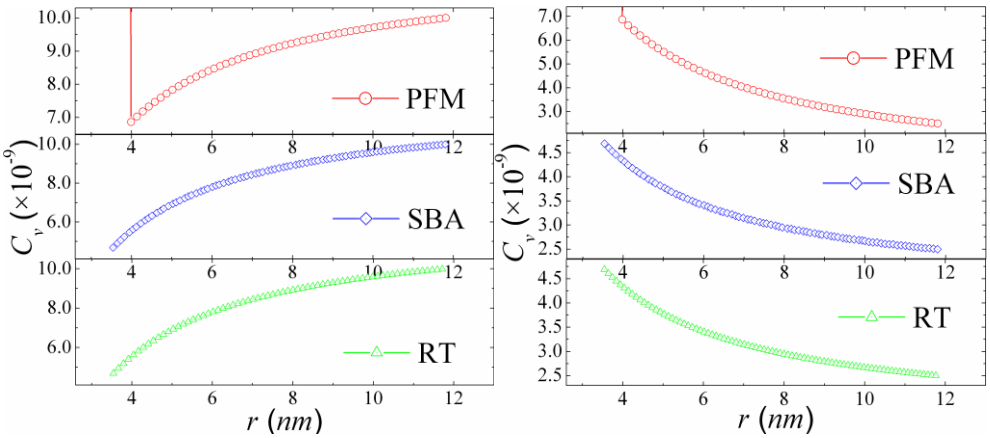

(*a*) (*b*)

Fig. 6.1. Concentration profiles after $t = 10^{-5}$ *s* for the cases of void growth (*a*, $C_b = 10^{-8}$) and shrinkage (*b*, $C_b = 2.5\times10^{-9}$) at $T = 1750$ K and $R_{ini} = 3.54$ *nm*. PFM, SBA and RT represent phase-field method, sharp boundary approach and rate theory, respectively.

In Fig. 6.1, we present the concentration profiles calculated with PFM, SBA and RT for two different vacancy concentrations at the external boundary ($r = L$), with both the temperature and the initial void radius kept unchanged. Values of $C_b = 10^{-8}$ and $C_b = 2.5\times10^{-9}$ correspond to the cases of void growth and shrinkage, respectively. According to the figure, PFM

reproduces quite well the characteristic r^{-1} behavior of the vacancy concentration distribution, which follows from the rate-theory approximation in the sharp boundary case.

Both in the PFM and in the SBA, whether void shrinkage or growth is realized depends on the value of the vacancy chemical potential at the void-metal interface compared to its value $\mu \cong k_B T \ln(C_b/C_{e\infty})$ at the volume boundary $r = L$. The difference is that in the SB case this value is equal to $k_B T \ln(C_{eR}/C_{e\infty})$, while in the diffuse interface approach it is given by equation (4.27). Note that, despite very sharp spatial dependence of vacancy concentration within the diffuse interface, the chemical potential calculated with equation (4.27) remains practically constant (Fig. 6.2).

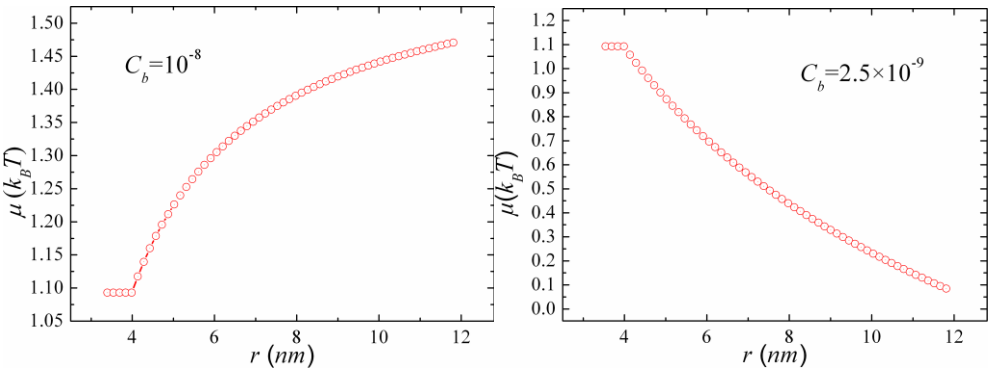

(*a*) (*b*)

Fig. 6.2. Profiles of the chemical potential, μ, after $t = 10^{-5}$ *s* calculated with

equation (4.27) for the cases of void growth (*a*) and shrinkage (*b*) at T = 1750 K and R_{ini} = 3.54 *nm*.

When the chemical potential of vacancies at $r = L$ is larger than its value at the interface there is a positive flux of vacancies from the external boundary towards the void, which results in void growth (Fig. 6.3). In the opposite case, the shrinkage of void takes place due to the outflow of vacancies from the void into the matrix (Fig. 6.4). From Fig. 6.3*b* and Fig. 6.4*b* one can easily see that the void growth rates obtained with the PFM and SBA reach the steady-state values after a very short initial period. In other words, the characteristic time t_R required for the vacancy diffusion field to attain its steady-state profile is indeed much shorter than the time intervals considered in the numerical calculations. Since on the time scales under consideration the absolute values of the void radius changes are still relatively small, these changes are almost linear with time (Fig. 6.3*a* and Fig. 6.4*a*). Comparing the results presented in Fig. 6.3 and Fig. 6.4, one can find that, after the short initial periods, the void growth curves obtained by the three different methods demonstrate very similar behavior.

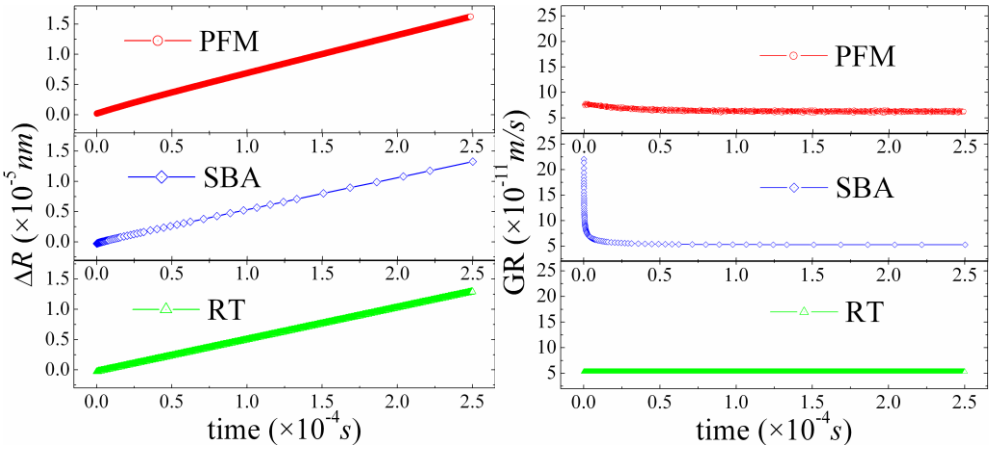

(*a*) (*b*)

Fig. 6.3. (*a*) Change in the void radius $\Delta R = R - R_{ini}$ versus time at T = 1100 K, C_b = 1.0×10^{-7}, R_{ini} = 1.02 *nm*. (*b*) Void growth rate (GR) versus time under the same conditions as in (*a*).

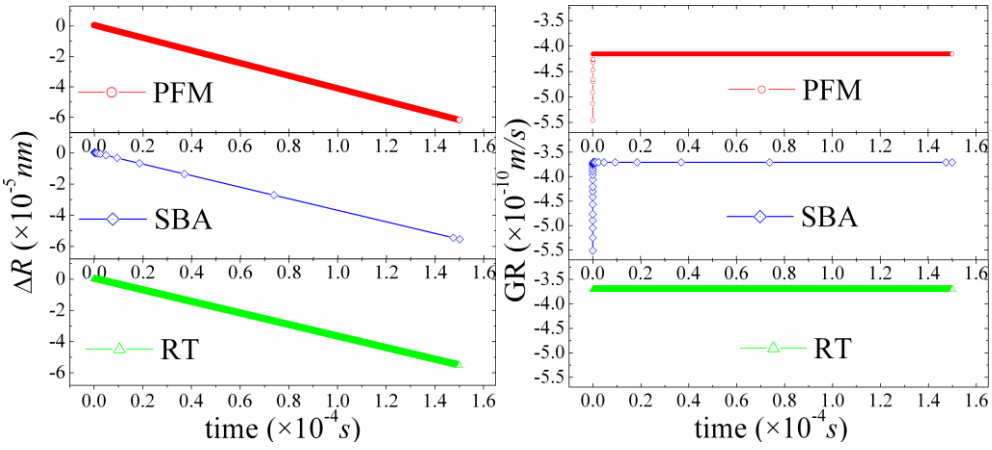

(*a*) (*b*)

Fig. 6.4. (*a*) Change in the void radius $\Delta R = R - R_{ini}$ versus time at T = 1750 K, C_b = 2.5×10^{-9}, R_{ini} = 2.95 *nm*. (*b*) Void growth rate (GR) versus time under the same

conditions as in (*a*).

Since the void radius is almost unchanged for a period which is far longer than the characteristic time, t_R, this time interval, t_R, and void growth rate can also be obtained by using the separation of variables and power series solution method to solve the diffusion equation (3.37) for fixed vacancy concentration at the void surface and volume boundary (see Appendix H). Fig. 6.5*a* shows the vacancy concentration profile obtained by equation

(H. 29) with the exponent n = 1000 at four different moments. The initial uniform distribution of vacancy concentration will relax to steady state distribution very quickly. This can also be seen from Fig. 6.5*b*. The difference between a non-steady state vacancy profile and the steady state profile (see equation (H. 35)) decreases to zero very quickly with time. The exact non-steady state growth rate seen in equation (H. 32) in Appendix H, which will approach the steady state growth rate (equation (3.39) or equation (H. 33)) within very short time intervals, t_R, which is about 10^{-5} *s*, as shown in Fig. 6.5c.

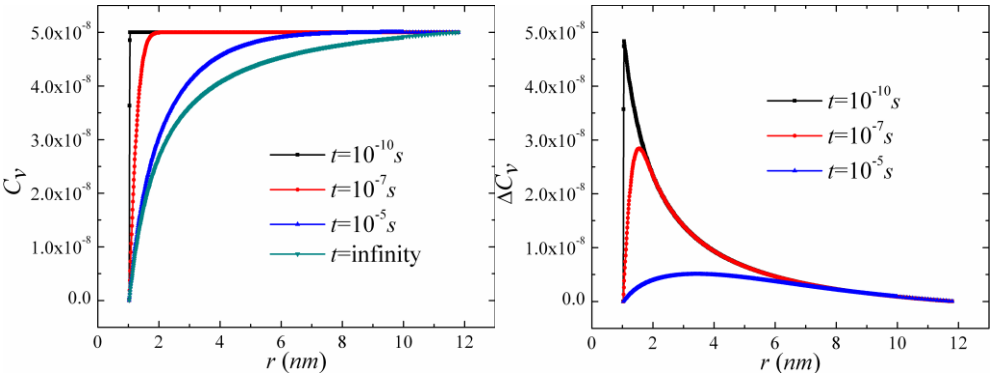

(a) (b)

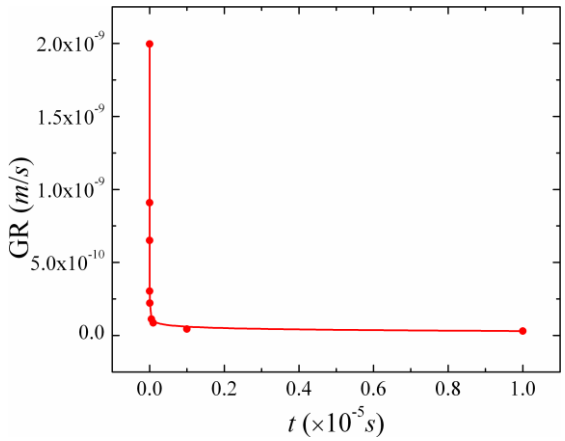

(c)

Fig. 6.5. Vacancy concentration profile, C_v, and growth rate (GR) versus time obtained through solving diffusion equation by using the separation of variables and power series method under the conditions of R = 1.02 nm, L = 11.8 nm and C_b = 5×10^{-5}. (a) the vacancy concentration profiles at three different moments and steady state (t = infinity), (b) the difference ΔC_v between the non-steady state vacancy concentration profile and the steady state vacancy concentration profile at three different moments, (c) the growth rate (GR) versus time.

1. At temperature 1100K

For a case with void radius 1 *nm* and $C_b = 10^{-7}$, $D = 4.9\times10^{-13}\ m^2/s$, $L = 11.81\ nm$, $R_{ini} = 1.02\ nm$ (corresponding to the case in Fig. 6.3), the time needed for the growth rate to drop to a value which is bigger than the steady state growth rate by 1/10 through numerical calculation using PDECHEB software package is $t_{num} = 1.8\times10^{-5}\ s$. And this time, obtained through the above separation of variables and power series solution method with choosing the exponent $n = 10$, is

$$R_{ratio} = \frac{\dot{R}_{ns} - \dot{R}_s}{\dot{R}_s} = \frac{2R}{L-R} S = \frac{1}{10} \Rightarrow t_a = 1.793\times10^{-5} s \tag{6.8}$$

The two values are almost the same. In fact, $n = 3$ is good enough because $S = \sum_{n=1}^{\infty} \exp\left[-\left(n\pi/\left(L-R\right)\right)^2 Dt\right]$ converges very fast. And even $n = 1$ is a good estimation for calculating the time. Then equation (H. 32) is reduced to

$$\dot{R}_{ns} = \frac{dR}{dt} = D\frac{dC(r,t)}{dr}\bigg|_{r=R} = \frac{2D(C_b - C_{eR})}{L-R} e^{-\left(\frac{\pi}{L-R}\right)^2 Dt} + \frac{DL(C_b - C_{eR})}{R\left(L-R\right)} \tag{6.9}$$

The vacancy concentration distribution is reduced to

$$\begin{aligned} C(r,t) = {} & \frac{2R(C_b - C_{eR})}{r\pi} \sin\left[\frac{\pi}{L-R}\left(r-R\right)\right] e^{-\left(\frac{\pi}{L-R}\right)^2 Dt} \\ & + \frac{LC_b - RC_{eR}}{L-R} - \frac{1}{r}(C_b - C_{eR})\frac{LR}{L-R} \end{aligned} \tag{6.10}$$

And equation (H. 36) is reduced to

$$R_{ratio} = \frac{\dot{R}_{ns} - \dot{R}_s}{\dot{R}_s} = \frac{2R}{L-R} e^{-\left(\frac{\pi}{L-R}\right)^2 Dt} \tag{6.11}$$

Through this first order approximation (exponent n = 1), the time needed for the growth rate to drop to a value which is bigger than the steady state growth rate by 1/10 is

$$\begin{aligned} & R_{ratio} = \frac{2R}{L-R} e^{-\left(\frac{\pi}{L-R}\right)^2 Dt} = \frac{1}{10} \\ & \Rightarrow t_a = -\left(\frac{L-R}{\pi}\right)^2 \frac{1}{D} \ln \frac{L-R}{20R} = 1.54 \times 10^{-5} s \end{aligned} \tag{6.12}$$

The difference between 1.54×10^{-5} *s* and 1.8×10^{-5} *s* is very small. Thus equation (6.9) can be used as an analytical formula to estimate the growth rate for the initial stage.

2. At temperature 1750K

For a case with void radius 1 *nm* and $C_b = 2.5 \times 10^{-9}$, $D = 2.8 \times 10^{-10}$ m^2/s, L = 11.81 *nm*, R_{ini} = 3.54 *nm* (corresponding to the case in Fig. 6.1b), the time needed for the growth rate to drop to a value which is bigger than the steady state growth rate by 1/10 through numerical calculation using PDECHEB software package is about $t_{num} = 5.2 \times 10^{-8}$ *s*. This time, obtained though the above separation of variables and power series solution method by choosing

n = 10, is

$$R_{ratio} = \frac{\dot{R}_{ns} - \dot{R}_s}{\dot{R}_s} = \frac{2R}{L-R} S = \frac{1}{10}$$
$$\Rightarrow t_a = 5.29 \times 10^{-8} s \tag{6.13}$$

For the first order estimation

$$R_{ratio} = \frac{2R}{L-R} e^{-\left(\frac{\pi}{L-R}\right)^2 Dt} = \frac{1}{10}$$
$$\Rightarrow t_a = -\left(\frac{L-R}{\pi}\right)^2 \frac{1}{D} \ln \frac{L-R}{20R} = 5.29 \times 10^{-8} s \tag{6.14}$$

These two are almost the same. Thus, for the case of high temperature, the equation (6.9) is a better approximation formula for the calculation of void growth rate than it is for relatively low temperature.

However, equation (6.9) is very poor for estimating the growth rate at t = 0 s, because $2D(C_b - C_{eR})/(L - R)$ is finite. Yet again, from equation (H. 32) the growth rate should be infinite, because $S = \sum_{n=1}^{\infty} a^{n^2} = \infty$ at t = 0 s. Thus the first order estimation for void growth rate is very poor at t = 0 s. And the growth rate is infinite at t = 0 s because the initial vacancy concentration at void surface r = R is C_b bigger than the thermal emission vacancy concentration, C_{eR}. So the first order term can only be used to estimate the growth rate and vacancy concentration distribution after the initial stage.

This is the reason that the first order term is a good estimation for void growth rate at high temperature: because the diffusion constant is large at high temperature, thus the required time for the initial relaxation period of the vacancy field can be small.

Thus, in order to obtain precise results, more higher-order terms are needed to be calculated. Since it is only valid for those cases without boundary motion, the separation of variables and power series method for solving the diffusion equation is good for the analysis of void evolution within a relatively small time interval but small time interval should be larger than the relaxation time of vacancy diffusion field because the void radius is almost unchanged within this time interval. From the above calculation and analysis, we can get a precise solution of the diffusion equation for the cases without boundary motion, or those with void radius almost unchanged, by using the separation of variables and power series method.

6.1.4 Void evolution with no vacancy emission

In this section we consider the void growth in a solution that is highly supersaturated, i.e., when $C_b >> C_{eR}$. In this case the effect of vacancy

emission on the void evolution is negligible. Indeed, from equation (3.39) the void growth rate in the RT approximation can be written as

$$\frac{dR}{dt} \cong \frac{DC_b}{R} \tag{6.15}$$

According to the foregoing, within sufficiently short time intervals, which, however, are much larger than the relaxation time of the vacancy diffusion field, the void growth rate remains almost unchanged. Thus, instead of instantaneous growth rates, the growth rates averaged over the corresponding time intervals can be used to study the relationship between the PFM and the SBA. This is the case for Fig. 6.6 – Fig. 6.8, in which the presented growth rates are results of the averaging over a time period of 10^{-4} *s*.

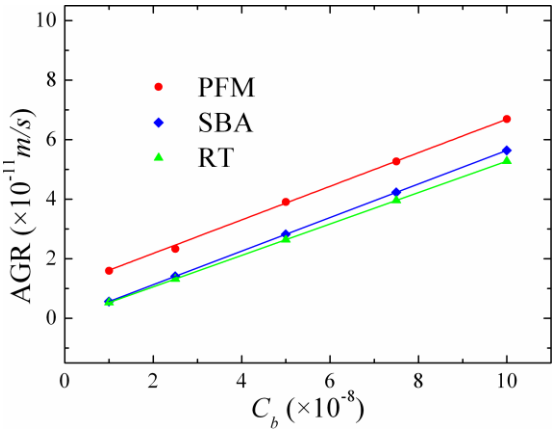

Fig. 6.6. Average void growth rate (AGR) as a function of vacancy concentration at the volume boundary, C_b, at T = 1100 K, R_{ini} = 1.02 *nm*.

In Fig. 6.6 the average void growth rate is shown as a function of the vacancy concentration, C_b, at the volume boundary. In agreement with equation (6.15), the void growth rates obtained by the three different methods are directly proportional to C_b. From Fig. 6.6, the slopes of the lines obtained with PFM, SBA and RT are about 5.67×10^{-4} *m*/*s*, 5.68×10^{-4} *m*/*s* and 5.28×10^{-4} *m*/*s*, respectively. Since vacancy emission from the void is negligible in the considered case, the difference in the absolute values between the PFM and SBA cannot be removed by varying the effective surface tension of the void. Most probably this difference is a property of the free-energy density (equation (4.9)) adopted in the present consideration. Note also that in the case of solidification similar differences are typically observed when the results of the phase-field model and the capillary approximation are compared [109].

Void growth rate as a function of initial void radius is presented in Fig. 6.7. According to equation (6.15), in this case the void growth rate should be inversely proportional to the radius of the void. Fig. 6.7 demonstrates that this tendency is reproduced quite well in the phase-field approach.

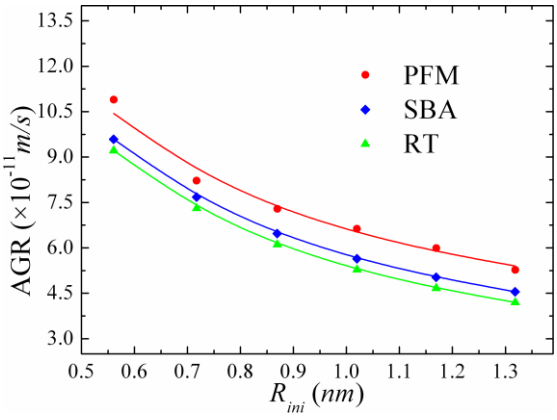

Fig. 6.7. Average void growth rate (AGR) as a function of initial void radius, R_{ini}, at T = 1100 K, $C_b = 1.0\times10^{-7}$.

Within the temperature range at which the vacancy emission from voids still remains negligible, the temperature dependence of void growth rate is entirely determined by the vacancy diffusion coefficient $D = D_0\exp(-E_v^m/k_BT)$ (equation (6.15)). Fig. 6.8 shows that the growth rate increases with temperature in the same way for all three methods.

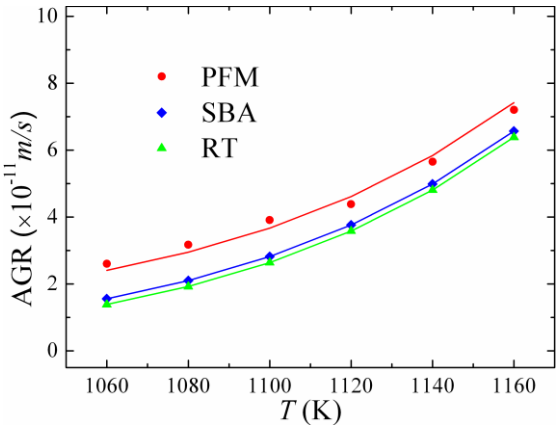

Fig. 6.8. Average void growth rate (AGR) as a function of temperature, T, at C_b = 5.0×10^{-8} and R_{ini} = 1.02 *nm*.

6.1.5 Void evolution in the vicinity of critical size

In the sharp boundary case the critical size of the void R_c corresponds to the maximum of free energy change caused by the void formation [24] (see equation (3.19)). From the kinetic point of view, R_c is the unstable stationary solution of equation (3.39); i.e.,

$$R_c = 2\gamma_s\Omega \Big/ \left[k_B T \ln\left(C_b / C_{e\infty}\right)\right] \tag{6.16}$$

It is easy to see from equation (3.39) that a subcritical void shrinks over time, while a supercritical one keeps growing. Obviously, the void evolution in the vicinity of critical size is very sensitive even to small changes in the environmental parameters, such as, for example, the void surface tension and the vacancy concentration at the volume boundary, C_b. Since the phase-field model is only an approximation for the sharp-boundary case, the most significant deviations between these two approaches should be expected when void sizes are close to the critical one. As an example, in the following we consider the behavior of the average void growth rate near the critical

size at 1750 K. The calculated growth rates are results of the averaging over a time period of 10^{-5} *s*. The time period is chosen an order of magnitude shorter than in the foregoing section because vacancy migration at 1750 K is several orders of magnitude faster than at 1100 K.

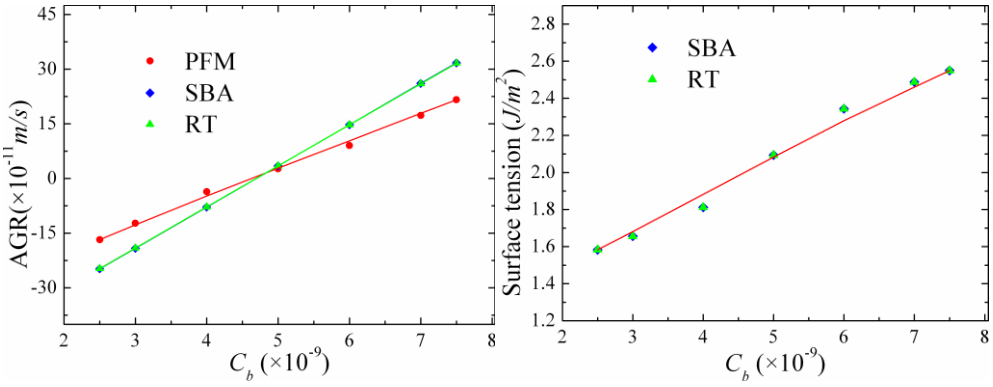

(*a*) (*b*)

Fig. 6.9. (*a*) Average void growth rate (AGR) as a function of vacancy concentration at the volume boundary, C_b, at T = 1750 K, R_{ini} = 3.54 *nm*. (*b*) Matching value of the surface tension coefficient γ_s as a function of vacancy concentration at the volume boundary, C_b.

Fig. 6.9*a* shows that in both approaches void growth rate increases linearly with the vacancy concentration at the volume boundary. The critical value of C_b corresponding to the zero growth rate is about 4.69×10^{-9} in the case of SBA and RT and about 4.58×10^{-9} in the case of PFM. On the other

hand, the slopes of the curves obtained with SBA and PFM are 11.3×10^{-2} *m/s* and 7.67×10^{-2} *m/s*, respectively; i.e., unlike in the case described in section 6.1.4, there is a substantial difference between them. However, due to the sensitivity of void evolution to the surface tension coefficient, these curves can be matched by varying the value of this coefficient. The matching values as a function of vacancy concentration at the boundary are presented in Fig. 6.9*b*.

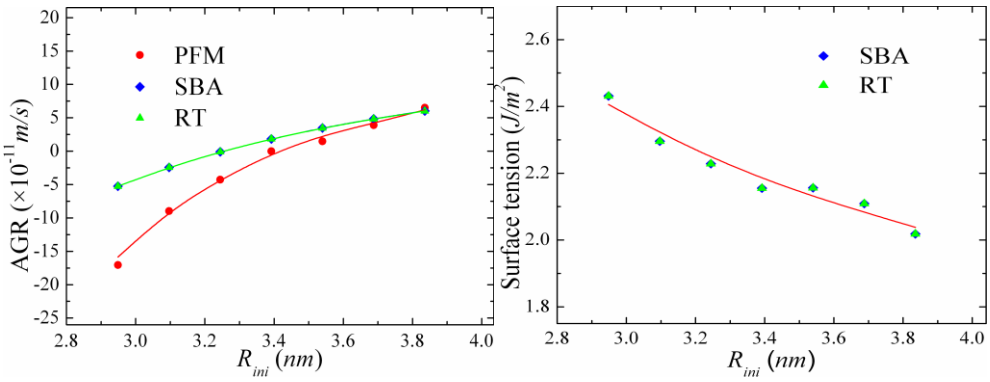

(*a*) (*b*)

Fig. 6.10. (*a*) Average void growth rate (AGR) as a function of initial void radius, R_{ini}, at T = 1750 K, C_b = 5.0×10^{-9}. (*b*) Matching value of the surface tension coefficient, γ_s, as a function of initial void radius.

As far as the effect of the initial void radius on the void growth rate is concerned, the average void growth rate as a function of initial void radius is

shown in Fig. 6.10*a*. From this figure, the critical void radius is approximately equal to 3.25 *nm* in the case of SBA and RT and to 3.42 *nm* in the case of PFM. As in Fig. 6.9a, there is a substantial difference in the slopes of the curves obtained with SBA and PFM. This difference can be also removed by varying the value of the surface tension coefficient (Fig. 6.10*b*). According to equation (6.16), the higher vacancy concentration at the boundary of the volume corresponds to the lower critical void size. Thus, both from Fig. 6.9*b* and from Fig. 6.10*b* it follows that the effective interfacial tension, or the gradient-energy coefficient, should be a decreasing function of the void radius for the void growth rates resulting from the PFM and the SBA to match, in the vicinity of critical size.

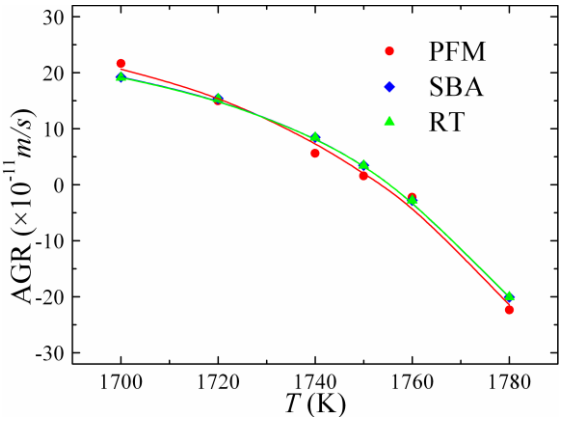

Fig. 6.11. Average void growth rate (AGR) as a function of temperature, T, at C_b = 5.0×10^{-9} and R_{ini} = 3.54 *nm*.

Finally, Fig. 6.11 demonstrates the effect of temperature on the void growth rate. Clearly, there is a good agreement between the two approaches. PFM and SBA give the critical temperatures at which void growth rate changes its sign as 1754 K and 1755.5 K, respectively. Since vacancy emission from the void plays a dominant role in the void evolution in the vicinity of this critical temperature, the void growth rate decreases with the temperature increase. This is unlike the case in section 6.1.4, where the effect of temperature is entirely determined by the temperature dependence of the vacancy diffusion coefficient.

6.2 Single void dynamics in spherical coordinates in copper

6.2.1 Model parameters and material parameters

The model configuration and solution methods for PFM and SBA are the same as in the section 6.1, as are the boundary conditions and initial conditions. In PFM, a spherical domain with the radius L = 10.93 *nm* is discretized along the radial direction into a uniform grid of grid size l = 0.228 *nm*. The value of l is chosen to be less than the characteristic width of

the interface, which is determined by the gradient energy coefficient κ. For the numerical scheme to be stable the time step τ is taken to be $\tau = 5\times10^{-16}$ s. The material parameters of copper used in the simulations are listed in Table 6.2. Temperatures in the calculations are chosen so that the void evolution may be revealed, both in temperature ranges where they are significantly affected and in those where they are practically unaffected by the vacancy emission from the void.

Table 6.2

Material parameters for copper.

Parameter	Value
Vacancy formation energy, E_v^f [a]	1.28 eV
Vacancy migration energy, E_v^m [a]	0.7 eV
Vacancy diffusivity pre-exponential, D_0 [a]	1.3×10^{-5} m^2/s
Surface tension, γ_s [b]	1.3 J/m^2
Lattice constant, a_0 [a]	3.615 A
Atomic volume, Ω	$a_0^3/4$

[a] Reference [107].

[b] Reference [108].

To mimic the real experimental conditions all numerical calculations are

performed for very low values of vacancy concentration C_b (~ 10^{-8} – 10^{-7}).

6.2.2 Vacancy concentration profile and chemical potential profile

As in section 6.1, since the void growth rate does not explicitly depend on time and only depends on the void radius, R, the vacancy concentration at boundary, C_b, and the temperature, T, indirectly through the thermal emission vacancy concentration, C_{eR}, and diffusion constant, D, the characteristics of void dynamics under different R, C_b and T will be studied. Again, instead of considering the void evolution over long time periods, during which significant changes in the void radius can be realized, we just compare the void growth rates at different values of the initial void radius, R_{ini}. Equivalence in the growth rates would obviously mean equivalence in the void evolution during the corresponding period of time. The considered time intervals, t, of void evolution in the simulation are far greater than the characteristic times required for a vacancy diffusion field that is relaxing from an initial uniform spatial distribution, to approach its steady-state spatial distribution. This characteristic time is of the order of $t_R = R_{ini}^2/(2D)$.

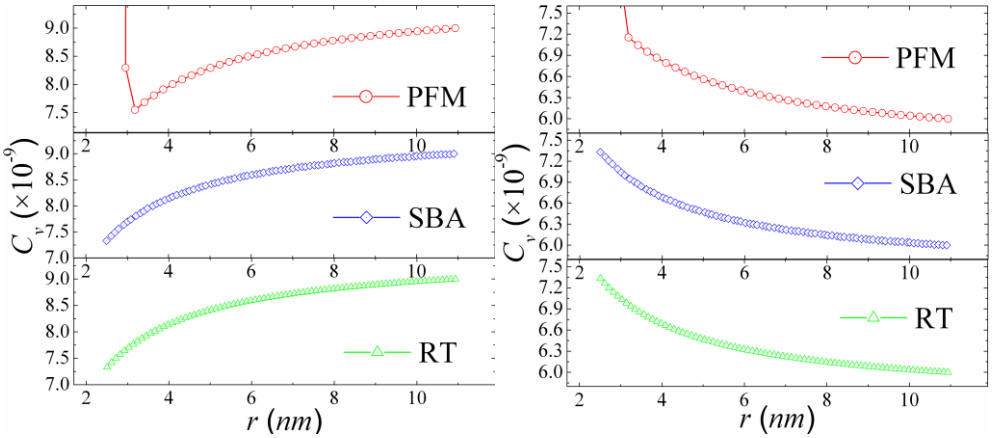

(*a*) (*b*)

Fig. 6.12. Concentration profiles after $t = 10^{-5}$ *s* for the cases of void growth (*a*, $C_b = 9\times10^{-8}$) and shrinkage (*b*, $C_b = 6\times10^{-8}$) at $T = 850$ K and $R_{ini} = 2.505$ *nm*.

Fig. 6.12 show the concentration profiles calculated with PFM, SBA and RT for two different vacancy concentrations at the external boundary ($r = L$), under the same temperature and the initial void radius. The values of $C_b = 9\times10^{-8}$ and $C_b = 6\times10^{-8}$ correspond to the cases of void growth and shrinkage, respectively. The concentration profiles obtained with PFM are very similar to those obtained with SBA and RT and reproduce quite well the characteristic r^{-1} behavior of the vacancy concentration distribution, which is a steady state distribution of vacancy concentration, from the rate theory approximation.

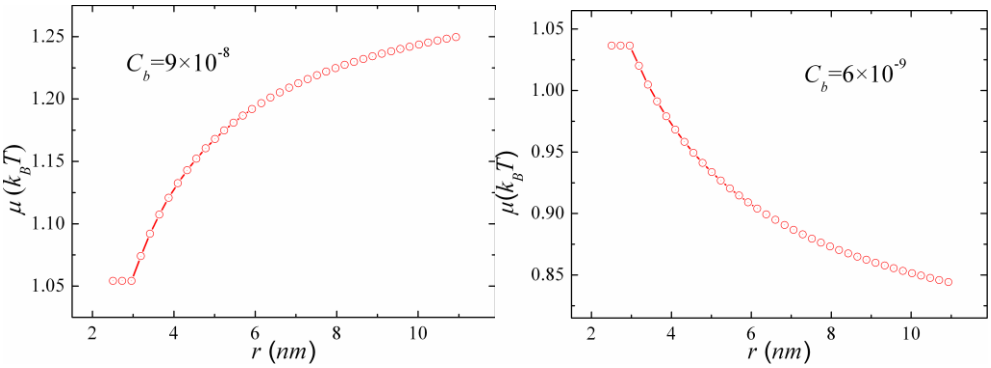

(*a*) (*b*)

Fig. 6.13. Profiles of the chemical potential, μ, after $t = 10^{-5}$ *s* calculated with eq. (6) for the cases of void growth (*a*) and shrinkage (*b*) at T = 850 K and R_{ini} = 2.505 *nm*.

Since the fluxes of vacancies are governed by the gradient of chemical potential in both PFM and SBA, the void evolution depends on the difference between the vacancy chemical potential $\mu \cong k_BT\ln(C_b/C_{e\infty})$ at the matrix boundary $r = L$ and at the void-metal interface. The value of chemical potential at void surface in the SBA is equal to $k_BT\ln(C_{eR}/C_{e\infty})$, while within the diffuse interface in the PFM it is given by equation (4.27). For the PFM to perfectly reproduce the SBA, the chemical potential within the diffuse interface should also be equal to $k_BT\ln(C_{eR}/C_{e\infty})$. Despite very sharp spatial dependence of vacancy concentration within the diffuse interface, the chemical potential calculated with equation (4.27) remains practically

constant (Fig. 6.13).

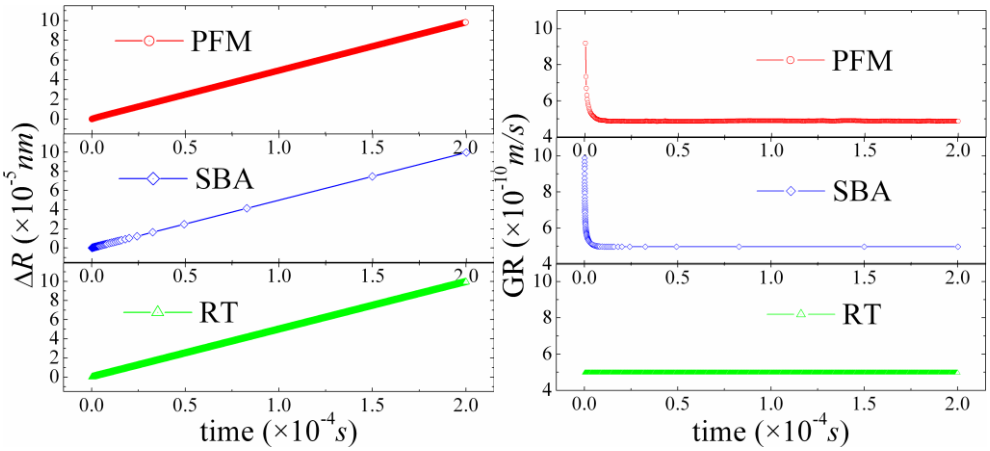

(*a*) (*b*)

Fig. 6.14. (*a*) Change in the void radius, $\Delta R = R - R_{ini}$, versus time at T = 550 K, $C_b = 10^{-7}$, R_{ini} = 1.126 *nm*. (*b*) Void growth rate (GR) versus time under the same conditions as in (*a*).

If the chemical potential at $r = L$ is larger than its value at the interface, this gives rise to a driving force that makes vacancies flow from the external boundary towards the void, which results in void growth (Fig. 6.14). For the inverse case, the driving force produces the outflow of vacancies from the void into the matrix (Fig. 6.15). Since in the matrix the Cahn-Hilliard equation (4.82) in PFM reproduces the diffusion equation (3.35) in SBA, whether the void grows or shrinks can also be explained through the

comparison between the vacancy concentration value at $r = L$ and at the transition point between the diffuse interface and the matrix. When the vacancy concentration at the transition point between the diffuse interface and the matrix is equal to that at $r = L$, the void will neither grow nor shrink, which is an unstable equilibrium state. This is indicated from equation (3.39) for the SBA case also, because the void growth rate is zero when C_b is equal to C_{eR}.

From Fig. 6.14*b* and Fig. 6.15*b* one can easily see that the void growth rates obtained with the PFM and SBA reach the steady-state values after a very short initial period. In other words, the characteristic time t_R required for the vacancy diffusion field to attain its steady-state profile is indeed much shorter than the time intervals considered in the numerical calculations. Since on the time scales under consideration the absolute values of the void radius variations are still relatively small, these changes are almost linear with time (Fig. 6.14*a* and Fig. 6.15*a*). Comparing the results presented in Fig. 6.14 and Fig. 6.15, one finds that, after the short initial periods, the void growth curves obtained by the three different methods indicate very similar behavior.

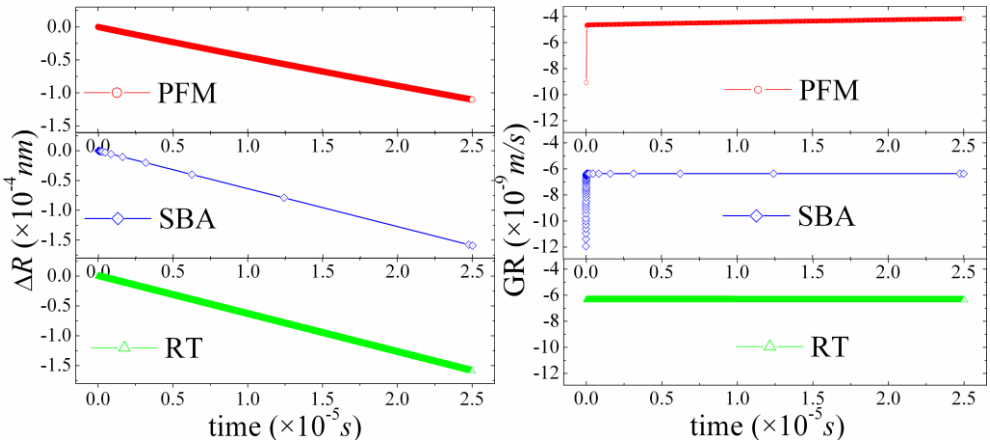

(*a*) (*b*)

Fig. 6.15. (*a*) Change in the void radius, $\Delta R = R - R_{ini}$, versus time at T = 850 K, $C_b = 6\times10^{-8}$, R_{ini} = 2.505 *nm*. (*b*) Void growth rate (GR) versus time under the same conditions as in (*a*).

6.2.3 Void evolution under strong supersaturation

In this section the void growth under the condition of a solution of high supersaturation, i.e., $C_b >> C_{eR}$, will be considered. The number of vacancies emitted from the void surface is far smaller than that for those flowing into the void. Thus, it has no effect on the void growth rate as equation (6.15) shows. It is the same as that in the molybdenum cases, in which, due to the very dilute vacancy concentration in the matrix and small diffusion coefficient (which is about 5×10^{-12} m^2/s at 550 K), the void growth rate

remains almost unchanged over short time intervals (which, however, are much larger than the relaxation time of the vacancy diffusion field). Thus, instead of the instantaneous growth rates, the growth rates averaged over the corresponding time intervals can be used to study the relationship between the PFM and the SBA. In Fig. 6.16 - Fig. 6.18, the presented growth rates are results of the averaging over a time period of 2×10^{-4} *s*.

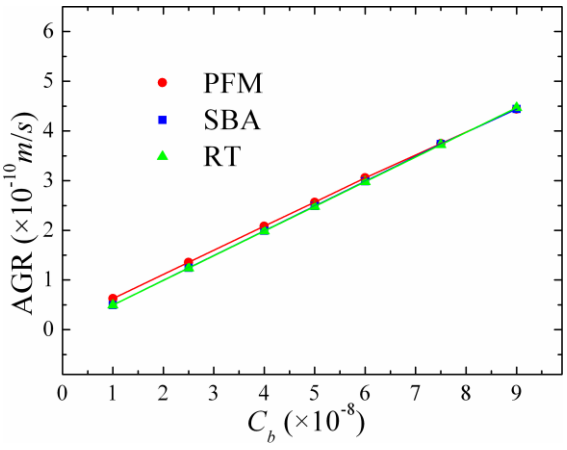

Fig. 6.16. Average void growth rate (AGR) as a function of vacancy concentration at the volume boundary, C_b, at T = 550 K, R_{ini} = 1.126 *nm*. The curve of SBA coincides with that of RT, and the following corresponding cases are the same.

In Fig. 6.16 the average void growth rate is shown as a function of the vacancy concentration C_b at the volume boundary. The void growth rates obtained by the three different methods are directly proportional to C_b, which

is consistent with equation (6.15). In Fig. 6.16, the slopes of the lines obtained with PFM, SBA and RT are about 4.77×10^{-3} *m/s*, 4.93×10^{-3} *m/s* and 4.97×10^{-3} *m/s*, respectively. These three lines almost coincide with each other, except for the low vacancy concentration cases.

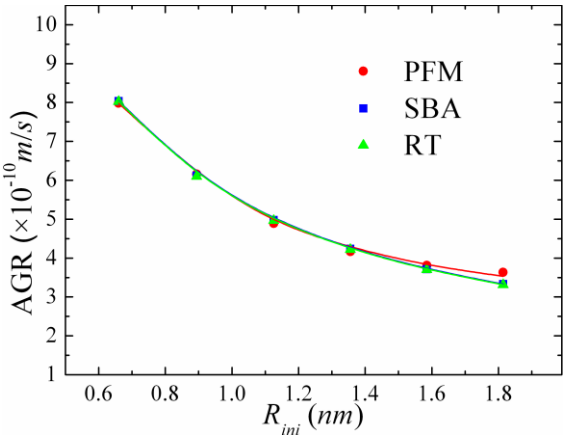

Fig. 6.17. Average void growth rate (AGR) as a function of initial void radius, R_{ini}, at T = 550 K, $C_b = 10^{-7}$.

Fig. 6.17 shows the void growth rate as a function of initial void radius R_{ini}. In this case the temperature T and the vacancy concentration C_b at the volume boundary are fixed. The fixation of T leads to the vacancy diffusion coefficient D being fixed as well. According to equation (6.15), the void growth rate should be inversely proportional to the radius of the void. Fig. 6.17 demonstrates that this tendency is reproduced quite well in the PFM.

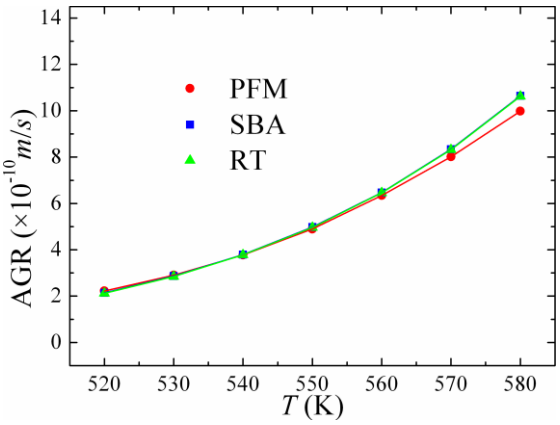

Fig. 6.18. Average void growth rate (AGR) as a function of temperature, T, at C_b = 10^{-7} and R_{ini} = 1.126 *nm*.

Since the initial void radius and C_b are temperature independent, and C_{eR} remains negligible compared to the values for C_b at 550K, the temperature dependence of the void growth rate is entirely determined by the vacancy diffusion coefficient $D = D_0\exp(-E_v^m/k_BT)$ (equation (6.15)). Thus, the void growth rate increases with temperature as a function of $\exp(-1/T)$. Fig. 6.18 shows this behavior for the results obtained with all three methods.

6.2.4 Void evolution in the vicinity of critical size

In the sharp boundary case, according to classical nucleation theory, a supersaturated solution is in a meta-stable state which is stable for

infinitesimal fluctuations due to the formation of the surface of the void, and unstable for relative large fluctuations which can overcome the barrier formed by surface free energy. The critical energy for the formation of a void is determined by a competition between a volume term which favors creation of the void and a surface term which favors its dissolution, which is the maximum in the free energy change caused by the void formation [24]. The void evolution in the vicinity of critical size is very sensitive even to small changes in the environmental parameters, such as the void surface tension and the vacancy concentration at the volume boundary, C_b, as is discussed in section 6.1.5. Thus, the void evolution in the vicinity of critical size easily brings some errors to the PFM simulations. Since the PFM is only an approximation for the SBA, the most significant deviations between these two approaches should be expected when void sizes are close to the critical one. As an example, the following mainly considers behavior of the average void growth rate near the critical size at around 850 K. The calculated growth rates are results of the averaging over a time period of 2.5×10^{-5} *s* which is of an order of magnitude shorter than in the foregoing section because vacancy migration at 850 K is several orders of magnitude faster than at 550 K.

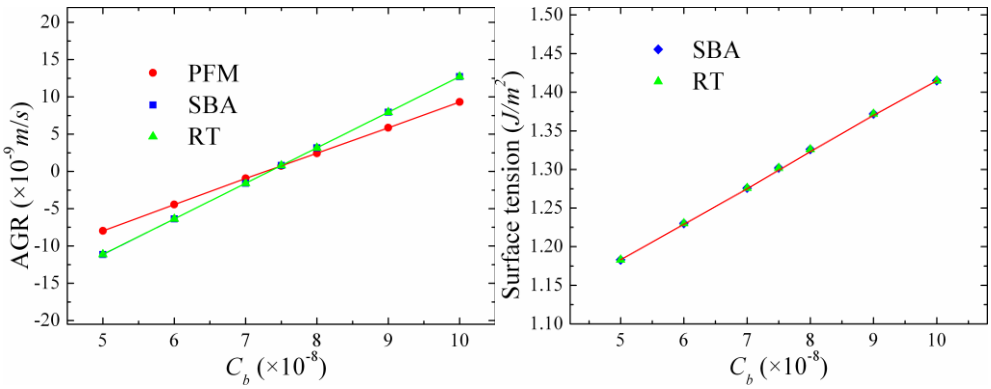

(*a*) (*b*)

Fig. 6.19. (*a*) Average void growth rate (AGR) as a function of vacancy concentration at the volume boundary, C_b, at T = 850 K, R_{ini} = 2.505 *nm*. (*b*) Matching value of the surface tension coefficient γ_s as a function of vacancy concentration at the volume boundary.

According to equation (6.15), the void growth rate only depends on the vacancy concentration at the volume boundary, C_b, when the temperature, T, and initial void radius, R_{ini}, are fixed. Fig. 6.19*a* shows that, in both the PFM and the SBA approach, void growth rate increases linearly with the vacancy concentration at the volume boundary. The critical value of C_b corresponding to the zero growth rate is about 7.33×10^{-9} in the case of SBA and RT and about 7.28×10^{-9} in the case of PFM. The slopes of the curves obtained with SBA and PFM are 4.77×10^{-1} *m*/*s* and 3.46×10^{-1} *m*/*s*, respectively; i.e., unlike in the foregoing section, the difference between them is relatively big.

However, like in the molybdenum cases in section 6.1.5, due to the sensitivity of void evolution to the surface tension coefficient, these curves can be matched by varying the value of this coefficient. The matching values, as a function of vacancy concentration at the boundary, are presented in Fig. 6.19*b*.

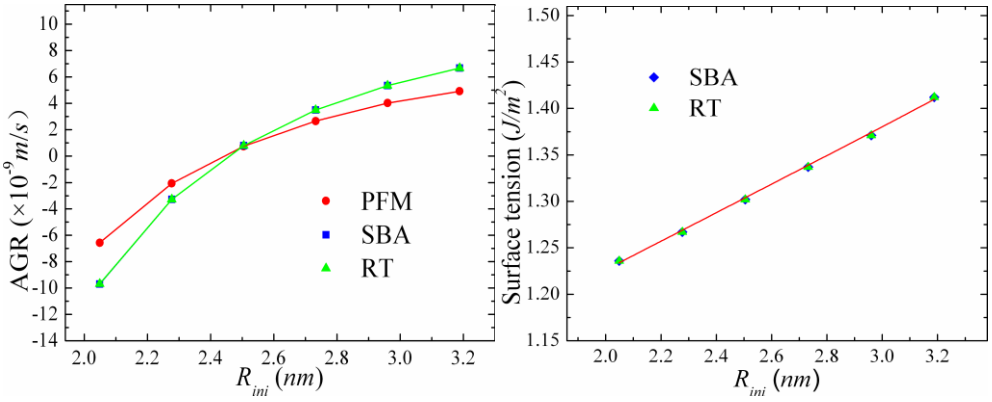

(*a*) (*b*)

Fig. 6.20. (*a*) Average void growth rate (AGR) as a function of initial void radius, R_{ini}, at T = 850 K, C_b = 7.5×10^{-8}. (*b*) Matching value of the surface tension coefficient γ_s as a function of initial void radius.

The average void growth rate as a function of initial void radius, R_{ini}, is shown in Fig. 6.20*a*. In this case, the average void growth rate increases with the void radius, which is totally different from the corresponding case in the foregoing section. Here, the thermal emission vacancy concentration, C_{eR}, is

comparable to C_b and decreases significantly as void radius increases. C_{eR}, rather than void radius, plays the dominant role in determining the void growth. From Fig. 6.20*a*, the critical void radius is approximately equal to 2.46 *nm* in the case of SBA and RT and to 2.44 *nm* in the case of PFM. As in Fig. 6.19, there is a substantial difference in the slopes of the curves obtained with SBA and PFM. This difference can be removed by varying the value of the surface tension coefficient (Fig. 6.20*b*).

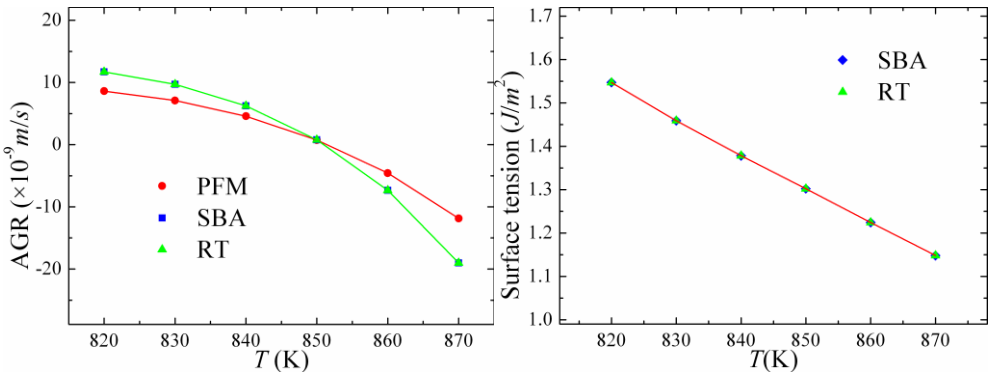

(*a*) (*b*)

Fig. 6.21. Average void growth rate (AGR) as a function of temperature, *T*, at C_b = 7.5×10^{-8} and R_{ini} = 2.505 *nm*.

Finally, Fig. 6.21 demonstrates the effect of temperature on the void growth rate. PFM and SBA give the critical temperature, at which average void growth rate changes its sign, as equal to 851.4 K and 851 K,

respectively. Since vacancy emission from a void plays a dominant role in the void evolution in the vicinity of the critical point, void growth rate decreases with increasing temperature. This is unlike in section 6.2.3, where the effect of temperature is entirely determined by the temperature dependence of the vacancy diffusion coefficient. The difference in the slopes of the curves obtained with SBA and PFM can be also removed by varying the value of the surface tension coefficient (Fig. 6.21*b*).

In summary, for cases with spherical coordinates of void evolution around the critical point, the corresponding values of system parameters obtained with PFM match very well those obtained with SBA. Only the trends of void evolution predicted by PFM are a little bit different from the predictions made with SBA. These small differences may be due to the nature of PFM, in which the sharp boundary at the void surface is treated as a diffusive interface. In these cases, the void evolution is sensitive to the system parameters, which may deviate simulation results obained with PFM from those with SBA. Around the critical point at a relative low temperature, either the void size is small, or the equilibrium vacancy concentration in the matrix is extremely dilute. Any small uncertainty errors from the numerical scheme or other problems will make the simulations result errors large. Around the critical point at a relative high temperature, although the void

size and the equilibrium vacancy concentration can be relatively large, the increase of temperature will increase the thickness of the interface, which will make the results obtained with PFM deviate from those obtained with SBA. The particular form of free-energy density adopted in the current study may lead to the differences in these trends as well, because the thickness of the interface is dictated by the competition between the bulk chemical potential and the chemical potential due to gradient energy.

The characteristic spatial scales of the void-metal diffuse interface are about one or two lattice constants, across which the variation of vacancy concentration is several orders of magnitude. This may bring some errors to the simulation, especially for the void evolution around the critical point. The dynamic equivalence between PFM and SBA requires the gradient energy coefficient to be dependent on the void size, which may be particularly true for the voids with sizes close to the critical one. This presents a challenge for modeling the evolution of an ensemble of voids under irradiation. One possible way to solve this problem is to use the method of matched asymptotic expansion [13, 33] to relate the PFM to the SBA. In this case the gradient-energy coefficient may become dependent on the void size even for voids, the sizes of which are significantly larger than critical.

6.3 Single void dynamics in 3D Cartesian coordinates in molybdenum

6.3.1 Boundary conditions and initial conditions

In this section a single void evolution in a cubic volume will be studied. Equation (4.82) is numerically solved by using the numerical scheme described in section 5.2. A single spherical void is put in the center of a cubic domain with side-length 2L. The boundary conditions are written as follows:

$$C_v(\mathbf{r},t)\big|_{\mathbf{r}\in\partial V} = C_b,\ \nabla^2 C_v\big|_{\mathbf{r}\in\partial V} = 0,\ \nabla(\nabla^2 C_v)\big|_{\mathbf{r}\in\partial V} = 0 \qquad (6.17)$$

where ∂V is the domain boundary which is the six faces of the cubic domain. The initial condition is $C_v(\mathbf{r},t=0)\big|_{\|\mathbf{r}-L\|\le R_{ini}} \cong 1$ within the void and $C_v(\mathbf{r},t=0) = C_b$ for other areas in the domain outside the void. Here, the void radius R is defined the same way as in the previous spherical coordinate case (see equation (6.3)).

6.3.2 Model parameters and material parameters

Material parameters used in the calculations correspond to the case of

molybdenum. They are listed in Table 6.1. The cubic domain with the side-length $2L$ = 21.26 *nm* is discretized into $48 \times 48 \times 48$ uniform cubic grids with the side-length l = 0.4429 *nm* which is about three times that it used in section 6.1.2. The gradient energy coefficient is also the same as that used in section 6.1.2, i.e., I_2 in the equation (4.79) is assumed to be equal to unity. For the numerical scheme to be stable the time step, τ, is taken to be 5×10^{-12} *s*, which is bigger than that used in section 6.1.2 because here the grid size is larger.

6.3.3 Vacancy concentration profile

Fig. 6.22*a* and *b* show the vacancy concentration contour on cross section planes of a three-dimensional domain of a case of void growth. The void is in the center of the cubic domain and the vacancy concentration is minimal in the adjacent vicinity of the surrounding void surface. This is indicated in Fig. 6.22*b* as well. The vacancy concentration profile is similar to that in the spherical coordinate case. The vacancy concentration in the void is unity; it decreases drastically from unity to an order of 10^{-10} across the interface. The vacancies will diffuse in the matrix from the system boundary to the lowest vacancy concentration position and flow into the void further through uphill

diffusion within the interface.

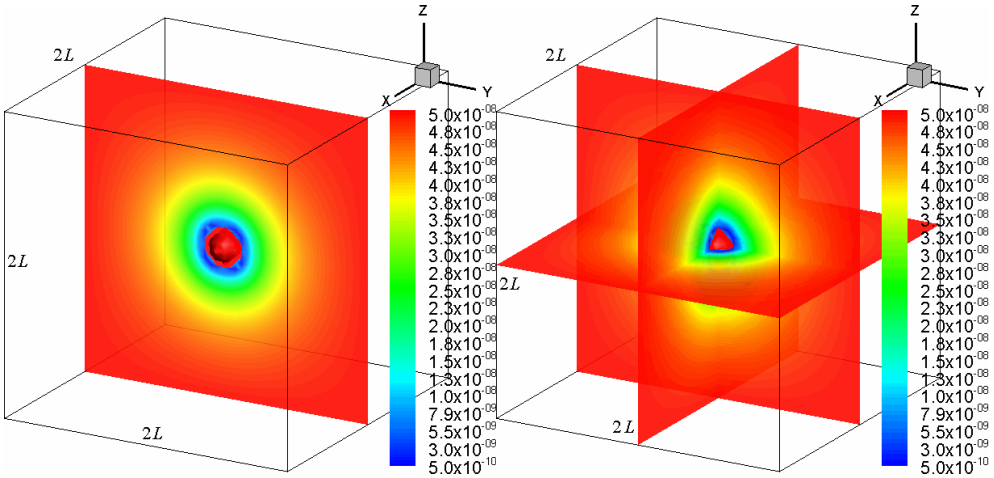

(*a*) (*b*)

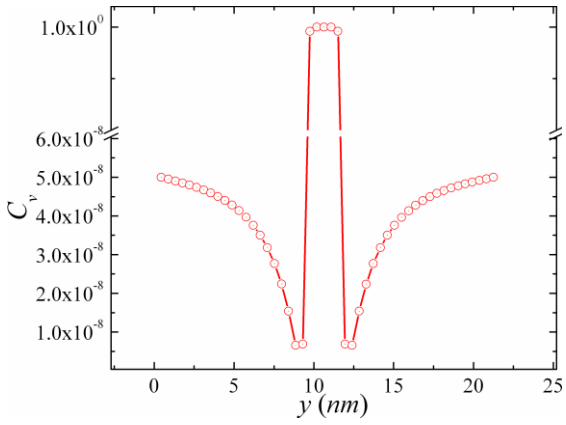

(*c*)

Fig. 6.22. Concentration profiles at $t = 10^{-4}$ *s* for the cases of void growth under the conditions $C_b = 5\times10^{-8}$, T = 1100 K and R_{ini} = 0.88 *nm*. (*a*) The contour of the vacancy concentration in three dimensions, with a cross section plane whose

direction is along *x*-direction at $x = L$. (*b*) The vacancy concentration contour on the three cross section planes along the *x*-, *y*- and *z*- directions, respectively. (*c*) The vacancy concentration profile along the *y*-direction at $x = L$ and $z = L$.

Fig. 6.23*a* shows that the void radius increases with time in a void growth case. Fig. 6.23*b* shows the corresponding process of void growth rate versus time. After an initial short period of large growth rate, the growth rate approaches to a constant value, which exhibits the same behavior as in the case of void growth in a spherical domain (see sections 6.1.3 and 6.2.2).

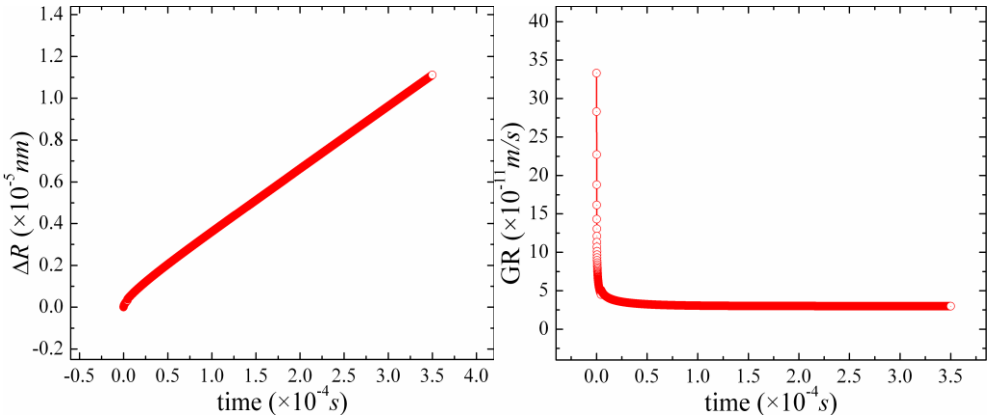

(*a*) (*b*)

Fig. 6.23. (*a*) Change in the void radius $\Delta R = R - R_{ini}$ versus time at $T = 1100$ K, $C_b = 6.0\times10^{-8}$, $R_{ini} = 1.366$ *nm*. (*b*) Void growth rate (GR) versus time under the same conditions as in (*a*).

6.3.4 Void evolution without vacancy emission

In this section, void evolution under different conditions will be studied. This void growth is similar to the cases of void growth studied with spherical coordinates (see section 6.1.4). The void evolution is under the condition of high supersaturation of vacancy concentration. Similarly to the cases of void evolution in the spherical domain, instead of instantaneous growth rate, the average growth rates will be used in the following study of void evolution under different conditions. These average rates are the results of averaging over a time period of 3.5×10^{-4} *s*. A case of void growth behavior within such a time period is shown in Fig. 6.23. This time interval is very short, but it is much larger than the relaxation time of the vacancy diffusion field, and the void growth rate remains almost unchanged. This is discussed in section 6.1.4. According to equation (6.15), for large supersaturation at volume boundary, the growth rate should linearly increase with time. Fig. 6.24 shows this behavior very well.

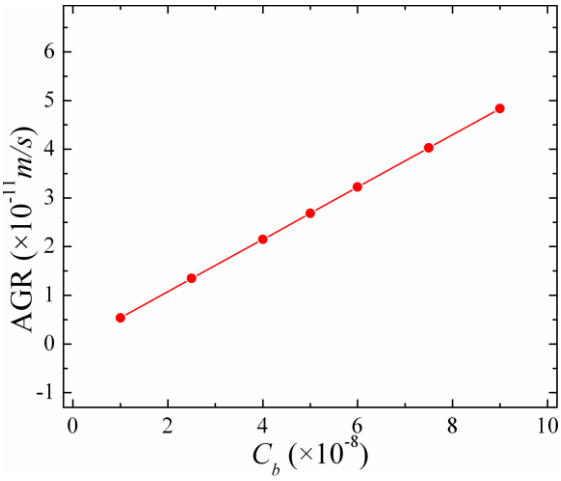

Fig. 6.24. Average void growth rate (AGR) as a function of vacancy concentration at the volume boundary, C_b, at T = 1100 K, R_{ini} = 1.366 *nm*.

Fig. 6.25 shows the average growth rate versus the initial void radius. This is similar, but with a larger range of initial void radius, to the case in the spherical domain, shown in Fig. 6.7, where the curve shows an inverse relationship between the average growth rate and the initial void radius. Fig. 6.26 shows the average growth rate change with temperature. The trend of the curve in Fig. 6.26 is also similar to that in Fig. 6.8, and shows that the average growth rate increases with the temperature. The reason for this has been discussed in section 6.1.4. Through the above study of void evolution in a cubic domain with the Cartesian coordinates, one can find that the void dynamics in a cubic domain with the Cartesian coordinates are very similar to those in a spherical domain with the spherical coordinates.

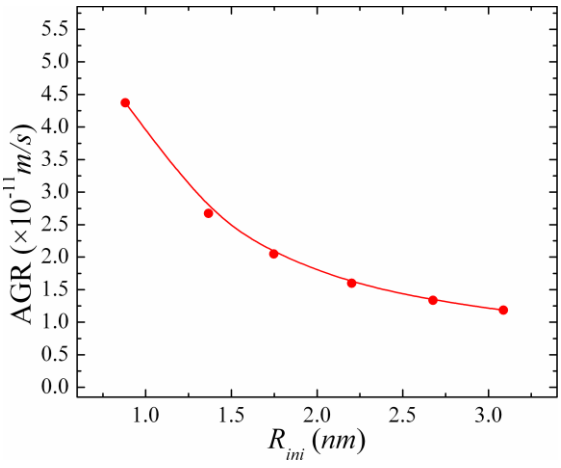

Fig. 6.25. Average void growth rate (AGR) as a function of initial void radius, R_{ini}, at T = 1100 K, $C_b = 5.0\times10^{-8}$.

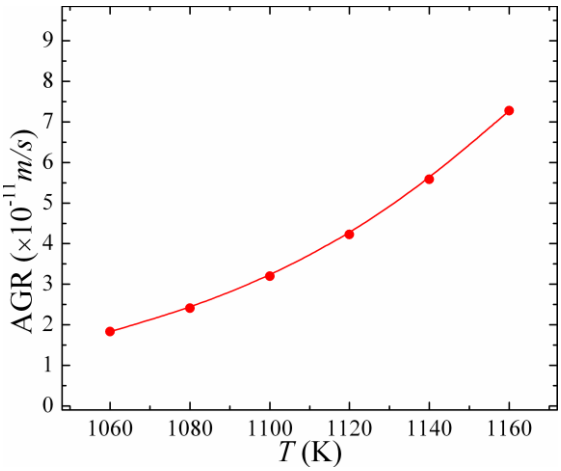

Fig. 6.26. Average void growth rate (AGR) as a function of temperature, T, at $C_b = 1.0\times10^{-7}$ and R_{ini} = 2.2 *nm*.

Chapter 7: Conclusions and recommendations for future work

7.1 Conclusions

A quantitative study of single void evolution in the phase-field framework with thermodynamic consistency has been conducted. Through constructing the free energy functional of a system with only vacancies and voids presence [24], with the principles of the non-equilibrium thermodynamics of void evolution correctly built in and with the physical mechanism maintained, the phase-field method can numerically emulate single void dynamics at very low vacancy concentrations, which correspond to the real experimental conditions. The key points for realization of a successful phase-field modeling of void evolution are as follows:

1. The void-metal sharp interface is mimicked by using a diffuse interface via the combination effects of gradient energy and bulk free energy, which should ensure the thermodynamic equivalence of the physical and the emulated void in the PFM.

2. Due to the local conservation of vacancies, the Cahn-Hilliard equation

should be used. In this way, the vacancy concentration becomes an order parameter.

3. Since the vacancy concentration is unity in the void in the PFM instead of zero in reality, the thermodynamic potential of Gibbs free energy in the SBA should be interpolated for the regions, such as in the interface and void, in which vacancy concentrations are far greater than thermal equilibrium concentration, by using phenomenological terms.

4. In order to reproduce the kinetic characteristic of the void growth or shrinkage, the vacancy concentration profile in the matrix in the PFM should be the same as that in the SBA. The vacancy concentration in the void should be identical unity. The uphill diffusion should only occur within the narrow diffuse interface, in void growth cases.

The goal of this thesis has been to build a phase-field model which can correctly depict the evolution of single void under different conditions, through investigating the thermodynamics of void nucleation and evolution and benchmarking the results obtained by the PFM with those obtained by the SBA. In this thesis, the following work has been done.

1. A bulk free energy has been proposed, based on the thermodynamic

potential used in the SBA. It is a double well function with two global minima at thermal equilibrium vacancy concentration and unity, respectively.

2. By following the phase-field theory proposed by A. A. Semenov, the gradient energy coefficient, which is related to the surface tension, for a flat surface and for a curved surface of a spherical void, have been derived. The relationship between the gradient energy coefficient and the width of interface has been analyzed also.

3. Based on the proposed free energy functional, and on the variable mobility which related to the diffusion coefficient, the Cahn-Hilliard equation can be reduced to the diffusion equation in the matrix, and uphill diffusion will only occur within the diffuse interface.

4. By solving the Cahn-Hilliard equation with spherical coordinates, the phase-field numerical modeling of a single void evolution after nucleation in a spherical domain has been performed under different system conditions, by using the experimental material parameters of molybdenum and copper. The results of this modeling have been compared to the results obtained with the SBA. The vacancy concentration profiles in the matrix obtained with the PFM are almost

the same as those obtained with the SBA. At relatively low temperatures, when vacancies emitted from voids are negligible, the trends of void evolution predicted by the PFM agree quite well with those obtained with the SBA. For cases of void evolution around a critical point, which is an unstable equilibrium state between the growth state and shrinkage state, the results of average void growth rate versus system parameters obtained with the PFM match very well those obtained with the SBA. The trends of void evolution predicted by the PFM are a little bit different from those by SBA.

5. The single void evolutions in a cubic domain after nucleation, with the Cahn-Hilliard equation solved using Cartesian coordinates, have been studied under different system conditions by using the experimental material parameters of molybdenum. The simulation results of the PFM of single void evolution, using three-dimensional Cartesian coordinates, show the same behavior as those obtained when using the spherical coordinates. In contrast to the PFM, with spherical coordinates, this PFM with three-dimensional Cartesian coordinates can be used to study the evolution of multiple voids. The complex morphological and topological changes, such as coalescence and break-up of the boundary, can be easily captured. Other types of defects or new phases, such as

interstitials and dislocations, can be incorporated into this PFM with three-dimensional Cartesian coordinates as well. Thus the spatial correlation between the voids, and even the dislocations, can be captured by using the point defects as the media for spatial correlation. The elastic interaction between the dislocations and point defects can be taken into account as well.

7.2 Recommendations for future work

The present work has succeeded as a study of single void evolution and present significant progress in the three-dimensional phase-field simulation of void evolution. But there is still much to do. The following items are recommended.

1. Incorporate the self-interstitials into the model. The self-interstitials cannot form the volume type of defect clusters, as voids do, but they have strong interaction with line defect - dislocation, which are sinks and sources of self-interstitials as well. For the sake of convenience, the influence of single self-interstitials on the void evolution should be studied without considering dislocation. The dislocation should be

incorporated into the model at step 3. Thus, the governing equation of self-interstitials can use the diffusion equation, and the free energy functional of self-interstitials can directly use the free energy of classical thermodynamics. However, due to the three-dimensional isotropic migration of dumbbell and one-dimensional anisotropic migration of crowdions in crystalline close-packed directions, the anisotropic diffusion constant should be used. Due to the difference of formation energy between dumbbell and crowdion, their thermal equilibrium concentrations will be different, and this will result in the difference of their corresponding proportions in the self-interstitials. Since the dumbbell and crowdion convert to each other under thermal fluctuation, the difference in their proportions in self-interstitials may be reflected by configuring the anisotropic diffusion constant and both types of self-interstitials may be treated as one type. The vacancies and self-interstitials are kinds of matter and anti-matter. They will annihilate each other when they meet. Thus, the recombination rate term should be added to both the Cahn-Hilliard equation, which governs the vacancy diffusion and to the diffusion equation, which governs the self-interstitials diffusion.

2. In order to mimic the thermal fluctuation of defect concentration, the

stochastic term (Langevin noise term) should be added to the Cahn-Hilliard equation, and also to the diffusion equation. The Cahn-Hilliard equation will then be changed to the Cahn-Hilliard-Cook equation [110]. Also, the diffusion equation for self-interstitials should be added with a stochastic term. Here, the stochastic term is not used to represent the nucleation driving force. The nucleation process should be realized in other ways. The generation of vacancies and self-interstitials in the irradiated metal is a random process. Thus, the generation of vacancies and self-interstitials can also be mimicked by a stochastic term.

3. If the extended defects dislocation, which is the origin of the dislocation bias effect, is incorporated into the model, the Allen-Cahn equation should be used to describe the spatiotemporal evolution of long range order parameters, which will represent the phases of dislocation. Since dislocation is one type of extended defect, as the void, a correct phase-field modeling of dislocation with thermodynamics consistency should first be built, just as has been done for single void evolution in the present work. Similar to the surface tension and corresponding thermal emission vacancy concentration in the void case, there is a line tension and stacking-fault around the dislocation and corresponding

thermal emission vacancy concentration (see the introductions in section 2.4.2.1). They can be mimicked by a gradient energy term as well. In contrast to the small elastic interaction between the voids and the vacancies, there are large elastic interactions between the dislocations and the vacancies and self-interstitials, and these should be taken into account. This will be a very complicated task, because there are many types of dislocations, such as vacancy dislocation loops, self-interstitial dislocation loops and dislocation networks, and there are several slip planes on which there is a Burgers vector of dislocation.

Appendices

Appendix A The derivation of void growth rate

According to the Fick's first law, the flux density of vacancies is given by

$$\mathbf{J}_v = -D\nabla n(\mathbf{r},t) = -\frac{1}{\Omega} D\nabla C_v(\mathbf{r},t) \tag{A. 1}$$

Due to the mass conservation the continuity equation can be written as follows:

$$\frac{dN_v}{dt} + \oint_S \mathbf{J}_v \cdot d\hat{\mathrm{S}} = \frac{dV}{\Omega dt} + \oint_S \mathbf{J}_v \cdot d\hat{\mathrm{S}} = 0 \tag{A. 2}$$

where N_v is the number of vacancies in a void and V is the volume of the void, Ω the atomic volume, $n(\mathbf{r},t) = C_v(\mathbf{r},t)/\Omega$, $C_v(\mathbf{r},t)$ vacancy concentration whose value range is from zero to unity. For a case of spherical void with spherical coordinates, equation (A. 2) can be rewritten as follows:

$$\frac{d}{dt}\left(\frac{4\pi R^3}{3\Omega}\right) + 4\pi R^2 J_v\big|_{r=R} = 0 \tag{A. 3}$$

where $J_v\big|_{r=R}$ is the vacancy flow density at void surface, which has following relations with vacancy concentration and diffusion coefficient according to equation (A. 1).

$$J_v\big|_{r=R} = -\frac{1}{\Omega} D \frac{\partial C_v(r,t)}{\partial r}\bigg|_{r=R} \tag{A. 4}$$

where R is the void radius. Equation (A. 3) becomes

$$\frac{dR(t)}{\Omega dt} + J_v\big|_{r=R} = 0 \tag{A. 5}$$

Combining equation (A. 4) and equation (A. 5) one can get

$$\frac{dR(t)}{dt} = -\Omega J_v\big|_{r=R} = D \frac{\partial C_v(r,t)}{\partial r}\bigg|_{r=R} \tag{A. 6}$$

Above equation indicates that the void growth rate is proportional to the vacancy concentration gradient at the void surface.

Appendix B The derivation of void growth rate in RT

In steady state, the vacancy concentration distribution will not vary with time, which means that the derivative of vacancy concentration with respect to time is zero.

$$\frac{\partial C_v(r,t)}{\partial t} = 0 \tag{B. 1}$$

$$D\frac{1}{r^2}\frac{\partial}{\partial r}\left[r^2\frac{\partial C_v(r)}{\partial r}\right] = 0 \tag{B. 2}$$

Equation (B. 2) has following type of general solution

$$C_v(r) = B - \frac{A}{r} \tag{B. 3}$$

Applying boundary conditions $C_v(r) = C_{veR}$ at $r = R$ and $C_v(r) = C_b$ at $r = L$ to equation (B. 3) one can get

$$\begin{cases} A = (C_b - C_{veR})\dfrac{RL}{L-R} \\ B = \dfrac{L}{L-R}C_b - \dfrac{R}{L-R}C_{veR} \end{cases} \tag{B. 4}$$

thus, the solution of equation (B. 2) is

$$C_v(r) = \frac{L}{L-R}C_b - \frac{R}{L-R}C_{veR} - \frac{1}{r}(C_b - C_{veR})\frac{RL}{L-R} \tag{B. 5}$$

where R is the void radius, L the radius of the system. The flux density

distribution is given by

$$J(r) = -\frac{D}{\Omega}\frac{\partial C_v(r)}{\partial r} = -\frac{D(C_b - C_{veR})}{\Omega}\frac{LR}{L-R}\frac{1}{r^2} \quad \text{(B. 6)}$$

At the void surface, the flux density is given by

$$J(r)|_{r=R} = -\frac{D(C_b - C_{veR})}{\Omega}\frac{L}{R(L-R)} \quad \text{(B. 7)}$$

Therefore, the void growth rate is

$$\frac{dR}{dt} = -\Omega J(r)|_{r=R} = D(C_b - C_{veR})\frac{L}{R(L-R)} \quad \text{(B. 8)}$$

If $L >> R$, then

$$\frac{dR}{dt} = D(C_b - C_{veR})\frac{1}{R} \quad \text{(B. 9)}$$

At steady state, the void growth rate is inversely proportional to the void radius, and proportional to the difference of the vacancy concentration between at the system boundary and at the void surface.

Appendix C The derivation of the expression of chemical potential in the PFM

The variation of free energy functional is

$$\begin{aligned}
\delta F(C_v) &= \delta \frac{1}{\Omega}\int_V \left[f_0(C_v) + \alpha (\nabla C_v)^2 \right] d^3r \\
&= \frac{1}{\Omega}\left\{ \delta \int_V f_0(C_v) d^3r + \alpha \delta \int (\nabla C_v)^2 d^3r \right\} \\
&= \frac{1}{\Omega}\int_V \left[f_0(C_v + \delta C_v) - f_0(C_v) \right] d^3r + \frac{\alpha}{\Omega}\int_V \left\{ \left[\nabla (C_v + \delta C_v) \right]^2 - (\nabla C_v)^2 \right\} d^3r \\
&= \frac{1}{\Omega}\left\{ \int_V \left[\frac{\partial f_0(C_v)}{\partial C_v} \delta C_v \right] d^3r + \alpha \int_V \left[(\nabla C_v + \nabla \delta C_v)(\nabla C_v + \nabla \delta C_v) - (\nabla C_v)^2 \right] d^3r \right\} \\
&\approx \frac{1}{\Omega}\left\{ \int_V \left[\frac{\partial f_0(C_v)}{\partial C_v} \delta C_v \right] d^3r + \alpha \int_V \left[2\nabla \delta C_v \cdot \nabla C_v \right] d^3r \right\} \\
&= \frac{1}{\Omega}\left\{ \int_V \left[\frac{\partial f_0(C_v)}{\partial C_v} \delta C_v \right] d^3r + 2\alpha \int_V \left[\nabla \cdot (\delta C_v \nabla C_v) - \nabla^2 C_v \delta C_v \right] d^3r \right\} \\
&= \frac{1}{\Omega}\left\{ \int_V \left[\frac{\partial f_0(C_v)}{\partial C_v} \delta C_v \right] d^3r + 2\alpha \oiint (\delta C_v \nabla C_v) \cdot \mathbf{n} dS - 2\alpha \int \left[\nabla^2 C_v \delta C_v \right] d^3r \right\}
\end{aligned} \tag{C. 1}$$

For the cases that the vacancy concentration is fixed at the system boundary $\delta C_v = 0$, or there are no vacancies flowing in or out through system boundary, or the periodic boundary condition, $\nabla C_v \cdot \mathbf{n} = 0$, we have following relations

$$\oiint (\delta C_v \nabla C_v) \cdot \mathbf{n} dS = 0 \tag{C. 2}$$

where $\mathbf{n}$ is the unit vector normal to the system boundary, S the closed surface of the system. It should be noted here, exactly, the vacancy flux density is $\mathbf{J}_v = M(C_v)\nabla \mu_v(C_v) \neq D\nabla C_v$, such as in the interface region. However, in the matrix, especially at volume boundary, $\mathbf{J}_v = D\nabla C_v$ holds.

Thus, for vacancy conservation, it has $\mathbf{J}_v \cdot \mathbf{n} = D\nabla C_v \cdot \mathbf{n} = 0$

Therefore, the variation of free energy functional is

$$\delta F\left(C_v\right) = \frac{1}{\Omega}\int_V \left[\frac{\partial f_0\left(C_v\right)}{\partial C_v} - 2\alpha\nabla^2 C_v\right]\delta C_v d^3 r \qquad \text{(C. 3)}$$

and the chemical potential is

$$\mu\left(C_v\right) = \Omega\frac{\delta F\left(C_v\right)}{\delta C_v} = \frac{\partial f_0\left(C_v\right)}{\partial C_v} - 2\alpha\nabla^2 C_v \qquad \text{(C. 4)}$$

Appendix D The chemical potential in equilibrium state in the PFM

The boundary conditions and the Green's formula:

$$\oiint(\delta C_v \nabla C_v)\cdot d\mathbf{S} = \int_V \left[\delta C_v \nabla^2 C_v + (\nabla \delta C_v)(\nabla C_v)\right] d^3 r \qquad \text{(D. 1)}$$

Here S is the closed surface of the volume V. The variation of free energy functional is

$$\begin{aligned}\delta F(C_v) &= F(C_v + \delta C_v) - F(C_v) \\ &= \frac{k_B T}{\Omega}\int_V \left[\phi(C_v + \delta C_v) - \phi(C_v^0) + \kappa^2 \left(\nabla(C_v + \delta C_v)\right)^2\right] d^3 r \\ &\quad - \frac{k_B T}{\Omega}\int_V \left[\phi(C_v) - \phi(C_v^0) + \kappa^2 \left(\nabla C_v\right)^2\right] d^3 r \\ &= \frac{k_B T}{\Omega}\int_V \left[\frac{\partial \phi(C_v)}{\partial C_v} - 2\kappa^2 \nabla^2 C_v\right] \delta C_v(\mathbf{r}) d^3 r\end{aligned} \qquad \text{(D. 2)}$$

In equation (D. 1) $\delta C_v(\mathbf{r})$ is an arbitrary deviation satisfying the conservation relation

$$\int_V \delta C_v(\mathbf{r}) d^3 r = 0 \qquad \text{(D. 3)}$$

Thus, the functional $F(C_v(\mathbf{r}))$ reaches its extremum when $C_v(\mathbf{r})$ is a solution of the following equation:

$$\frac{d\phi(C_v)}{dC_v} - 2\kappa^2 \nabla^2 C_v = const \qquad \text{(D. 4)}$$

Appendix E The estimation of interface thickness

In order to analyze and get the approximate value of the thickness of interface, we can expand the right hand side of equation (4.37) in the Taylor series around C = 0.5 which is at the middle of the interface and the maximum of bulk free energy also by assuming that κ is independent to the vacancy concentration. C_{ve} is very small even at a very high temperature, which is about 10^{-12} at 1100K. It can be omitted by comparing to $\phi_b(0.5)$ which is far bigger than unity.

$$\begin{aligned}
\Delta l &= \kappa \int_{C_{veR}}^{1-C_{veR}} \left[\phi_b(C(\mathbf{r})) + C_{ve}\right]^{-\frac{1}{2}} dC_v \\
&= \kappa \int_{C_{veR}}^{1-C_{veR}} \left\{ \left[\phi_b(0.5)\right]^{-\frac{1}{2}} - \frac{1}{2}\left[\phi_b(0.5)\right]^{-\frac{3}{2}}(C-0.5) + \frac{3}{8}\left[\phi_b(0.5)\right]^{-\frac{5}{2}}(C-0.5)^2 + \cdots \right\} dC \\
&= \kappa \left\{ \left[\phi_b(0.5)\right]^{-\frac{1}{2}} C - \frac{1}{2}\left[\phi_b(0.5)\right]^{-\frac{3}{2}} 0.5C(C-1) + \frac{1}{8}\left[\phi_b(0.5)\right]^{-\frac{5}{2}}(C-0.5)^3 + \cdots \right\} \Big|_{C_{eR}}^{1-C_{eR}} \\
&\approx \kappa \left[\phi_b(0.5)\right]^{-\frac{1}{2}} \\
&= \kappa \left[\phi_{b\max}\right]^{-\frac{1}{2}}
\end{aligned} \tag{E. 1}$$

where $\phi_{b\max}$ is the maximum of bulk free energy $\phi_b(C(\mathbf{r}))$. In the above derivation process κ is assumed to be independent to the vacancy concentration. The larger the maximum of bulk free energy is, the error of approximation of $\kappa\left[\phi_{b\max}\right]^{-\frac{1}{2}}$ to the interface width will be smaller, because the higher order terms in Taylor series are inversely proportional to the maximum of bulk free energy.

Appendix F The transformation of coordinates of diffusion equation

Let

$$x = \frac{r - R}{L - R} \tag{F. 1}$$

where x varies between 0 ($r = R$) and 1 ($r = L$).

Then $r = R + (L - R)x$. Therefore,

$$\frac{\partial C_v(r,t)}{\partial r} = \frac{\partial x}{\partial r}\frac{\partial C_v(x,t)}{\partial x} = \frac{1}{L-R}\frac{\partial C_v(x,t)}{\partial x} \tag{F. 2}$$

$$\begin{aligned}\frac{\partial C_v(r,t)}{\partial t} &= \frac{\partial C_v(x,t)}{\partial t} + \frac{\partial C_v(x,t)}{\partial x}\frac{\partial x}{\partial t} \\ &= \frac{\partial C_v(x,t)}{\partial t} + \frac{\partial C_v(x,t)}{\partial x}\frac{1-x}{L-R}\left(-\frac{dR}{dt}\right) \\ &= \frac{\partial C_v(x,t)}{\partial t} - \frac{1-x}{L-R}\frac{dR}{dt}\frac{\partial C_v(x,t)}{\partial x}\end{aligned} \tag{F. 3}$$

Substituting equations (F. 2) and (F. 3) into equation (3.37), one gets

$$\begin{aligned}\frac{\partial C_v(x,t)}{\partial t} - \frac{1-x}{L-R}\frac{dR}{dt}\frac{\partial C_v(x,t)}{\partial x} = &\frac{1}{\left[R+(L-R)x\right]^2}\frac{1}{L-R}\frac{\partial}{\partial x} \\ &\left\{D\left[R+(L-R)x\right]^2\frac{1}{L-R}\frac{\partial C_v(x,t)}{\partial x}\right\}\end{aligned} \tag{F. 4}$$

or

$$\left[R+(L-R)x\right]^2(L-R)\left[\frac{\partial C_v(x,t)}{\partial t}-\frac{1-x}{L-R}\frac{dR}{dt}\frac{\partial C_v(x,t)}{\partial x}\right] = \frac{\partial}{\partial x}\left\{D\left[R+(L-R)x\right]^2\frac{1}{L-R}\frac{\partial C_v(x,t)}{\partial x}\right\} \quad \text{(F. 5)}$$

The void growth rate can be written as follows:

$$\frac{dR}{dt}=D\frac{\partial C_v(r,t)}{\partial r}\bigg|_{r=R}=D\frac{1}{L-R}\frac{\partial C_v(x,t)}{\partial x}\bigg|_{x=0} \quad \text{(F. 6)}$$

Appendix G The free energy dissipation in the diffusion process of vacancies governed by the Cahn-Hilliard equation

The free energy functional can be written as follows:

$$F\left(C_v(\mathbf{r},t)\right)=\frac{k_BT}{\Omega}\int_V\left[\phi_b(C_v(\mathbf{r},t))+\kappa^2(\nabla C_v(\mathbf{r},t))^2\right]dV \tag{G. 1}$$

$$\mu\left(C_v(\mathbf{r},t)\right)=\Omega\frac{\delta F\left(C_v(\mathbf{r},t)\right)}{\delta C_v(\mathbf{r},t)}=k_BT\left[\frac{d\phi_b\left(C_v(\mathbf{r},t)\right)}{dC_v(\mathbf{r},t)}-2\kappa^2\nabla^2C_v(\mathbf{r},t)\right] \tag{G. 2}$$

The free energy changed with time is

$$\begin{aligned}
&\frac{dF\left(C_v\right)}{dt}=\frac{k_BT}{\Omega}\int_V\left[\frac{d\phi_b(C_v)}{dt}+2\kappa^2\nabla C_v\cdot\frac{d\nabla C_v}{dt}\right]dV\\
&=\frac{k_BT}{\Omega}\int_V\left[\frac{dC_v}{dt}\frac{d\phi_b(C_v)}{dC}+2\kappa^2\nabla C_v\cdot\nabla\frac{dC_v}{dt}\right]dV\\
&=\frac{k_BT}{\Omega}\left\{\int_V\left[\frac{dC_v}{dt}\frac{d\phi_b(C_v)}{dC}-2\kappa^2\frac{dC_v}{dt}\nabla^2C_v\right]dV+2\kappa^2\oiint_S\left[\frac{dC_v}{dt}\nabla C_v\right]\cdot\mathbf{n}dS\right\}\\
&=\frac{k_BT}{\Omega}\left\{\int_V\frac{dC_v}{dt}\left[\frac{d\phi_b(C_v)}{dC_v}-2\kappa^2\nabla^2C_v\right]dV+2\kappa^2\oiint_S\left[\frac{dC_v}{dt}\nabla C_v\right]\cdot\mathbf{n}dS\right\}\\
&=\frac{1}{\Omega}\int_V\frac{dC_v}{dt}\mu\left(C_v\right)dV+\frac{k_BT}{\Omega}2\kappa^2\oiint_S\left[\frac{dC_v}{dt}\nabla C_v\right]\cdot\mathbf{n}dS\\
&=\frac{1}{\Omega}\int_V\mu\left(C_v\right)\nabla\cdot\left[M\left(C_v\right)\nabla\mu\left(C_v\right)\right]dV+\frac{k_BT}{\Omega}2\kappa^2\oiint_S\left[\frac{dC_v}{dt}\nabla C_v\right]\cdot\mathbf{n}dS\\
&=\frac{1}{\Omega}\oiint_S\left[\mu\left(C_v\right)M\left(C_v\right)\nabla\mu\left(C_v\right)+k_BT2\kappa^2\frac{dC_v}{dt}\nabla C_v\right]\cdot\mathbf{n}dS\\
&-\frac{1}{\Omega}\int_VM\left(C_v\right)\left[\nabla\mu\left(C_v\right)\right]^2dV\\
&=-\frac{1}{\Omega}\oiint_S\mathbf{J}_e\cdot\mathbf{n}dS-\frac{T}{\Omega}\int_V\frac{dS_i}{dt}dV
\end{aligned} \tag{G. 3}$$

where, **n** is the unit vector normal to the system boundary, and $\mathbf{J}_e$ is the flux density of entropy which flow in or out through the system boundary. It is written as follows:

$$\begin{aligned}\mathbf{J}_e &= -\mu(C_v)M(C_v)\nabla\mu(C_v) - k_B T 2\kappa^2 \frac{dC_v}{dt}\nabla C_v \\ &= \mu(C_v)\mathbf{J}_v + k_B T 2\kappa^2 \nabla C_v \nabla\cdot\mathbf{J}_v\end{aligned} \tag{G. 4}$$

which indicates that the entropy flux is related to the vacancy flux. According to the principle of minimum entropy production, entropy production rate is

$$\frac{dS_i}{dt} = \frac{1}{T}M(C_v)\left[\nabla\mu(C_v)\right]^2 \tag{G. 5}$$

Since we study the free energy dissipation of a spontaneous process of vacancy diffusion in a system, there should be no vacancies flowing in or out through system boundary and without the production and annihilation of vacancies in the system. Thus, following boundary conditions should be satisfied.

$$\mathbf{J}_v\cdot\mathbf{n} = M(C_v)\nabla\mu(C_v)\cdot\mathbf{n} = D\nabla C_v\cdot\mathbf{n} = 0 \tag{G. 6}$$

Equation (G. 6) only holds at the system boundary, which has been discussed in Appendix C. Since $D \neq 0$ and $M(C_v) \neq 0$, thus $\hat{n}\bullet\nabla C_v = \hat{n}\bullet\nabla\mu = 0$ at the system boundary. And entropy flux density at the system boundary is

$$\mathbf{J}_e \cdot \mathbf{n} = \mu\left(C_v\right)\mathbf{J}_v \cdot \mathbf{n} + k_B T 2\kappa^2 \left(\nabla C_v \cdot \mathbf{n}\right)\left(\nabla \cdot \mathbf{J}_v\right) = 0 \qquad \text{(G. 7)}$$

Above equation means that, under the conditions of vacancies conservation and of without vacancies flowing in and out through the system boundary, there is no entropy flowing in and out through the system boundary. Thus equation (G. 3) becomes

$$\frac{dF\left(C_v\right)}{dt} = -\frac{T}{\Omega}\int_V \frac{dS_i}{dt} dV \qquad \text{(G. 8)}$$

Since the entropy produced by the spontaneous process of vacancy diffusion in the system always increases with time ($dS_i/dt \geq 0$, see equation (G. 5)), the free energy of the system will decrease with time ($dF/dt \leq 0$). In equilibrium state, the entropy production rate is zero, thus

$$\frac{dF\left(C_v\right)}{dt} = -\frac{T}{\Omega}\int_V \frac{dS_i}{dt} dV = 0 \qquad \text{(G. 9)}$$

which means that there is no free energy dissipation in equilibrium state.

Appendix H Solving diffusion equation of fixed boundary position case using separation of variables and power series solution method

The separation of variables and power series solution method will be used to solve the diffusion equation for a case with fixed vacancy concentration at the void surface and at the system boundary (void radius R unchanged). The diffusion equation with spherical coordinates is

$$\frac{\partial C(r,t)}{\partial t} = \frac{1}{r^2}\frac{\partial}{\partial r}\left(Dr^2 \frac{\partial C(r,t)}{\partial r} \right) \tag{H. 1}$$

Boundary conditions:

$$C_L = C_b \quad \text{at} \quad r = L, \tag{H. 2}$$

$$C_R = C_{eR} \quad \text{at} \quad r = R \tag{H. 3}$$

where L is the radius of the system; the thermal emission vacancy concentration, C_{eR} is a constant, which means that the thermal emission vacancy concentration will almost not change with time or the void radius varies very slowly with time.

Due to the linearity of equation (H. 1), the solution of it can be defined as the sum of two functions $v(r,t)$ and $w(r)$:

$$C(r,t) = v(r,t) + w(r) \tag{H. 4}$$

$v(r,t)$ depends on position and time, $w(r)$ is temporal independent. Both of them are the solutions of equation (H. 1). For $w(r)$, we have

$$\frac{1}{r^2}\frac{\partial}{\partial r}\left(Dr^2\frac{\partial w(r)}{\partial r}\right) = \frac{\partial w(r)}{\partial t} = 0 \tag{H. 5}$$

So the function $w(r)$ is the steady-state distribution of vacancy concentration. The solution of equation (H. 5) under the boundary conditions $w_L = C_b$ at $r = L$ and $w_R = C_{eR}$ at $r = R$ is

$$w(r) = \frac{LC_b - RC_{eR}}{L-R} - \frac{1}{r}(C_b - C_{eR})\frac{LR}{L-R} \tag{H. 6}$$

The solution process of equation (H. 5) is shown in Appendix C. Substituting equation (H. 4) into equation (H. 1) gets us

$$\frac{\partial v(r,t)}{\partial t} = \frac{D}{r^2}\frac{\partial}{\partial r}\left(r^2\frac{\partial v(r,t)}{\partial r}\right) \tag{H. 7}$$

The boundary conditions of equation (H. 7) are

$$v_L = C_L - w_L = C_b - C_b = 0 \quad \text{at} \quad r = L, \tag{H. 8}$$

$$v_R = C_R - w_R = C_{eR} - C_{eR} = 0 \quad \text{at} \quad r = R \tag{H. 9}$$

The method of separation of variables will be used to solve equation (H. 7).

Assume the solution of equation (H. 7) is a product of two functions which is written as follows:

$$v(r,t) = X(r)T(t) \tag{H. 10}$$

Substituting equation (H. 10) into equation (H. 7) gets

$$\frac{1}{X(r)r^2}\frac{d}{dr}\left(r^2\frac{dX(r)}{dr}\right) = \frac{dT(t)}{T(t)Ddt} = -k^2 \tag{H. 11}$$

Thus, the partial differential equation (H. 7) becomes two ordinary differential equations

$$\frac{\partial T(t)}{T(t)} = -k^2 D\partial t \tag{H. 12}$$

$$\frac{1}{r^2}\frac{\partial}{\partial r}\left(r^2\frac{\partial X(r)}{\partial r}\right) + k^2 X(r) = 0 \tag{H. 13}$$

The solution of equation (H. 12) is

$$T(t) = Ee^{-k^2 Dt} \tag{H. 14}$$

The solution of equation (H. 13) can be written as follows:

$$X(r) = \left[A\frac{\sin k(r-R)}{r} + B\frac{\cos k(r-R)}{r}\right] \tag{H. 15}$$

Then

$$v(r,t)=\left[A\frac{\sin k\left(r-R\right)}{r}+B\frac{\cos k\left(r-R\right)}{r}\right]Ee^{-k^2Dt} \qquad \text{(H. 16)}$$

where, $r \geq R$. Appling boundary conditions (H. 8) and (H. 9) to equation (H. 16) we can get

$$B\frac{1}{R}Ee^{-k^2Dt}=0,\ \ B=0, \qquad \text{(H. 17)}$$

$$A\frac{\sin\left[k\left(L-R\right)\right]}{L}Ee^{-k^2Dt}=0, \qquad \text{(H. 18)}$$

$$\sin\left[k\left(L-R\right)\right]=0 \ \text{ and } \ k=\frac{n\pi}{L-R} \qquad \text{(H. 19)}$$

Thus

$$X\left(r\right)=\frac{A}{r}\sin\left[\frac{n\pi}{L-R}\left(r-R\right)\right] \qquad \text{(H. 20)}$$

and

$$\begin{aligned} v(r,t)&=\frac{AE}{r}\sin\left[\frac{n\pi}{L-R}\left(r-R\right)\right]e^{-\left(\frac{n\pi}{L-R}\right)^2Dt} \\ &=\frac{F}{r}\sin\left[\frac{n\pi}{L-R}\left(r-R\right)\right]e^{-\left(\frac{n\pi}{L-R}\right)^2Dt} \end{aligned} \qquad \text{(H. 21)}$$

For each one of k there is a solution function to equations (H. 12) and (H. 13). There are infinite solution functions to equations (H. 12) and (H. 13) because n is integer whose value is from 1 to infinity. Those functions are orthogonal eigen-functions.

The general solution of equation (H. 7) can be written as follows:

$$v(r,t)=\sum_{n=1}^{\infty}\frac{F_n}{r}\sin\left[\frac{n\pi}{L-R}(r-R)\right]e^{-\left(\frac{n\pi}{L-R}\right)^2 Dt} \tag{H. 22}$$

Then the solution of equation (H. 1) is

$$\begin{aligned} C(r,t) &= v(r,t)+w(r) \\ &= \sum_{n=1}^{\infty}\frac{F_n}{r}\sin\left[\frac{n\pi}{L-R}(r-R)\right]e^{-\left(\frac{n\pi}{L-R}\right)^2 Dt} \\ &+\frac{LC_b-RC_{eR}}{L-R}-\frac{1}{r}(C_b-C_{eR})\frac{LR}{L-R} \end{aligned} \tag{H. 23}$$

Now we need to obtain the value of F_n which can be solved by taking advantage of the orthogonality between those eigen-functions.

The initial concentration $C(r,0)$ is C_b, equation (H. 23) becomes

$$C_b-\frac{LC_0-RC_{eR}}{L-R}+\frac{1}{r}(C_0-C_{eR})\frac{LR}{L-R}=\sum_{n=1}^{\infty}\frac{F_n}{r}\sin\left[\frac{n\pi}{L-R}(r-R)\right] \tag{H. 24}$$

Multiply both side of equation (H. 24) by $r\sin\left[\frac{m\pi}{L-R}(r-R)\right]$ and integrate it from R to L gets

$$\begin{aligned} &\int_R^L\left[C_b-\frac{LC_b-RC_{eR}}{L-R}+\frac{1}{r}(C_b-C_{eR})\frac{LR}{L-R}\right]r\sin\left[\frac{m\pi}{L-R}(r-R)\right]dr \\ &=\int_R^L\sum_{n=1}^{\infty}\frac{F_n}{r}\sin\left[\frac{n\pi}{L-R}(r-R)\right]r\sin\left[\frac{m\pi}{L-R}(r-R)\right]dr \end{aligned} \tag{H. 25}$$

where

$$
\begin{aligned}
&\int_R^L \left[\frac{R(C_{eR}-C_b)}{L-R}+\frac{1}{r}(C_b-C_{eR})\frac{LR}{L-R}\right] r\sin\left[\frac{m\pi}{L-R}(r-R)\right]dr \\
&=\int_R^L \frac{R(C_{eR}-C_b)}{L-R} r\sin\left[\frac{m\pi}{L-R}(r-R)\right]dr+\int_R^L (C_b-C_{eR})\frac{LR}{L-R}\sin\left[\frac{m\pi}{L-R}(r-R)\right]dr \\
&=\frac{R(C_{eR}-C_b)}{L-R}\int_R^L r\sin\left[\frac{m\pi}{L-R}(r-R)\right]dr+(C_b-C_{eR})\frac{LR}{L-R}\int_R^L \sin\left[\frac{m\pi}{L-R}(r-R)\right]dr \\
&=\frac{R(C_{eR}-C_b)}{L-R}\frac{(R-L)}{m\pi}\int_R^L \left\{d\left[r\cos\left[\frac{m\pi}{L-R}(r-R)\right]\right]-\cos\left[\frac{m\pi}{L-R}(r-R)\right]dr\right\} \\
&+\frac{LR(C_b-C_{eR})}{m\pi}\int_R^L \left\{-d\cos\left[\frac{m\pi}{L-R}(r-R)\right]\right\} \\
&=\frac{R(C_b-C_{eR})}{m\pi}\left[L\cos m\pi-R\right]+0-\frac{LR(C_b-C_{eR})}{m\pi}\left[\cos m\pi-1\right] \\
&=-\frac{R^2(C_b-C_{eR})}{m\pi}+\frac{LR(C_b-C_{eR})}{m\pi} \\
&=\frac{(L-R)R(C_b-C_{eR})}{m\pi}
\end{aligned}
\tag{H. 26}
$$

and

$$
\begin{aligned}
&\int_R^L \sum_{n=1}^{\infty}\frac{F_n}{r}\sin\left[\frac{n\pi}{L-R}(r-R)\right] r\sin\left[\frac{m\pi}{L-R}(r-R)\right]dr \\
&=\sum_{n=1}^{\infty} F_n\int_R^L \sin\left[\frac{n\pi}{L-R}(r-R)\right]\sin\left[\frac{m\pi}{L-R}(r-R)\right]dr \\
&=F_m\int_R^L \sin^2\left[\frac{m\pi}{L-R}(r-R)\right]dr \\
&=F_m\int_R^L \frac{1-\cos\left[\frac{2m\pi}{L-R}(r-R)\right]}{2}dr \\
&=\frac{L-R}{2}F_m
\end{aligned}
\tag{H. 27}
$$

Thus

$$
\frac{(L-R)R(C_b-C_{eR})}{m\pi}=\frac{L-R}{2}F_m,\quad F_m=\frac{2R(C_b-C_{eR})}{m\pi} \tag{H. 28}
$$

and the vacancy concentration field is

$$C(r,t)=\sum_{n=1}^{\infty}\frac{2R(C_b-C_{eR})}{n\pi r}\sin\left[\frac{n\pi}{L-R}(r-R)\right]e^{-\left(\frac{n\pi}{L-R}\right)^2 Dt}+\frac{LC_b-RC_{eR}}{L-R}-\frac{1}{r}(C_b-C_{eR})\frac{LR}{L-R} \quad \text{(H. 29)}$$

Therefore the void growth rate is

$$\begin{aligned}\frac{dR}{dt}&=D\left.\frac{dC(r,t)}{dr}\right|_{r=R}\\&=\frac{2D(C_b-C_{eR})}{L-R}S(t)+\frac{DL(C_b-C_{eR})}{R(L-R)}\end{aligned} \quad \text{(H. 30)}$$

where,

$$S(t)=\sum_{n=1}^{\infty}e^{-\left(\frac{n\pi}{L-R}\right)^2 Dt} \quad \text{(H. 31)}$$

For $L >> R$

$$\dot{R}_{ns}=\frac{dR}{dt}=-J=D\left.\frac{\partial C(r,t)}{\partial r}\right|_{r=R(t)}=\frac{D(C_b-C_{eR})}{R}+\frac{2D(C_b-C_{eR})}{L-R}S(t) \quad \text{(H. 32)}$$

$$\dot{R}_{s}=\frac{dR}{dt}=-J=D\left.\frac{\partial C(r,t)}{\partial r}\right|_{r=R(t)}=\frac{D(C_b-C_{eR})}{R} \quad \text{(H. 33)}$$

where $\dot{R}_{ns}$ is growth rate of non-steady state and $\dot{R}_{s}$ is growth rate of steady state. From the comparison of equation (H. 32) and equation (H. 33), one can find that there is a decay term that depicts the decrease of the growth rate due to the relaxation of initial uniform distribution of vacancy concentration to steady state distribution.

$$\Delta\dot{R} = \dot{R}_{ns} - \dot{R}_s = \frac{2D(C_b - C_{eR})}{L - R} S(t) \qquad \text{(H. 34)}$$

The term $S(t)$ decay to zero with time t (see formula (H. 31)). The decay speed is mainly determined by the diffusion constant. Through the comparison between equation (H. 29) and (H. 6), we can find that the differences between the non-steady state of vacancy concentration distribution and the steady state of vacancy concentration distribution are written as follows:

$$\Delta C(r,t) = C(r,t) - w(r,t) = \sum_{n=1}^{\infty} \frac{2R(C_b - C_{eR})}{n\pi r} \sin\left[\frac{n\pi}{L-R}(r-R)\right] e^{-\left(\frac{n\pi}{L-R}\right)^2 Dt} \qquad \text{(H. 35)}$$

$$R_{ratio} = \frac{\dot{R}_{ns} - \dot{R}_s}{\dot{R}_s} = \frac{2R}{L-R} S(t) \qquad \text{(H. 36)}$$

$\Delta C(r,t)$ originates from the initial uniform vacancy concentration distribution in the matrix. It decreases with time quickly.

References

[1] C. Cawthorne, and E. J. Fulton, Nature **216**, 575 (1967).

[2] D. I. R. Norris, Nature **227**, 830 (1970).

[3] J. H. Evans, Nature **229**, 403 (1971).

[4] J. H. Evans, B. L. Eyre, and S. Mahajan, Philosophical Magazine **26**, 813 (1972).

[5] J. H. Evans, and M. Eldrup, Nature **254**, 685 (1975).

[6] W. G. Wolfer, and M. Ashkin, Journal of Applied Physics **47**, 791 (1976).

[7] C. H. Woo, and B. N. Singh, Physica Status Solidi B-Basic Research **159**, 609 (1990).

[8] C. H. Woo, and B. N. Singh, Philosophical Magazine A-Physics of Condensed Matter Structure Defects and Mechanical Properties **65**, 889 (1992).

[9] B. N. Singh, C. H. Woo, and A. J. E. Foreman, Materials Science Forum **97**, 75 (1992).

[10] J. W. Cahn, Acta Metallurgica **9**, 795 (1961).

[11] D. Kondepudi, and I. Prigogine, *Modern Thermodynamics: From Heat*

Engines to Dissipative Structures (Wiley, Chichester, 1998).

[12] J. W. Cahn, and J. E. Hilliard, Journal of Chemical Physics **28**, 258 (1958).

[13] H. Emmerich, Advances in Physics **57**, 1 (2008).

[14] V. P. Skripov, and A. V. Skripov, Uspekhi Fizicheskikh Nauk **128**, 193 (1979).

[15] A. D. Brailsford, and R. Bullough, Journal of Nuclear Materials **44**, 121 (1972).

[16] R. Bullough, and R. S. Nelson, Physics in Technology **5**, 29 (1974).

[17] H. C. Yu, and W. Lu, Acta Materialia **53**, 1799 (2005).

[18] S. Rokkam *et al.*, Modelling and Simulation in Materials Science and Engineering **17**, 064002 (2009).

[19] P. C. Millett *et al.*, Modelling and Simulation in Materials Science and Engineering **17**, 064003 (2009).

[20] P. C. Millett *et al.*, Computational Materials Science **50**, 949 (2011).

[21] S. Y. Hu, and C. H. Henager, Journal of Nuclear Materials **394**, 155 (2009).

[22] S. Y. Hu, and C. H. Henager Jr, Acta Materialia **58**, 3230 (2010).

[23] Y. Li *et al.*, Journal Of Nuclear Materials **407**, 119 (2010).

[24] A. A. Semenov, and C. H. Woo, Journal of Nuclear Materials **411**, 144

(2011).

[25] A. A. Semenov, and C. H. Woo, Acta Materialia **60**, 6112 (2012).

[26] J. W. Gibbs, *Collected Works. Thermodynamics* (Longmans, Green & Co, London, 1878), Vol. 1.

[27] T. Blesgen, Analysis **28**, 125 (2008).

[28] M. Volmer, and A. Weber, Z. Phys. Chem. **119**, 277 (1926).

[29] R. Bullough, B. L. Eyre, and K. Krishan, Proceedings Of the Royal Society of London. A. Mathematical and Physical Sciences **346**, 81 (1975).

[30] A. D. Braislford, and R. Bullough, Journal of Nuclear Materials **69-70**, 434 (1978).

[31] R. Bullough, B. L. Eyre, and K. Krishan, Proceedings Of The Royal Society of London Series a-Mathematical Physical and Engineering Sciences **346**, 81 (1975).

[32] G. Caginalp, and W. Xie, Physical Review E **48**, 1897 (1993).

[33] K. R. Elder *et al.*, Physical Review E **64** (2001).

[34] J. W. Cahn, and S. M. Allen, Le Journal de Physique Colloques **38**, C7 (1977).

[35] S. M. Allen, and J. W. Cahn, Acta Metall **27**, 1085 (1979).

[36] G. J. Fix, in *Free Boundary Problems: Theory and Applications*, edited by A. Fasano, and M. PrimicerioPitman, Boston, 1983), pp. 580.

[37] J. S. Langer, in *Directions in Condensed Matter Physics*, edited by G. Grinstein, and G. Mazenko (World Scientific, Singapore, 1986), pp. 165.

[38] J. B. Collins, and H. Levine, Physical Review B **31**, 6119 (1985).

[39] G. Caginalp, and P. Fife, Physical Review B **33**, 7792 (1986).

[40] G. Caginalp, and P. Fife, Physical Review B **34**, 4940 (1986).

[41] O. Penrose, and P. C. Fife, Physica D **43**, 44 (1990).

[42] O. Penrose, and P. C. Fife, Physica D **69**, 107 (1993).

[43] A. A. Wheeler, W. J. Boettinger, and G. B. McFadden, Physical Review A **45**, 7424 (1992).

[44] R. Kobayashi, Physica D **63**, 410 (1993).

[45] J. A. Warren, and W. J. Boettinger, Acta Metallurgica et Materialia **43**, 689 (1995).

[46] A. Karma, and W.-J. Rappel, Physical Review E **53**, R3017 (1996).

[47] A. Karma, and W.-J. Rappel, Physical Review E **57**, 4323 (1998).

[48] N. Provatas, N. Goldenfeld, and J. Dantzig, Physical Review Letters **80**, 3308 (1998).

[49] A. Karma, Physical Review Letters **87** (2001).

[50] W. J. Boettinger *et al.*, Annual Review Of Materials Research **32**, 163 (2002).

[51] L. Q. Chen, and Y. Wang, JOM **48**, 13 (1996).

[52] Y. H. Wen, Y. Wang, and L. Q. Chen, Acta Materialia **47**, 4375 (1999).

[53] T. W. Heo, S. Bhattacharyya, and L. Q. Chen, Solid State Phenomena **172-174**, 1084 (2011).

[54] L. Q. Chen, and W. Yang, Physical Review B **50**, 15752 (1994).

[55] I. Steinbach *et al.*, Physica D **94**, 135 (1996).

[56] D. Fan, and L. Q. Chen, Acta Materialia **45**, 611 (1997).

[57] M. T. Lusk, Proceedings of the Royal Society of London. Series A: Mathematical, Physical and Engineering Sciences **455**, 677 (1999).

[58] R. Kobayashi, J. A. Warren, and W. Craig Carter, Physica D: Nonlinear Phenomena **140**, 141 (2000).

[59] I. S. Aranson, V. A. Kalatsky, and V. M. Vinokur, Physical Review Letters **85**, 118 (2000).

[60] A. Karma, D. A. Kessler, and H. Levine, Physical Review Letters **87** (2001).

[61] A. Karma, and A. E. Lobkovsky, Physical Review Letters **92** (2004).

[62] R. Spatschek *et al.*, Physical Review Letters **96** (2006).

[63] S. Nambu, and D. A. Sagala, Physical Review B **50**, 5838 (1994).

[64] Y. L. Li *et al.*, Applied Physics Letters **78**, 3878 (2001).

[65] J. Wang *et al.*, Acta Materialia **52**, 749 (2004).

[66] Y. Zheng, B. Wang, and C. H. Woo, Acta Materialia **56**, 479 (2008).

[67] K. Toshiyuki, and O. Hidehiro, Materials Transactions **44**, 2503 (2003).

[68] J. X. Zhang, and L. Q. Chen, Philosophical Magazine Letters **85**, 533 (2005).

[69] J. X. Zhang, and L. Q. Chen, Acta Materialia **53**, 2845 (2005).

[70] T. Koyama, Science and Technology of Advanced Materials **9**, 013006 (2008).

[71] F. Léonard, and R. C. Desai, Physical Review B **58**, 8277 (1998).

[72] S. Y. Hu, and L. Q. Chen, Acta Materialia **49**, 463 (2001).

[73] Y. U. Wang *et al.*, Applied Physics Letters **78**, 2324 (2001).

[74] Y. U. Wang *et al.*, Acta Materialia **49**, 1847 (2001).

[75] S. Y. Hu *et al.*, Journal Of Applied Physics **96**, 229 (2004).

[76] R. Poduri, and L. Q. Chen, Acta Materialia **44**, 4253 (1996).

[77] Y. Wang, L. Q. Chen, and A. G. Khachaturyan, Journal Of The American Ceramic Society **79**, 987 (1996).

[78] D. Y. Li, and L. Q. Chen, Acta Materialia **46**, 2573 (1998).

[79] V. Vaithyanathan, and L. Q. Chen, Scripta Materialia **42**, 967 (2000).

[80] X. Q. Ma *et al.*, MRS Online Proceedings Library **677**, AA4.14 (2001).

[81] X. Q. Ma *et al.*, Computational Materials Science **23**, 283 (2002).

[82] H. Mehrer, Journal of Nuclear Materials **69-70**, 38 (1978).

[83] F. W. Young, Journal of Nuclear Materials **69-70**, 310 (1978).

[84] W. Schilling, Journal of Nuclear Materials **69-70**, 465 (1978).

[85] D. Nguyen-Manh, A. P. Horsfield, and S. L. Dudarev, Physical Review B **73**, 020101 (2006).

[86] P. M. Derlet, D. Nguyen-Manh, and S. L. Dudarev, Physical Review B **76**, 054107 (2007).

[87] J. Steigman, W. Shockley, and F. C. Nix, Physical Review **56**, 13 (1939).

[88] R. P. Johnson, Physical Review **56**, 814 (1939).

[89] F. Kroupa, and P. B. Price, Philosophical Magazine **6**, 243 (1961).

[90] Y. N. Osetsky *et al.*, Philosophical Magazine A **80**, 2131 (2000).

[91] S. L. Dudarev, Philosophical Magazine **83**, 3577 (2003).

[92] G. H. Kinchin, and R. S. Pease, Reports On Progress In Physics **18**, 1 (1955).

[93] M. Kiritani, and H. Takata, Journal Of Nuclear Materials **69-70**, 277 (1978).

[94] T. D. de la Rubia *et al.*, Physical Review Letters **59**, 1930 (1987).

[95] T. D. de la Rubia *et al.*, Journal Of Materials Research **4**, 579 (1989).

[96] J. L. Katz, and H. Wiedersich, The Journal of Chemical Physics **55**, 1414 (1971).

[97] L. Landau, and E. Lifshitz, *Statistical Physics Part 1* (Robert Maxwell,

M.C., 1980), Vol. 5.

[98] J. Feder *et al.*, Advances In Physics **15**, 111 (1966).

[99] L. Onsager, Physical Review **37**, 405 (1931).

[100] A. Gokhman, and J. Boehmert, Radiation Effects and Defects in Solids **158**, 499 (2003).

[101] L. Q. Chen, Annual Review Of Materials Research **32**, 113 (2002).

[102] L. Q. Chen, and J. Shen, Computer Physics Communications **108**, 147 (1998).

[103] Y. He, Y. Liu, and T. Tang, Applied Numerical Mathematics **57**, 616 (2007).

[104] A. C. O'reilly, J. M. Beck, and K. Words, (University of Colorado Boulder, 2006).

[105] S. Q. Shi, M. Liao, and M. P. Puls, Modelling and Simulation in Materials Science and Engineering **2**, 1065 (1994).

[106] M. Berzins, and P. M. Dew, Acm Transactions on Mathematical Software **17**, 178 (1991).

[107] P. Ehrhart, in *Landolt-Börnstein: Numerical Data and Functional Relationships in Science and Technology- New Series, Group III, Crystal and solid state physics*, edited by H. Ullmaier (Springer-Verlag, Berlin, 1991).

[108] A. A. Semenov, and C. H. Woo, Physical Review B **66**, 024118 (2002).

[109] P. Harrowell, and D. W. Oxtoby, Journal Of Chemical Physics **80**, 1639 (1984).

[110] H. E. Cook, Acta Metall **18**, 297 (1970).